Computational Modelling of Plasma Membrane Electrophysiology and Calcium Dynamics in Microglia

Alireza Poshtkohi, B.Sc., M.Sc.

Faculty of Computing and Engineering

University of Ulster

A thesis submitted for the degree of

Doctor of Philosophy

June 2023

I confirm that the word count of this thesis is less than 100,000 words.

Note on Access to Contents

I hereby declare that with effect from the date on which the thesis is deposited in the Library of the University of Ulster, I permit the Librarian of the University to allow the thesis to be copied in whole or in part without reference to me on the understanding that such authority applies to the provision of single copies made for study purposes or for inclusion within the stock of another library. This restriction does not apply to the British Library Thesis Service (which is permitted to copy the thesis on demand for loan or sale under the terms of a separate agreement) nor to the copying or publication of the title and abstract of the thesis. IT IS A CONDITION OF USE OF THIS THESIS THAT ANYONE WHO CONSULTS IT MUST RECOGNISE THAT THE COPYRIGHT RESTS WITH THE AUTHOR AND THAT NO QUOTATION FROM THE THESIS AND NO INFORMATION DERIVED FROM IT MAY BE PUBLISHED UNLESS THE SOURCE IS PROPERLY ACKNOWLEDGED.

Abstract

Microglia, a type of glial cell, perform many tasks while interacting with neurons, astrocytes, and oligodendrocytes. Despite moderate advances in the characterisation of microglia in laboratory rodents, very little information is known about the physiology of microglia in the human brain. This is a challenging task and consequently this thesis attempts to advance knowledge of microglia function through mathematical modelling. Microglia restructure their intracellular actin cytoskeleton to enable motility; this requires a complex molecular cascade involving a set of ionic channels, membrane-coupled receptors, and cytosolic components. In this research, we develop a theoretical foundation for studying P2-mediated calcium and PI3K/Akt signalling in human microglial cells. Firstly, a detailed mathematical model is built for the dynamics of human P2XRs in microglia. Subsequently, experimental whole-cell currents are used to derive the P2X-mediated electrophysiology of human microglia (sodium and calcium dynamics, and membrane potential). Secondly, microglial-directed motility involves a complex family of intracellular signalling pathways that are mainly controlled by P2Y-mediated cytosolic calcium (Ca^{2+}) signalling and activation of the PI3K/Akt pathway. This thesis addresses the development of mathematical models for these two complex aspects of microglial functions and investigates the interconnecting role of PI3K pathway to Ca^{2+}.

Our predictions reveal new quantitative insights into how P2Rs regulate ionic concentrations in terms of physiological interactions and transient responses. Simulation results show that kink-like, intricate Ca^{2+} responses mediated by P2XRs arise from a complex cooperative activation of both P2XRs, and ionic extruders and pumps. More importantly, the proposed model supports our hypothesis that calcium influx via P2YR and P2XR can explain the experimentally observed twin peaks in the phosphorylated Akt. To the best of our knowledge, this is the first biophysical model that aims to predict complicated Akt and P2-mediated Ca^{2+} responses in microglia. The biophysical models provide direction for new fundamental experimental research.

TABLE OF CONTENTS

LIST OF FIGURES

LIST OF TABLES

ACKNOWLEDGEMENTS

First and foremost, I wish to give special thanks to my supervisor, Professor Liam McDaid, who encouraged me initially in 2017 to join their esteemed research team, whose focus on computational neuroscience has changed my scientific life since then. Liam's support and great guidance tremendously helped to keep my work on track throughout my study at the University of Ulster. I would also like to greatly appreciate my chief PhD supervisor, Dr John Wade at Ulster University, and Dr Junxiu Liu, my third PhD supervisor, for their unlimited advice and for giving great insight into my research, which played a major role in my contribution to a field for which I have decided to dedicate the rest of my life. John's fantastic expertise in the mathematical modelling of biological systems and round-the-clock support with quick hints on computational modelling aspects were of two utmost influences on my success.

I am likewise thankful for the dedication and efforts of my external advisors, Dr Mark Dallas and Dr Angela Bithell, both from the School of Pharmacy at the University of Reading. Their incredible points of view on experimental neuroscience and biology constituted a cornerstone of the underlying mathematical theories that I developed for my project. Many hours of fruitful discussion with Mark and his absolutely insightful inputs on my developed biophysical models in tandem with his impact as a role model have committed me to someday becoming an experimental physiologist, who is keen to exploit his mathematical knowledge for understanding the physiology of the brain in pursuit of unravelling mysteries involved in brain dysfunction.

I gratefully acknowledge the financial support of Ulster University for a prestigious VCRS scholarship on my project and top-tier open-access journals over the duration of my PhD.

Finally, I wish to greatly thank my mother and father, whose devotion and commitment to providing an amazingly peaceful environment prior to my PhD education was key to growing my talents in mathematics and computer science which would later end up with my successful PhD completion. Their unconditional love and mental support during the strange years of the pandemic over the phone unbelievably eased my PhD experience thousands of miles away from my hometown.

"I never made one of my discoveries through the process of rational thinking."

*…..**Albert Einstein***

Dedicated to my parents

Effat** and **Abdollah

Also for all leading pioneers in

mathematics**, **biophysics** and **neuroscience

particularly

Alan Hodgkin** and **Andrew Huxley

Chapter 1. Introduction

1.1 Introduction

The human brain is by far the most complex single structural object found in the visible universe, where 2.5 petabytes of memory in the human brain is comparable to the storage capacity needed to store all the astronomical structure information of the known universe [1]. Highly complex tasks can be processed by the brain, such as speech, memory, thoughts, and every process that controls the body. The computational capability of the brain is attributed to a complex net of neurons and synaptic connections. This highly complex structure of cells coexists with other networks of glial cells. The ratio of glia to neurons accounts for about 1.5:1 in the white matter and increases to about 3.5:1 if both white and grey matter are considered [2]. One type of glial cells is referred to as *microglia*.

Microglia play key roles and perform essential tasks in the central nervous system (CNS) during brain development, regulation of homeostasis and pathologies involved in brain diseases. Therefore, they directly interact with almost all components in the CNS. Microglial cells are also responsible for many main tasks such as clearing dead neurons and persevering tissue consistency. Moreover, they are the first agents of the CNS immune system to fight against viral, bacterial, and fungal infections. Perturbation of ionic homeostasis in the microenvironment of microglia can activate them. Upon activation, they can cause different types of cell migration, cytokine production, proliferation, and so forth. Five to twenty per cent of the total brain cells are composed of microglia, which are known as major factors in brain diseases and health [3].

Microglia, brain-resident macrophages, go through a variety of morphological configurations reliant on variable physiological conditions. The structure of microglia varies significantly from ramified to amoeboid-like cells [4, 5]. They involve a set of membrane-coupled receptors [5], which enable the microglia to sense concentration changes in their environment in order to begin either process extension or whole-cell chemotaxis. Three major types of purinergic receptors have been identified in microglia,

including, adenosine receptors (A_1, A_{2A}, A_{2B} and A_3), P2X receptors ($P2X_1$, $P2X_4$ and $P2X_7$) and P2Y receptors ($P2Y_2$, $P2Y_6$ and $P2Y_{12-14}$), three of which are more predominant in microglial directed motility, viz., $P2X_4$, $P2X_7$ and $P2Y_{12}$ both *in vitro* and *in vivo*, where spontaneous secondary messenger calcium (Ca^{2+}) transients play a key role [6-10]. Furthermore, they regulate different mechanisms, including, cell death, proliferation, migration, and differentiation. Uncontrolled activation of microglial cells leads to the production of proinflammatory cytokines, which affect different brain diseases such as Alzheimer's and Parkinson's [11].

One of the important elements to control the level of Ca^{2+} in intracellular space is adenosine triphosphate (ATP) which directly activates purinergic P2X receptors in eukaryotic cells [12]. After binding ATP, a channel pore opens allowing Ca^{2+} and other ions to traverse across the cell. It has been shown that Ca^{2+} actively participates in triggering the PI3K (phosphoinositide 3-kinase) pathway through calcium uptake from extracellular space for actin polymerisation [6, 13].

Adenosine diphosphate (ADP) also plays a vital role in regulating calcium via activation of the G protein-coupled $P2Y_{12}$ receptors which in turn gives rise to Ca^{2+} release from intracellular stores, particularly the endoplasmic reticulum (ER), through conversion of PIP_2 (phosphatidylinositol 4,5-bisphosphate) into IP_3 (inositol trisphosphate) macromolecules. Ca^{2+} release from ER stores also stimulate Ca^{2+} release-activated Ca^{2+} (CRAC) channels for an influx of Ca^{2+} to compensate for the intracellular stores and calcium-activated potassium channel (KCa3.1) channel for efflux of potassium [18]. These complex events activate PI3K and phospholipase C (PLC) pathways, which subsequently results in the activation of Protein kinase B (PKB, also known as Akt). Akt promotes process extension and chemotaxis by reorganisation of the actin cytoskeleton [19]. Ca^{2+} ions either indirectly or directly participate as a major regulator in most of the underlying pathways of these channels and receptors. For example, the IP_3 receptor, PI3K and parts of the $P2Y_{12}$ receptor depend on Ca^{2+} kinetics.

Although a body of literature elaborates on how microglia function in rodents (like rats and mice, see [14]), their role in human microglia has been investigated much less, mainly due to the difficulty faced in the study of human microglia *in situ* and preparing host tissue samples. Whereas studies in rodent cell lines are important to understand the physiology of

microglia, an increasing amount of evidence shows dramatic differences between human and animal microglia in terms of pharmacology, biochemistry and genome [15]. Despite major progress made on microglia-related neurodegeneration in rodents, it has failed to provide effective treatment for human brain diseases to date. Research on rodent and human microglia discloses dissimilarities in proliferation, cytokine production, gene expression, and so on, and thus makes rodent microglial data unsuitable when one intends to predict human microglia dynamics [16]. Many other challenges do also exist to study microglia for drug discovery strategies [17-19]. Therefore, robust, and scalable cellular models of human microglia should be constructed that facilitate an understanding of the physiology of microglia for drug development. Employing realistic human microglia is a vital step towards this essential aim.

Mathematical modelling and computer simulation are powerful tools whereby we can analyse complex biological systems, particularly, neural phenomena involved in brain dysfunction. The main goal of this thesis is to develop mathematical models in order to bridge the gap between the lack of human microglial data and information about the physiology of microglia for the key agents that regulate microglial functions such as ATP-triggered P2X, ADP-meditated $P2Y_{12}$ calcium signalling transduction and actin polymerisation towards microglial motility. Cytosolic calcium dynamics are vital to microglia function. To the best of our knowledge, this is the first mathematical model of microglia to accurately capture the complicated behaviour of Ca^{2+} dynamics observed in experimental studies while also describing the electrophysiology of microglia aimed at their directed motility. There is no unified and comprehensive model for the underlying dynamics in microglia starting from ligand binding to P2X/P2Y receptors to IP_3 generation and finally leading to the Ca^{2+} uptake from extracellular space and the Ca^{2+} release from the ER into the cytosol. Most of the models herein are developed from first principles with a few state variables for simplicity. Recent studies promote the urge for understanding microglia because microglial functions play critical roles in both normal physiological and pathological dynamics of the brain. Understanding the interactions and different shapes of transients of the model state variables will aid in the study of the link between purinergic receptors and brain dysfunction in terms of calcium behaviour. The biophysical models

developed in this thesis will improve our quantitative understanding of microglial physiology.

1.2 Thesis Contribution and Organisation

This thesis encompasses a considerable body of research into the biophysical modelling of human microglia. Several mathematical models are developed to investigate microglial functions in terms of receptor activation, Ca^{2+} dynamics and actin polymerisation with the aim of broadening our knowledge of microglial cells with respect to physiology and transient dynamics. Therefore, the proposed computational framework provides a strong foundation that can guide biological experimentation in human microglia. To date, there have not been any mathematical models developed using human microglial data. Not only have some human experiments failed to characterise some aspects of microglial receptor activation, but also there is an extremely scarce set of data to develop new biophysical models. This thesis targets these two major challenges through mathematical modelling. This research has been published in two peer-reviewed journals, which are cited in Appendix C. Consequently, the key contributions presented in this thesis are as follows:

- Development of two novel P2X biophysical models for capturing human $P2X_7$ and $P2X_4$ currents inspired by the Hodgkin and Huxley (HH) formalism for action potentials in neurons [20] and involving exponential dependency of kinetic rates on the agonist in the model.
- Development of a comprehensive mathematical model for human P2X-mediated plasma membrane electrophysiology (i.e., sodium and calcium dynamics, and membrane potential) in microglia comprising of $P2X_4$ and $P2X_7$ receptors, the Na^+/Ca^{2+} exchanger (NCX), Ca^{2+} extrusion by the plasma membrane Ca^{2+} ATPase (PMCA), and Ca^{2+} and Na^+ leak channels.
- Development of a new IP_3R (IP_3 receptor) model along with a complete biophysical model to capture human microglial Ca^{2+} data from activation of $P2Y_{12}$ receptor to Ca^{2+} release from intracellular stores consisting of SERCA (sarco/endoplasmic reticulum Ca^{2+}-ATPase) and Ca^{2+} leak channel.

- A new hypothesis that calcium influx via P2YR and P2XR can explain the experimentally observed twin peaks in the pAkt profile. It is realised by developing a novel PI3K/Akt model to support the hypothesis.
- Insightful predictions, and comprehensive simulation and quantitative results for P2X-mediated plasma membrane electrophysiology and calcium dynamics, P2Y-mediated calcium dynamics, and P2-mediated actin dynamics in human microglia.

The contributions of this work are discussed within Chapters 4 to 6 in detail. A brief organisation of the chapters is given below.

A review of the physiology of glial cells is first presented in Chapter 2. Microglia biology is elaborated with its complex signal transduction pathway that is made up of several purinergic receptors, pumps and exchangers. A greater detail is given for the biological components that contribute to the elevation of intercellular Ca^{2+} and Akt, which are also key to controlling the directed motility of microglia. Then, a concise and effective introduction to the mathematical modelling of biological processes is discussed on top of the concept of the law of mass action in Chapter 3, which lays the foundation for the majority of models proposed in subsequent chapters. In the next chapters, the key part of model development for the rest of the thesis is described. Parameter estimation plays an essential role in the success of the developed models in order to capture experimental data. A class of optimisation algorithms used in later chapters is described. Finally, in three separate subsections, the demonstration of related works sheds light on the contributions of this thesis for which new, simpler biophysical models are developed for the complicated machinery of human microglia biology. This section also reviews previous models for ionotropic and metabotropic receptors, and PI3K/Akt pathway.

In Chapter 4, the full development of all mathematical models for this thesis is presented. A detailed mathematical model is built for the dynamics of human P2XRs in microglia. Subsequently, experimental whole-cell currents are used to derive the P2X-mediated electrophysiology of human microglia (i.e., sodium and calcium, dynamics, and membrane potential). The complex P2Y-mediated signalling in microglia required several mathematical models. Because the $P2Y_{12}$ receptor leads not only to a dramatic elevation of intracellular Ca^{2+} but is also a major driver of the PI3K pathway, mathematical models are

developed to study these players in microglia functions. A complete biophysical model comprising of a novel model of IP_3 receptor coupled to other cytosolic components is constructed whose response is capable of getting fitted to human Ca^{2+} microglial data. In this chapter, it is hypothesised that ADP-meditated $P2Y_{12}$ and P2X Ca^{2+} influxes aggerate to give the overall $[Ca^{2+}]_i$ in the microglia soma. Subsequently, a new PI3/AKT model is built that uses this time dependant $[Ca^{2+}]_i$ profile to activate the PI3K/pAkt via CaMKII (Ca^{2+}/calmodulin-dependent protein kinase II). This model will support that calcium influx via P2YR and P2XR can justify the experimentally observed twin peaks in the pAkt data. This chapter also discusses challenges faced in parameter estimation of the models, in which smart decisions are made so that the underlying function optimiser can find the best fit to an ensemble of model parameters. Finally, a full curve fitting algorithm extending an evolutionary strategy is provided that will be used to fit all models in this thesis to complex experimental data sets.

The results and predictions of the models come in two separate chapters, i.e., Chapter 5 and Chapter 6.

While Chapter 5 deals with simulation results of P2X-mediated electrophysiology in human microglia, Chapter 6 focuses on the directed motility of microglia. Firstly, predictions reveal new quantitative insights into P2XRs on how they regulate ionic concentrations in terms of physiological interactions and transient responses. The entire model shows that intricate intracellular ion dynamics (kink-like transient responses) arise from the coupled interaction between $P2X_4$ and $P2X_7$ receptors, the Na^+/Ca^{2+} exchanger (NCX), Ca^{2+} extrusion by the plasma membrane Ca^{2+} ATPase (PMCA), and Ca^{2+} and Na^+ leak channels. Secondly, simulated results provide interesting quantitative insights into different ADP-mediated P2Y calcium and Akt dynamics. For example, cytosolic calcium only spreads in the cytosol in a short amount of time for long ADP pulse exposures, and for certain ADP amplitudes, pAkt behaves intricately by generating kink-like transient responses.

Finally, conclusions of the thesis are made in Chapter 7 followed by a discussion on the contributions carried out throughout it. Possible extensions to the models presented within the thesis that can take more functional aspects of microglia into account are provided for further study by including diverse channels and receptors, which were not

modelled during this project. Future work on the mathematical foundation grounded in this thesis can shed deeper light on predicting *in vivo* physiology of microglial cells.

Chapter 2. Literature Review – A Physiological Perspective

2.1 Introduction

Following the advancement of our understanding of brain structure, other types of brain cells have contributed to further perception of the functional organisation of the brain, one of which is microglia. Microglial cells are macrophages of the brain and show highly motile behaviour even in the normal brain. They own a great deal of transudation pathways that make them capable of communicating with neurons and macroglial cells. This becomes possible through a rich network of membrane-coupled and intercellular receptors (such as neurotransmitter receptors), channels, pumps and exchangers. Upon activation of microglia (which is for example detected by a complex cascade of neurotransmitters and chemical signals), they are converted into activated microglial cells and migrate to the site of an injury or a pathogen. The dynamics of microglia can be modified through intercellular or extracellular biochemical events and signalling agents. An essential process upon activation of microglia which is regulated in a very complex manner is the release of cytosolic Ca^{2+} and the uptake of extracellular Ca^{2+}. Neuronal networks can be potentially regulated by microglia as a function of their complex interactions. Consequently, it has become necessary to develop experimental and theoretical techniques for studying microglial functions. Microglia are an example of highly complex biological systems due to their enormous underlying pathways and non-linear components. In this chapter, the relevant aspects of the physiology of glial cells with a strong emphasis on biological processes underpinning microglia used in this thesis are described, because the understanding of several physiological features of microglia in terms of receptor and channel activity is essential to analyse and develop mathematical models in the next chapters of this thesis.

2.2 Physiology of Glial Cells

The brain contains two main classifications of cells, namely, neurons and glia [3]. Neurons are electrically excitable and form an extremely complicated cellular network for many different tasks like perception and memory. In contrast, glial cells are special-purpose, non-electrically excitable, cells in the CNS that provide a wide range of supportive functions such as myelin formation, protection of neural space and homeostasis. CNS glia consist of astrocytes, oligodendrocytes, Schwann cells and microglia [21] as shown in Figure 2.1.

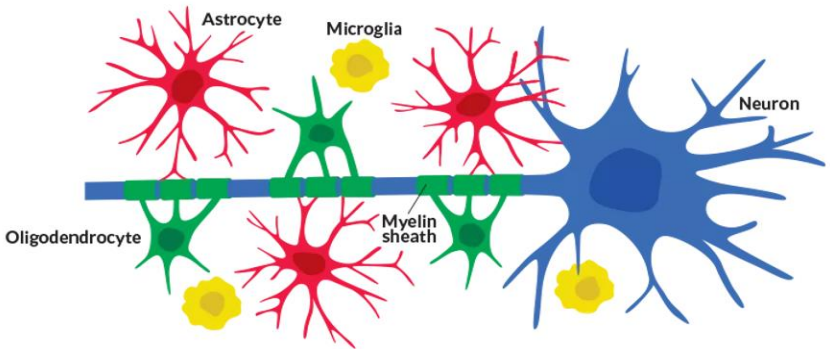

Figure 2.1. Different types of cells in the CNS [3].

2.3 Astrocytes, Oligodendrocytes and Schwann Cells

There are two main subclasses of astrocytes, protoplasmic and fibrous, due to their morphological differences and locations in the CNS [1]. The former is found in grey matter and by their many branches envelops synapses. The latter is present in white matter and has many fibre-style processes to envelop nodes of Ranvier. Studies have shown that both astrocyte types establish substantial junctions with blood vessels. Astrocytes are well-organised and spread over the entire CNS (brain and spinal cord) in a uniform manner such that no region of the CNS lacks them. They perform many functions from development to adulthood. In development, astrocytes essentially participate in the movement of forming axons. They have extensive contact with blood vessels by several bidirectional paths that allow them to regulate blood flow in CNS spots locally. Changes are mediated by

astrocytes in the blood flow during neural activities. Since astrocyte branches enwrap synapses, they are important agents in persevering the extracellular fluid content and homeostasis of synaptic communications. Astrocytes are also known to modulate synaptic transmission by releasing macromolecules such as glutamate, ATP and gamma-aminobutyric acid (GABA). There is evidence that astrocytes provide significant energy to the CNS through metabolism and are involved in supporting the blood-brain barrier. Astrocytes express sodium (Na^+), potassium (K^+) and Ca^{2+} channels which are voltage-gated and cause inward currents, however, these glial cells do not generate action potentials. It is known that increasing the intracellular Ca^{2+} in astrocytes plays a significant role in astrocyte-astrocyte/neuron communication. Astrocytes also benefit from a broad spectrum of receptors and neurotransmitters. Both ionotropic (iGluR, P2X and GABA) and metabotropic (mGluR, P2Y, cytokines, endothelin) receptors are expressed in astrocytes, and the activation of these receptors results in the stimulation of complicated pathways in order to process information as a result of the interaction with other neural and non-neural cells. For example, GluR is divided into three distinct subtypes, including, NMDA (N-methyl-D-aspartate), KA (kainite) and AMPA (α-amino-3-hydroxy-5-methyl-4-isoxazolepropionic acid). AMPA and KA receptors pass sodium and potassium whereas NMDA receptors are highly permeable to Ca^{2+}. mGluR evokes intracellular second messenger expressed by $InsP_3$ (inositol 1,4,5-trisphosphate)/DAG (diacylglycerol) and cAMP (cyclic adenosine monophosphate) cascades. The influx of Ca^{2+} into the cell finally generates Ca^{2+} waves that control the activity of a set of neural cells [22-26]. Two different pathways have been identified that regulate this type of communication. The first is direct communication through gap junctions between two adjacent neural cells. The second mediator depends on membrane receptors like NDMA that are activated by the release of gliotransmitters. Because astrocytes actively participate in brain homeostasis, they require a central focus for studying neurodegenerative diseases like Alzheimer's.

Oligodendrocytes are a type of glia and are responsible for insulating axons from the extracellular environment by enwrapping them (by producing myelin) and therefore speeding up the transmission of electrical signals between presynaptic and postsynaptic neurons [3]. They usually have a few numbers of processes for enwrapping axons and a rounded soma, and their size depends on their type. They can find and respond to neuronal

activity through purinergic signalling. This signalling modulates their differentiation and development. $P2X_{1-4}$, $P2X_7$, $P2Y_{1-2}$, $P2Y_4$, $P2Y_{12-13}$ and four types of adenosine receptors are expressed in oligodendrocytes [27]. There is a wealth of evidence that purinergic signalling is key to myelin production, therefore, extensive research is needed to characterise the operation of all of these receptors.

Schwann cells comprised of four types are found in the peripheral nervous system (PNS) and mostly provide myelin production (like oligodendrocytes). They are twisted around axons of sensory and motor neurons in the PNS. They also take part in forming nodes of Ranvier. Schwann cells express $P2X_7$, $P2Y_1$ and $P2Y_2$ receptors [28].

2.4 Microglia

Motile microglial cells play a key defensive role in CNS through their role in clearing pathogens and active maintenance of neurons and synapses. Recently, microglia have attracted wide attention from international researchers, because of their great importance in health, ageing and neurodegenerative diseases like Alzheimer's and Parkinson's [29-31]. Microglia go through a variety of morphological configurations reliant on defensive needs and location. The structure of microglia can be expressed from ramified to amoeboid cells [4, 5]. In healthy brain tissue at rest, microglia have fine processes with a small cell body, which is called a ramified morphology. Microglia are drastically different from classical macrophages in this perspective. Any perturbation in the brain homeostasis, which signifies danger in the CNS, quickly creates strong changes in their shape. Microglia in this state are referred to as activated microglia.

In this section, we focus on the role of microglial functions. There is a multitude of channels and receptors that contribute to the normal physiological function of microglia. We will also discuss how microglia exploit the underlying messaging system to discover a broad range of dangers in pathological conditions and accordingly deal with them.

2.4.1 Biological Functions

Microglia perform diverse functions in normal and pathological conditions [14]. Evidence shows that microglial cells are highly involved in neural cell death in the human CNS, in which dying cells are phagocytised. Microglia benefit from sensing the healthy brain to monitor any unusual neural change. *In vivo* imaging has shown that microglia extend and retract their processes contingently in the brain tissue. During acute brain injury, astrocytes and other damaged cells secrete ATP by which microglial cells are activated quickly.

Microglia function as both a source and a target of cytokines [32]. Cytokines trigger microglia when neurons are injured. Microglia also produce proinflammatory cytokines such as TNF-α, IL-1 and IL-6. Although these cytokines are typically meant to prevent more damage to different parts of the CNS tissue, they may appear as a toxin to neurons and glial cells. Increasing evidence shows that the repeated activation of microglia can result in the emergence or complication of neurodegenerative disorders.

Dysfunction of the normal physiology of microglial cells is found in autism disorder, Alzheimer's, and other brain-related diseases [33, 34]. Microglia are known to have a major role in neuropathic pain through P2X receptors and GABA transmission. Dysfunction or perturbation of the normal function of microglia can give rise to developmental disorders. Synaptic striping (a process through which microglia specifically eliminate synapses from damaged neurons) is known to be regulated by microglia. This mechanism may have implications for neuroprotective consequences. There is also evidence that microglia and synapses interact with each other [35]. Recent studies promote the urge to understand microglia because microglial functions play critical roles in both normal physiological and pathological dynamics of the brain [4, 31].

2.4.2 Morphological Configuration & Pathways

Figure 2.2 demonstrates several different functional cycles of microglia. Microglial cells are extremely sensitive to the molecular composition of their environment. Moreover, they roam their specific area by moving their long processes around, which is called surveillance or resting state. After a danger is encountered (e.g., damaged cells and apoptotic cells), the

cell begins directed motility by extending its processes towards it as the other processes are retracted. In some cases, the soma is also conveyed along with the process. The locomotion emerges from a complex chain of molecular events that results in the reformation of the actin cytoskeleton. When a microglial cell locates a danger by amoeboid movement, it will be activated and phagocytose (swallow) a dying cell or a pathogen. Microglia are members of the macrophage family that engulf and digest cellular debris, cancer cells, microbes, and so forth. Activated microglia can also proliferate, and release cytokines such as TNF-α (Tumour Necrosis Factor) and IL-1β (Interleukin) that in turn influence different cellular mechanisms [14].

While much more research is needed to understand the cellular events that are involved in microglia activation, we know much less about the time after. Therefore, the main goal of the present PhD thesis is on providing mathematical/computational tools and theories in order to understand microglia functions after activation. The models can shed light on the cellular events that will arise from a complex response system assembled by different channels, receptors, and messenger systems.

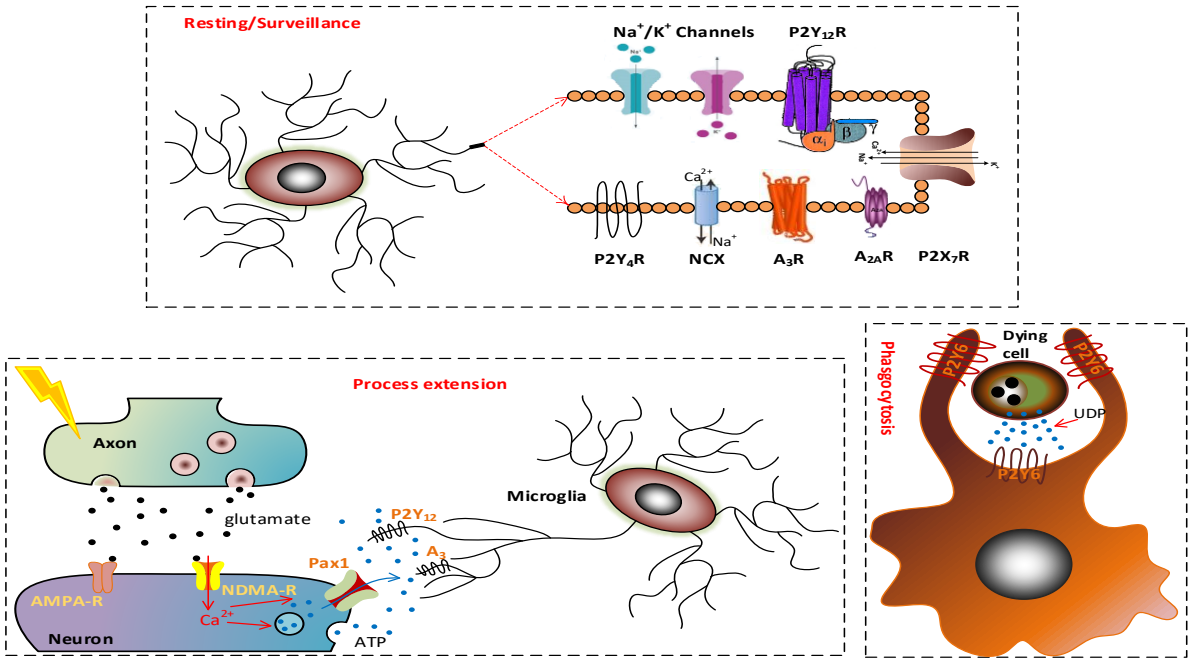

Figure 2.2. Different functional cycles [5] of microglia during the discovery of danger in the brain using purinergic signalling.

2.4.3 Environmental Sensing (Ion Receptors and Channels)

In this section, microglial receptors and ion channels, which will be mathematically investigated throughout this thesis, are surveyed. Ion channels are permeable plasma membrane proteins that control the bidirectional flow of ions in nervous cells. They do a wide range of tasks in the CNS from generating action potentials in neurons to message passing between different neural cells. Two important classes of ion channels are ionotropic and metabotropic [36]. Ionotropic receptors are ligand-gated ion channels which conduct ion flows such as Na^+, K^+ and Ca^{2+} and have at least three protein subunits [37]. When a neuron or glia emits a messenger, it binds to the target receptor(s) and activates the channel(s).

Metabotropic receptors, also known as G protein-coupled receptors, are activated by first-messenger neurotransmitters (e.g., ATP and ADP) on their external ligands and in turn they trigger a cascade of intracellular pathways by second messengers such as InsP3 and cAMP [38]. These receptors elicit long-time-scale cellular phenomena as compared to ionotropic channels. Second messengers trigger intracellular physiological responses by activating cytosolic receptors and pathways—as an example, the release of Ca^{2+} from the endoplasmic reticulum through an IP_3-sensitive channel. The understanding of these channels is a very demanding issue in molecular biology and neuroscience and therefore mathematical modelling of these receptors is used to determine their function more completely.

2.4.4 P2X Receptors

P2XRs have trimeric configurations and are known to be membrane proteins. Studies have shown that the biophysical properties of their subunits involve tasks such as binding to ATP, ion permeation and trafficking through the membrane. P2X receptors are also widely spread throughout neurons and glia at the protein level and mRNA in humans. One of the important elements to control the level of Ca^{2+} in intracellular space is ATP by directly activating purinergic P2X receptors in eukaryotic cells [12]. After binding ATP, a channel pore opens for calcium and other ions to traverse across the cell.

$P2X_7$ activation also releases proinflammatory cytokines, as microglial $P2X_7$ receptors have likewise been associated with neuropathic pain. Single-channel recordings are used to study the regions of P2X receptors in ion permeation and characterise their dynamics. $P2X_7$ receptors are stimulated by ATP and result in an extrusion of K^+ followed by IL1 secretion [39].

$P2X_4$ is a purinergic receptor that is also activated by ATP and is involved in the motility of microglia, particularly, its inhibition prevents chemotaxis [6] where it also regulates the phosphatidylinositol-3-kinase (PI3K)/Akt pathway. Chemotaxis is performed by the generation and degradation of phosphatidylinositol (3,4,5)-trisphosphate [PtdIns(3,4,5)P_3] on the microglia membrane. It forms a key role in actin polymerisation and directional microglial motility. PI3K pathway modulates [PtdIns(3,4,5)P_3] and cytoskeletal rearrangements [40]. $P2X_4$ activation not only increases the level of cytosolic Ca^{2+} but also the Src kinase is evoked which is furthermore a modulator of the PI3K pathway [41]. The $P2X_4$ receptor, which is stimulated at micromolar ranges of ATP, induces a steeply peaked current and desensitizes within seconds. Millimolar ATP triggers $P2X_7$ receptors and keeps a high amount of current during the ATP application as compared to $P2X_4$ receptors.

2.4.5 $P2Y_{12}$ Receptor

G-protein coupled receptors like $P2Y_{12}$, which reside on cell surfaces, in microglia are important signalling mechanisms to transfer information into the cell by activating a complicated secondary messenger system. Therefore, this can lead to changes in the conformation of ion channels inside intracellular or membrane-coupled regions. The $P2Y_{12}$ receptor is a protein specific to microglia [42] and is actively responsible for directed motility and chemotaxis. Its activation gives rise to Ca^{2+} release from intracellular stores, particularly, the endoplasmic reticulum (ER), which instead stimulates CRAC channels for an influx of Ca^{2+} to compensate the intracellular stores and KCa3.1 channel for an efflux of potassium [18]. $P2Y_{12}$ activation gives rise to modulating a two-pore channel for an efflux of potassium [4, 43].

2.4.6 Adenosine Receptors (P1)

P1 adenosine receptors are a family of G protein-coupled receptors that are activated by adenosine, which is an organic compound produced by the hydrolysis of ATP [44]. Four types of these receptors have been identified and expressed in microglia, including, A_1, A_{2A}, A_{2B} and A_3 [45-48]. There is a body of evidence that A_1, A_{2A}, and A3 are involved in the migration of microglia, where the A_3 and A_{2A} receptors are respectively responsible for process extension and process retraction [46, 49, 50].

2.4.7 Ion Channels

A more realistic characterisation of microglia activation, in order to study its electrophysiology, will be established by including those channels that contribute to changes in the membrane potential. Research works have discovered distinct types of potassium channels in microglia involved in functions such as proliferation and ramification, including, inward and delayed rectifiers, and voltage-dependent/independent calcium-activated K^+ channels. Furthermore, microglia include other anionic and cationic channels such as H^+, Na^+, Ca^{2+} release-activated Ca^{2+} and voltage-dependent/independent Cl^- [14].

Voltage-gated ion channels, which are ion-specific and a subtype of transmembrane proteins, are elicited by the membrane potential in which an ion channel is formed. The conformation of the channel is modulated by the membrane potential for opening or closing the channel. These channels consist of several subunits and are deployed such that ions can travel through a central pore due to electrochemical gradients. Voltage-gated variants of Na^+, K^+ and Ca^{2+} have been determined in microglial cells [51, 52]. Changes in ion concentrations evoke the opening and closing of a voltage-gated channel.

Microglia also express sodium-calcium exchanger (NCX) and plasma membrane Ca^{2+} ATPase (PMCA). The NCX is an antiporter that electrochemically exchanges three Na^+ ions for one Ca^{2+} ion across the cell membrane. It works in two different operational modes (forward or reverse) depending on the membrane potential and the transmembrane Na^+ and Ca^{2+} gradients, in non-excitable neural cells like microglia. The PMCA pump is a high-

affinity protein that preserves low cytosolic Ca^{2+} profiles by consuming ATP macromolecules and extruding one Ca^{2+} from inside microglia against its ionic gradient.

2.4.8 ER Regions and Store-Operated Ca^{2+} Entry

ER and mitochondria are two sources of intracellular Ca^{2+} stores in microglia. The free ER Ca^{2+} concentration is about 0.8mM and the SERCA pump is responsible to maintain it at a high level [14]. Depletion of the ER-Ca^{2+} stores, following the activation of membrane receptors that are coupled to PIP_2/IP_3 generation, activates store-operated Ca^{2+} entry (SOCE). SOCE is elicited following the activation of microglial P2Y receptors by Ca^{2+} release from internal calcium stores [50]. SOCE in human microglia is also modulated by membrane potential through P2X receptors in low levels of ATP [51]. SOCE plays a central role in tandem with $P2Y_{12}$ and P2X receptors in microglial calcium signalling and cytosolic calcium homeostasis.

2.4.9 PI3K/Akt Pathway

Microglia respond to chemoattractant gradient by sensing their microenvironment and aligning their internal signalling polarity which is established by PI3K (phosphoinositide-3-kinase) signalling cascade. Activation of the PI3K pathway elevates phosphatidylinositol 3,4,5-triphosphate (PIP_3), which triggers F-actin polymerisation at the leading edge of microglial cells. The complex events during $P2Y_{12}$R activation directly regulate the PI3K pathway, which subsequently results in the activation of Akt (Protein kinase B (PKB), a.k.a., Akt). Akt promotes process extension and chemotaxis by reorganisation of the actin cytoskeleton [19]. Therefore, PI3K signalling is known as a key ingredient for regulating microglia chemotaxis. Directed microglial motility through Akt requires a complex family of intracellular signalling pathways over which multi-component signalling, feedbacks and cross-talks take place. A multi-step process controls Akt activation by involving PI3K. Furthermore, several studies have shown that the metabotropic receptors A_{2A} and A_3 are involved in migration and process contraction, respectively. A_3 is influential on PI3K and PLC and Akt akin to $P2Y_{12}$ [22].

2.4.10 Ca^{2+}-Dependent Protein Kinase II (CaMKII)

CaMKII is a protein kinase regulated by the levels of Ca^{2+}. This enzyme takes part in many cellular pathways and also mediates Akt activation [53]. Dysfunction of this protein can lead to a wide range of brain malfunctions [54]. This enzyme can auto-phosphorylate when there is enough Ca^{2+}. In larger amounts of Ca^{2+}, this enzyme can persistently phosphorylate itself leading to the activation of CaMKII. This enzyme will play a central role in the cooperative regulation of the PI3K/Akt signalling by P2 receptors in the biophysical models presented in this thesis.

2.4.11 Available Experimental Data

The neuroscience community has published a number of experimental data, mostly on rodents, by which macroscopic aspects of microglial activation are studied. In this section, we give a brief overview of the existing experiments for microglia in the scope of this thesis, some of which are exploited to build mathematical models over the next chapters.

To understand how $P2X_4R$ is regulated, a series of patch-clamp experiments were performed in [55, 56] to characterise the time course of responses as a function of ATP. It was found that both the resting and activated rat microglia respond to the stimulation of this receptor. In [57], the properties of the plasma membrane $P2X_7$ receptor are studied in mouse microglia with a similar whole-cell patch-clamp configuration. Another work investigated the effect of ATP in the regulation of TNF-α secretion, where several data sets for P2X-mediated Ca^{2+} transients are also provided for rat microglial cell lines [58]. Although it showed that cytosolic Ca^{2+} is induced by ATP and a variety of different responses was observed upon P2XR activation, the work was unable to conclude which types of P2X receptors were in charge of generating the intricate responses. Patch-clamp electrophysiology in [59] was used to investigate the behaviour of ATP-gated $P2X_7$ receptor in human microglia. However, this work failed to modulate $P2X_4R$ in culture.

A very limited number of published papers study features of Ca^{2+} dynamics that are mediated by P2Y receptors in microglia. Three families of P2Y receptors (i.e., $P2Y_2$, $P2Y_6$ and $P2Y_{12}$ types) are confirmed and characterised in [60] by showing different patterns of

Ca^{2+} in low and high concentrations of P2Y ligands for rat microglial cells, where P2X receptors are selectively inhibited by their corresponding antagonist. *In situ* experiments validated the $P2Y_{12}R$ expression in response to ADP and Ca^{2+} released from internal stores for activated human microglia [61].

In [62], the authors showed the $P2Y_{12}R$ activation essentially gives rise to Akt phosphorylation and mediated chemotaxis in rat microglia. The experiment disclosed that the underlying PLC pathway is required and activated through ADP exposure and regulates Akt activation and PI3K pathway. The work concluded that Akt is actively responsible for regulating microglial chemotaxis.

2.5 Discussion

Microglial cells play different roles in the brain that are regulated by a complex network of receptors, channels, and pathways. A literature review was carried out within this chapter to provide a deeper understanding of the key agents in this network. More importantly, it was found that studying P2 signalling, which significantly regulates actin polymerisation, is a key step to gaining insights into microglial functions. Several other types of channels and receptors such as adenosine receptors and SOCE exist in microglia and in some cases experimental data is still lacking. This thesis limits its research scope only to P2X and P2Y-mediated signalling in microglia. Existing research provides a few raw data sets and does not explain how intercellular and membrane-coupled components of microglia interact in concert. Most of these works show macroscopic properties of microglial activation by basic electrophysiological measurements; therefore, important questions remain unanswered that mainly deal with explaining the microscopic aspect of these cells. The few existing human experimental models are very limited in providing insights into how human microglia are modulated. This thesis attempts to address these (and other) challenges in subsequent chapters. For example, it will be shown that the $P2X_7$ receptor must work in tandem with $P2X_4R$ to represent the experimental Ca^{2+} data in [58].

2.6 Summary

Neuroglia are important cells that provide supportive functions to the nervous system and are actively involved in brain diseases. Microglia play many important functions in healthy brain tissue. They survey their micro-environment continuously and are activated upon detecting dangers in the brain. A wide range of ionotropic and metabotropic receptors along with ion channels form complex machinery for coordinating the activated microglial cells, among which $P2X_4$, $P2X_7$ and $P2Y_{12}$ receptors drive significant dynamics of microglial functions such as intracellular Ca^{2+} transients and reorganisation of the actin cytoskeleton in providing directed motility. Understanding the microglia' electrophysiology can disclose its functions and provide therapeutic insights for different types of brain dysfunction because microglia are heavily involved in many tasks closely relevant to maintaining a healthy brain and providing support for the nervous system.

Chapter 3. Literature Review – A Mathematical Modelling Perspective

3.1 Introduction

Mathematical models are indispensable tools in formulating theories and are used extensively in neuroscience. Mathematical modelling can capture the complex dynamics of cells and provide insights and predictions about different aspects of cell functions. To understand complex microglial machinery, it is not adequate to characterise their individual molecules, receptors, or components. The relationship between microglia-specific molecules and signalling transduction pathways must be known. This is more important when it comes to learning how brain diseases such as Alzheimer's work in tandem with the activation of microglia.

Over recent years, the neuroscience community has made progress to provide some essential experimental data that can be harnessed by mathematical modelling to interpret results and predict new insights into brain dysfunction. Complex modulatory processes can be studied using mathematical modelling which can then be used to guide researchers in the deployment of new experimental setups. Analysis of complex pathophysiological processes in the immune nervous system could be proved as an essential tool for bridging the link between brain disease and microglia. A deeper knowledge of interactions in microglial involvement with brain diseases is key to discovering therapeutic strategies. Moreover, mathematical models can unravel unexpected properties of complex biochemical systems.

3.2 Mathematical Cell Modelling

3.2.1 Introduction

Mathematical models can be investigated through computer simulations. Models of biochemical systems are very complicated to deal with analytically, therefore, numerical solutions of a system of ordinary differential equations (ODEs) using the computational

power of computers can be used to predict the response of the state variables in question to different system conditions. Mathematical techniques are usually used to model signalling pathways and their kinetics that form the central control system of a wide range of cells. Cell membranes are a major transmission site for these pathways into the cell, where specific genes are activated, and different modelling techniques can capture the dynamic event-based nature of these processes. Two major techniques exist to model the kinematic mechanics of receptors [63, 64]: the reaction-network paradigm and the reaction-diffusion paradigm.

3.2.2 Basics

A few natural laws can be employed to model all the tasks that a cell does. The underlying rules are remarkably simple, but they can be applied to a complex network of basic biochemical reactions, which involve many substances and species, to mathematically describe the behaviour of these highly complex systems. Chemical reactions happen reliant on the law of mass action. It states that the rate of a chemical reaction, in which species such as ions and macromolecules interact to make new chemicals, corresponds to the product of the molar concentration of the involved reactants [65]. For example, a bidirectional reaction is described as:

$$\mathrm{A} + \mathrm{B} \underset{\mathrm{k}_2}{\overset{\mathrm{k}_1}{\rightleftarrows}} \mathrm{C} \tag{3.1}$$

where k_1 and k_2 are called forward/backward rate constants of the reaction, and A, B and C are reactants. The backward reaction is only shown when the forward reaction is not dominant. The ODE describing species A can be written as:

$$\frac{d[A]}{dt} = k_2[C] - k_1[A][B] \tag{3.2}$$

In this process, quantity A is converted into product C by the forward path and recovered by the backward path. Therefore, the rate at which [A] changes is proportional to the difference between [C] and the product of [A] and [B]. The law of mass action is not always convenient for complicated processes, but rather they take place as complex machinery using consecutive elementary reactions.

In the method of reaction-network paradigm, we assume uniform ion concentrations and benefit from an assortment of rate equations (the law of mass action) in chemical reactions, curve fitting and patch-clamp techniques [66, 67]. Typically, the modeller arranges a series of patch-clamp experiments to gather adequate data for the receptor in question to be modelled (for example, measuring time-domain current curves or a current-voltage characteristic curve). The experimenter can build a model based on information collected from the literature about the functional behaviour of the receptor represented as signalling pathways. The mathematical model of a pathway is a kind of Markov model that can be quantified by writing a set of first-order ODEs in conformance to the rate equations of the governing biochemical reactions. Curve fitting is employed to construct closed-form functions for experimental data by interpolation techniques and find parameters of the ODE system via either linear or nonlinear regression.

3.2.3 Markov Modelling

In computational biology, continuous-time Markov models with discrete states provide the ubiquitous basis for capturing the behaviour of transporters and ion channels [65, 68]. A Markov model, which is a kind of stochastic mathematical model, is usually employed to model systems that vary randomly. Markov models suppose that the model state only relies on its current state and is independent of the states in the past. Hodgkin and Huxley (HH) in 1952 developed one of the first Markov models to quantify the description of the action potential [20], which is still widely used and can be extended to many other voltage-gated currents. Although they were not aware of the underlying ionic dynamics, decades later it was proved that their assumption of individual ion channels, whereby the HH model was based, was correct. The model originally assumed transitions between two rapid conducting and nonconducting Markov states. Subsequently, these models have turned out to be very useful for interpreting experimental data and are often used to conduct experiments by assessing specific model predictions. Proteins can reside theoretically in an unlimited number of states; however, it turns out that a finite set of states can effectively represent their conformational changes.

Markov models can almost describe all biochemical processes fundamental to neurophysiology. A major use of Markov models in this thesis is to construct novel mathematical models for specific ion channels and receptors in microglia. Then, the individual channel models are integrated to study how the complex machinery drives microglial electrophysiology in terms of ion concentrations, membrane potential, protein activity, etc.

Before diving into realistic, complex Markov models, let's consider a simple two-state model below (which is also a basis for the HH formalism [20])

$$\mathrm{C} \underset{\beta(\mathrm{V})}{\overset{\alpha(V)}{\rightleftarrows}} \mathrm{O} \tag{3.3}$$

In this two-state system, C and O stand for *closed* and *open* states (note that they are actually probabilities), where kinetic rates are variable and depend on the membrane potential *V*. Two other assumptions on this somewhat simple model are made: (1) the channel has no memory, and (2) transitions in both directions happen immediately. The second assumption is the basic property of Markov models. The ODE equations associated with this reaction utilising the law of mass action can be written as

$$\frac{dC}{dt} = \beta(\mathrm{V})O - \alpha(V)C \tag{3.4}$$

$$\frac{dO}{dt} = \alpha(V)C - \beta(\mathrm{V})O \tag{3.5}$$

The model must conserve all the species because it is a closed system; therefore, it is expected that the sum of these two probabilities becomes unity, namely, $C + O = 1$. Subsequently, a single equation can express the open state by substitution as below

$$\frac{dO}{dt} = \alpha(V)(1 - O) - \beta(\mathrm{V})O \tag{3.6}$$

The remaining task is to determine the relationship between the kinetic rates α and β and the membrane potential. HH carried out an extensive set of patch-clamp experiments whereby the cell membrane was kept at different voltages, each of which showed distinct current profiles. Then, they approximated nicely fitted exponential functions to the resultant set of recorded rate coefficients with respect to voltage. In Chapter 4, we will employ rather a similar approach to build a model for P2X receptors in microglial cells.

Detailed Markov models of activation of ion channels and receptors usually consider four (or more) gating aspects [66, 69]:

- **Activation/binding:** receptor activation follows three main phases in which the agonist first binds the receptor, then this effect transduces down to the channel (coupling), and finally the ion channel opens (gating).
- **Deactivation/unbinding:** receptors require to be turned off after activation. Receptor inactivation can be affected by several agents such as ligand removal. Ligand binding is a reversible process where the ligand can dissociate from the receptor. Ligands can also degrade because they eventually turn into (are recycled) their original forming substances.
- **Sensitisation**: it is an increased activity of the receptor in the time course of the same ligand.
- **Desensitisation**: receptor desensitisation is a decreased responsiveness of a receptor which is encountered after prolonged exposure to an agonist. This is a feature common to most membrane receptors. As a result, desensitisation reduces the fraction of open channels, and for example, the current mediated by the receptor decreases.

Overall, receptor dynamics are vital to understanding the individual kinetics of receptors, but most important when multiple receptors are integrated to give insight into the time course of a sequence of ionic events within the cell. In the rest of this section, we elaborate on two examples of how Markov modelling is used in practice. The basic ideas given in this section will be used throughout Chapter 4.

As the first example, we model the AMPA receptor which is an ionotropic receptor that is activated by glutamate. Mechanistically, each AMPA receptor has four binding sites for a ligand. It has been shown that when at least two sites are occupied the receptor begins its activity. When the receptor is open, it can undergo rapid desensitisation and so the current diminishes. Figure 3.1 shows a typical AMPA-provoked current and its mathematical model using the Markov approach adapted from [70].

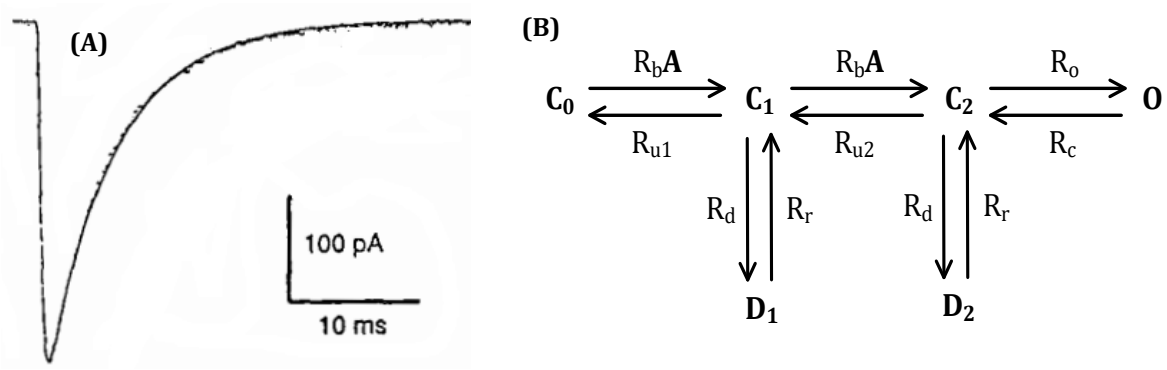

Figure 3.1. (A) AMPA-mediated current [70]. (B) A Markov-based model of the AMPA receptor [70].

Here, the inactivated receptor C_0 binds the agonist A and forms the conformation C_1. Following these stages, another ligand molecule binds the receptor and leads to the opening of the receptor. R_b and R_u are binding and unbinding rates, respectively. Receptor desensitisation is modelled by two states D_1 and D_2, which can desensitise C_1 and C_2 with the rate R_d. Note that the transition $D \xrightarrow{R_r} C$ models receptor resensitisation with the rate R_r. One can write a system of ODE for the topology in Figure 3.1(B), and after solving it the AMPA current is expressed by

$$I_{AMPA} = g_{AMPA} O (V_m - E_{AMPA}) \tag{3.7}$$

where g_{AMPA} is the maximal conductance of the receptor, O is the probability at which the receptor is open, V_m is the membrane potential, and E_{AMPA} is the reversal potential (the membrane voltage when the net flow of ions becomes zero) calculated by the Nernst equation (see [69] or Section 4.2.2). The model can be fitted to Figure 3.1(B) using an optimisation algorithm in order to estimate the model parameters (for example, see [71] or Sections 3.2.5 and 4.4).

In our second example, the focus is devoted to Michaelis-Menten kinetics, which explains enzyme-catalysed reactions [72]. This mathematical model supposes a rapidly reversible production of a complex after an enzyme and its substrate bind together. Assume

that E, S, ES and P respectively denote an enzyme, its substrates, an enzyme-substrate complex, and a product. This system can be expressed as

$$\mathrm{E} + \mathrm{S} \underset{k_r}{\overset{k_f}{\rightleftharpoons}} \mathrm{ES} \xrightarrow{k_{\mathrm{cat}}} \mathrm{E} + \mathrm{P} \tag{3.8}$$

where k_f, k_r, and k_{cat} are forward, reverse, and catalytic rate constants, respectively. In this reaction, the substrate reversibly binds to the enzyme and then the product is created after the formation of the enzyme-substrate complex. By directly applying the law of mass action, the equations governing this model can be written as

$$\frac{d[S]}{dt} = k_r[ES] - k_f[E][S] \tag{3.9}$$

$$\frac{d[E]}{dt} = (k_r + k_{cat})[ES] - k_f[E][S] \tag{3.10}$$

$$\frac{d[ES]}{dt} = k_f[E][S] - (k_r + k_{cat})[ES] \tag{3.11}$$

$$\frac{d[P]}{dt} = k_{cat}[ES] \tag{3.12}$$

3.2.4 Existing Models Used in the Thesis

In this section, several biophysical models that will be directly used throughout Chapter 4 are discussed.

3.2.4.1 Sodium Calcium Exchanger (NCX)

The NCX is an ion antiporter which resides on the cell surface. It electrochemically brings one Ca^{2+} out of the cell and three Na^{+} ions into the cell normally across the cell membrane [73]. This mode of working is called forward as compared to certain conditions at which it functions in a reverse mode to bring Ca^{2+} ions into the cell. Therefore, this exchanger works in two different operational modes (forward or reverse) depending on V_m and the transmembrane Na^{+} and Ca^{2+} gradients [74]. The normal function of NCX is critical for the regulation of Na^{+} and Ca^{2+} homeostasis whereby the Ca^{2+} concentration is kept low inside

the cell. The reversed NCX can result in intricate ionic responses (e.g., see Section 5.2.3) and is also involved in generating cardiac action potentials [75]. In addition, many physiological events depend on the NCX protein because of these complex interdependencies. The Na^+ and Ca^{2+} current densities of the exchanger in [74] are defined by

$$J_{NaNCX} = \bar{J}_{NCX}\left(\frac{[Na_i^+]}{[Na_x^+]}\right)^3 e^{\frac{\gamma FV_m}{RT}} - \frac{[\mathrm{Ca}^{2+}]_i}{[Ca_x^{2+}]} e^{\frac{(\gamma-1)FV_m}{RT}} \tag{3.13}$$

$$J_{CaNCX} = -\frac{2}{3}J_{NaNCX} \tag{3.14}$$

where $\bar{J}_{NCX}$ and γ are the NCX conductance and partition number, respectively [74]. The current density J_{NaNCX} has been obtained through a membrane-coupled protein that assumes both Na^+ and Ca^{2+} are abundant in the extracellular space. The current density therefore depends on the intracellular and extracellular concentrations of ions and V_m. The exchanger has a low affinity and binds moderately to Ca^{2+}. It transmits both Na^+ and Ca^{2+} ions quickly because of its high capacity and consequently the NCX is mainly responsible for removing Ca^{2+} that flows into the cytosol. It should be noted that in this thesis we have not included an allosteric factor into Eq. 3.13 (similar to [76, 77]) mainly due to a lack of experimental evidence that shows if NCX is allosterically regulated by intracellular Ca^{2+} in microglia. Therefore, in the future, if experimental data supports an allosteric effect on NCX for microglial cells then more complex models (eg., see [78] in cardiac cells) can be used and fitted to recorded data instead of Eqs. (3.13-3.14).

3.2.4.2 Plasma Membrane Ca^{2+} ATPase (PMCA)

The PMCA pump is a high-affinity protein that preserves low cytosolic Ca^{2+} profiles by consuming ATP macromolecules and extrudes Ca^{2+} from inside the microglia against its ionic gradient. The Ca^{2+} current density through PMCA is modelled using Michaelis-Menten kinetics [79], and is formulated by

$$J_{PMCA} = \bar{J}_{PMCA} \frac{[\mathrm{Ca}^{2+}]_i^{\,n}}{[\mathrm{Ca}^{2+}]_i^{\,n} + K_{PMCA}{}^{n}} \tag{3.15}$$

where $\bar{J}_{PMCA}$ and K_{PMCA} are the maximum current density and pump affinity respectively. n is the order of the Hill function. This pump removes Ca^{2+} and is also used to maintain Ca^{2+} at low levels in our model.

3.2.4.3 G Protein-Coupled Receptor (GPCR) Model

When ADP binds to $P2Y_{12}$ receptor on the microglia membrane surface, a simple model can capture the amount of IP_3 release [80] as follows

$$\frac{dIP_3^{ADP}}{dt} = r_{ip3} ADP - \frac{IP_3^{ADP}}{\tau_{ip3}} \tag{3.16}$$

where IP_3^{ADP} is the quantity of IP_3 produced by PLC pathway within the cytoplasm, r_{ip3} is the generation rate of IP_3^{ADP}.

Hydrolysis of membrane lipid phosphatidylinositol 4, 5–bisphosphate (PIP_2) through phosphoinositide-specific phospholipase C (PLC) can increase the level of IP_3. This behaviour and its activation rate that is also modulated by $[\mathrm{Ca}^{2+}]_i$ can be modelled through PLC_δ signalling [81] as below

$$PLC_\delta = PLC'_\delta Hill\left(\mathrm{Ca}^{2+}_{\mathrm{P2Y}}, 2, K_{PLC_\delta}\right) \tag{3.17}$$

where one can model the maximum IP_3 production [81] which depends on PLC_δ by

$$PLC'_\delta = \frac{\overline{PLC'_\delta}}{1 + \frac{IP_3}{K_\delta}} \tag{3.18}$$

and K_δ stands for inhibition constant of the PLC_δ activity. The standard Hill function has been used in Eq. (3.17) formulated by

$$Hill(x, n, K) \equiv \frac{x^n}{x^n + K^n} \tag{3.19}$$

where *x* is the substance in question. *n* and *K* are respectively the Hill coefficient (indicative of steepness of the response curve) and the midpoint of the Hill function at which the magnitude of the function becomes one-half.

IP_3 is mainly degraded through phosphorylation into inositol 1, 3, 4, 5-tetrakisphosphate (IP_4) which is catalysed by IP_3 3-kinase (3K) and regulated by $[Ca^{2+}]_i$ in a complicated manner. It is also dephosphorylated by inositol polyphosphate 5-phosphatase (5P). The degradation rate of IP_3 by these two events [81] can be modelled as

$$IP_3^{5p} \approx \bar{r}_{5p} IP_3 \tag{3.20}$$

$$IP_3^{3K} = \bar{v}_{3K} Hill(Ca_{P2Y}^{2+}, 4, K_D) Hill(IP_3, 1, K_3) \tag{3.21}$$

where $\bar{r}_{5p}$ is the rate of IP_3 degradation associated with IP_3^{5p}. $\bar{v}_{3K}$ is the maximum rate of degradation by IP_3^{3K}. K_D and K_3 are short for Ca_i^{2+} and IP_3 affinities of IP_3^{3K} for the two Hill functions.

Finally, the rate at which IP_3 changes with respect to time is described in terms of an ODE given by

$$\frac{dIP_3}{dt} = IP_3^{ADP} + PLC_\delta - IP_3^{5p} - IP_3^{3k} \tag{3.22}$$

3.2.4.4 CaMKII Model

The mathematical model used for CaMKII is adopted from [82] as given by Eqs. (3.23) to (3.25). It makes use of a single ODE whose first term has a complex relationship with Ca^{2+}

(as a hill function). Note that $[Ca_i^{2+}]_{tot}$ as modelled in the previous section is a contribution of both P2X and P2Y receptors to the cytosolic Ca^{2+} concentration. When $[Ca_i^{2+}]_{tot}$ does not change (i.e., $[Ca_i^{2+}]_{tot}$ is zero), all state variables of the equations stay at their rest values (here at a value of zero).

$$CaMK_{bound} = CaMK_0 \times \left(1 - CaMK_{trap}\right) \times Hill\left([Ca_i^{2+}]_{tot}, 1, K_{m,CaM}\right) \tag{3.23}$$

$$CaMK_{active} = CaMK_{bound} + CaMK_{trap} \tag{3.24}$$

$$\frac{dCaMK_{trap}}{dt} = \alpha_{CaMK} \times CaMK_{bound} \times CaMK_{active} - \beta_{CaMK} \times CaMK_{trap} \tag{3.25}$$

where $CaMK_{active}$, $CaMK_{bound}$ and $CaMK_{trap}$ are the fractions of active, bound and trapped CaMKII subunits, $CaMK_0$ is this fraction at equilibrium, and α_{CaMK} and β_{CaMK} are two rate constants [82].

3.2.5 Parameter Estimation

A system of ODEs can be obtained by applying a collection of simple elementary reactions like Eq. (4.1) for complex processes and has been widely used for mathematical modelling of biochemical, and dynamical systems. Parameters of the model, i.e., kinetic rate constants, along with initial conditions of a system of ODEs can describe the dynamics of the biochemical model. A significant task in such a modelling approach is to estimate the model parameters through experimental data, many of which are usually unknown. Complex models have many state variables that are either difficult to measure experimentally or have a dependency on other undiscovered pathways (the non-identifiability issue). Such ODE systems are extremely nonlinear, and their observable data contains noise.

Classical curve fitting approaches such as the Gauss-Newton algorithm exploit optimisation principles to minimise a cost function in terms of solving a non-linear least squares problem whereby a curve or mathematical function is constructed to have the best

fit to a set of data points. In order to use this algorithm for parameter estimation of a system of ODEs, all the system observables (state variables) must have corresponding data gathered from experiments. In a complex biological system or even for different cells, a few observables can be determined empirically, therefore, traditional curve fitting methods fail. Additionally, some local minimums or maximums, which are related to rate constants, can be found by ordinary optimisation techniques in large biochemical systems. Alternative optimisation algorithms have been proposed to address the above problems. This section briefly reviews two important techniques for such problems.

Evolution strategies (ES) are among those algorithms that are stochastic and derivation-free. ES is often used for numerically optimising a non-linear/non-convex minimisation problem. Evolutionary methods are inspired by natural selection that imitates biological evolution. The population of separate solutions are iteratively updated. Individuals are selected from the current population and nominated as parents for the next iteration for generating new children. The algorithm is repeated until an optimal solution is reached for the population. A multivariable normal distribution is used to sample new optimal solutions. Covariance Matrix Adaptation Evolution Strategy (CMA-ES) is a type of ES [83] that updates the covariance matrix of the distribution. Iteration over the covariance matrix results in second-order learning of the underlying cost function. CMA-ES can be seamlessly used to find appropriate values of the model parameters in terms of rate constants.

Another popular technique in contrast to ES is Markov Chain Monte Carlo (MCMC) [84]. MCMC takes advantage of a Bayesian inference criterion to approximate the complete posterior distribution of the model parameters. Combining Markov Chains and Monte Carlo provides sampling high-order probability distributions randomly that is based on the problematic dependency among many samples. It is made possible by constructing a Markov chain that contains those Monte Carlo samples. A Markov process predicts the future state of a model that is dependent only on the current state. Samples are created by a probability density probability of a function as a continuous random variable. An integral as a function of those variables is computed over the samples.

3.3 Related Work

In this section, a brief discussion of previous work relevant to microglia research is given that can better highlight the contributions made throughout this thesis in three directions: P2X/P2Y-mediated calcium signalling and PI3K/Akt signalling cascade involved in directed motility.

Microglia are involved in many neurodegenerative disorders, such as Parkinson's and Alzheimer's diseases, and are massively activated during brain injuries such as stroke [31, 85, 86]. There are many known hurdles to overcome in the study of microglia for drug discovery strategies [17-19]. Robust and scalable cellular models have to be built that help understand the biology of microglia for drug development.

Mathematical biology is an overarching enabling technology that bridges the gap between reported experiments and unexplored cell behaviours. Many mathematical models have been proposed for modelling the PI3K/Akt pathway, ionotropic and metabotropic receptors, and IP_3R channel of other types of cells other than microglia.

3.3.1 P2X-mediated Calcium Signalling in Human Microglia

Recent studies highlight the importance of increasing our understanding of microglia physiology since their functions play critical roles in both normal physiological and pathological dynamics of the brain. There is a need to develop reliable human cellular models to investigate the biology of microglia aimed at understanding the influence of purinergic signalling in brain dysfunction to provide novel drug discovery targets. To the best of our knowledge, there is no theoretical work and no successful experimental study of the simultaneous activation of several ionotropic receptors in human microglia. There is substantial evidence that both $P2X_4$ and $P2X_7$ receptors are expressed in microglial cells [14, 87, 88]. However, human microglia experiments failed to isolate functional $P2X_4$ receptors [59], therefore a modelling approach will deepen our understanding of the contribution of each of these receptors to Ca^{2+} and Na^{+} dynamics within human microglia. Moreover, our model predictions for human microglia and the comparison of the kink-like behaviour of their responses confirm that intricate intracellular Ca^{2+} transients arise from a

complex cooperative activation of both P2XRs and other ionic extruders and pumps. It is anticipated that the future *in situ* and *in vivo* experiments relative to human microglia research on P2XRs will be able to validate the theoretical findings supported by faithful biological inferences made in this thesis. There is a high demand to develop reliable cellular human models where microglia can be studied to further our understanding of neuroglia interactions.

Biophysically different Markov models have been widely used to describe the binding sites of P2XRs in whole-cell current configurations with eight or more state variables. For example, as shown in Figure 3.2, a typical rat $P2X_7$ current in HEK293 cells has a biphasic characteristic and eight states with ten parameters are necessary to capture the current as detailed in [66]. For different levels of the agonist, the receptor shows drastically different patterns ranging from monophasic, slowly developing currents (for ATP less than 1mM) to biphasic (for ATP greater or equal to 1mM).

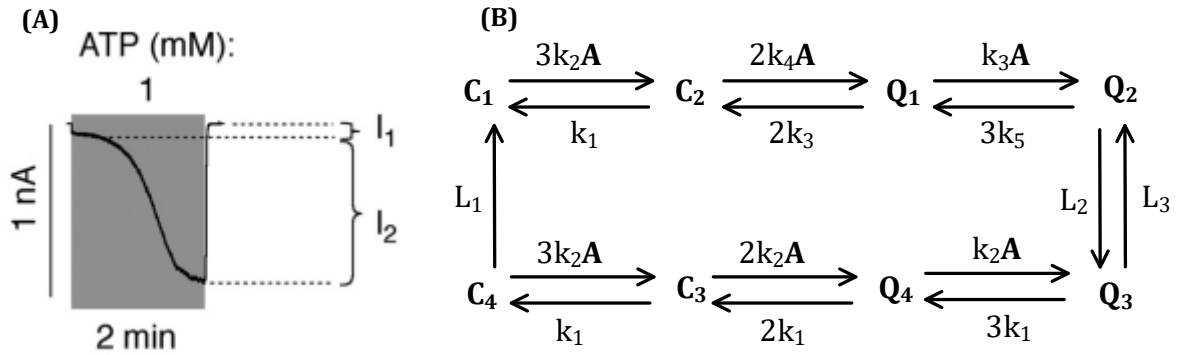

Figure 3.2. (A) A typical biphasic current of rat $P2X_7R$ in HEK293 cells [66]. I_1 is the initial rise in current which is accompanied with a growing current (I_2). (B). Markov-model of the $P2X_7$ receptor [66]. C_i and Q_i stand for closed and open channel pores, where the subscript i represents either sensitised (1 and 2) or unsensitised (3 and 4). The total current is expressed as $I_{P2X7} = g_{12}(Q_1 + Q_2)(V_m - E_{P2X7}) + g_{34}(Q_3 + Q_4)(V_m - E_{P2X7})$, where g is the maximal conductance of the receptor, V_m is the membrane potential, and E_{P2X7} is the reversal potential.

The authors in [89] developed a computational model for Ca^{2+} signalling by using experimental data for rat and mouse microglia mentioned in Section 2.4.11. They first built separate models for $P2X_4$ and $P2X_7$ receptors utilising rodent whole-cell patch-clamp

current data and reusing existing P2X Markov models. Then, the model was combined with a mass-action model of the PMCA channel and other components to reproduce the Ca^{2+} experimental data reported in [58]. Although the research refitted the entire model to Ca^{2+} data, the model was unable to reproduce the major properties of the experimental data. Additionally, they did not include Na^{+} signalling and membrane potential. On the other hand, the authors claim that the results provide quantitative insights into microglial function. What is obvious from the mismatch between the model predictions and experimental data makes the model an unsuitable candidate to explain P2X-mediated electrophysiology of microglia even in rodent microglial cells. In [90], several other issues with this model are reported as well.

In this thesis, a new mathematical model is developed for P2X receptors that avoids the complex Markov approach [91-93]. It is worth noting that eight-state Markov models [66, 89], such as Figure 3.2(b), were not successful in providing a good fit to the human data in [59, 94] (see [90]). Therefore, we developed a minimal model for hP2XRs as given in Section 4.2.

3.3.2 P2Y-mediated Calcium Signalling in Rat/Human Microglia

It is challenging to build computationally inexpensive biophysical models that can produce realistic behaviour of metabotropic ion channels. Modelling the IP_3 receptor has a long history due to its complexity. IP_3R is fundamental to many features in calcium responses. Their opening characteristics are significantly governed by ligands like IP_3 and Ca^{2+}. An extra hurdle for the mathematical modelling of IP_3R arises from the fact that they have three subclasses. This channel has usually a homotetrameric structure consisting of four subunits that are used to construct models. IP_3R can also be found in heterotetrameric structure, although we know very little about its kinetics in this mode. One of the pioneering IP_3R models was introduced in [95], which involves channel activation and deactivation via Ca^{2+}. It is an eight-state, complex Markov model with sixteen parameters and assumes the receptor is made up of three individual subunits. Each subunit has two Ca^{2+} binding sites for activation and inactivation, and an IP_3 binding site. The receptor can be sequentially in one state. The model was reduced further by a number of simplifying

assumptions [96]. Because IP_3 and Ca^{2+} bind quickly to their activating binding sites, it can be assumed that the dynamics of the states regarding these sites are negligible and thus the receptor works in a quasi-steady state. This results in a simplified Hodgkin–Huxley-style model with two-state variables. A type-2 complex IP_3 receptor model using ten Markov states with seventeen parameters in [97] is presented because other models do not comply with experimental data of the transient responses of the receptor.

In [67, 98], the author investigates the role of secondary messenger systems in single cells through $P2Y_2$ receptor by constructing a complex reaction network for the G-protein cascade, which is activated by uridine triphosphate (UTP). The model takes transient responses of calcium, IP_3 and PIP_2 into consideration. Equilibrium assumptions are incorporated into the model to derive simpler equations, but it may not be applied to other cells because every cell has different transient responses. A mathematical model that has been derived from an 8-state Markov model is reused for the IP_3 channel proposed by Li and Rinzel [96].

In [99], a mathematical model for P2-mediated calcium signalling in sensory neurons is developed by using basic kinetic reactions. The model, adopted from [100-103], includes signalling pathways regulating receptor activity and the G-protein cascade yields transient cytosolic calcium changes by reusing a legacy model of the IP_3 receptor [97]. The model is extremely complicated because of 90 species, 252 unknown parameters and 93 biochemical reactions. Because of the complexity, the authors used 9 different data sets for different cells to estimate the model parameters but were unable to find unique parameters. A multi-objective optimisation algorithm (Ensemble Simulated Annealing) was instead employed to find a near-optimal parameters that may be closer to the real ones.

Due to the complexity of the existing models and the lack of adequate experimental research in microglia, we develop a simple IP_3R model for the first time that is capable of capturing published microglial Ca^{2+} human data as explained in Section 4.3.1, where the existing models were not successful to provide good fits to experimental data (as also discussed in [90]).

3.3.3 PI3K/Akt-mediated Signalling Pathways in Microglia

Directed microglial motility through Akt requires a complex family of intracellular signalling pathways over which multi-component signalling, feedbacks and cross-talks take place. Therefore, developing a mathematical model for such a complex pathway to advance our understanding of the underlying biophysical mechanisms of kinase regulation is challenging. Parameter estimation of this biological model also becomes difficult because of the large number of model parameters that must be estimated. Consequently, several complex computational models of the PI3K/Akt signalling pathway have been reported in pursuit of finding therapeutic targets for various diseases [104-108]. The complexity of these models arises from a high number of ordinary differential equations (ODEs) and model parameters.

To the best of our knowledge, there is no accurate model to capture the intricate behaviour of this pathway in microglia, which is presented in Section 4.3.4 through a novel biophysical model. We make a hypothesis to explain how pAkt is regulated by observing the experimentally published data due to the simultaneous cooperation of P2 receptors. Then, the proposed model is shown that can capture the intricate behaviour.

3.3.4 Other General Microglia-Specific Mathematical Models

There is a scarce body of research into the mathematical modelling of microglial cells. We briefly refer to them in this section.

The work in [109] develops a mass-action cytokine model by assembling different pathways from the literature to study mainly TNFα signalling in rat microglia. Then, the complex model is fitted to experimental data for LPS-activated microglia. The model was also analysed to show the interaction of model components with each other.

In [110], a partial differential equation (PDE) model was built for microglial motion towards an implanted electrode in the rat brain, which aims at studying the purinergic pathway involved. It benefited from the established fact that long electrical stimulation of the brain causes the microglial cells to gather around the affected area. The authors also

analysed the influence of the electrode size on the model parameters which are governed by the underlying adenosine and purinergic receptors.

Stroke is a dominant cause of death all over the world and involves acute neural inflammation followed by a massive activation of microglial cells. Activated microglia can take two distinct phenotypes, namely, M1 and M2. In [111], a non-linear ODE model was formulated for representing the change of these two microglial phenotypes during ischemic stroke. The model also captured the interaction between this phenotypic change and cytokine secretion such as TNFα.

3.4 Discussion

Mathematical modelling and computer simulation are powerful tools by which we can analyse complex biological systems, particularly, neural phenomena involved in brain dysfunction. Three fundamental tools have been used for decades to model cellular-level processes since the inception of computational biology, including the law of mass action, biochemical networks and dynamical Markov models. They form the cornerstone of this thesis because they have tremendously helped move the field forward and are particularly ubiquitous among the computational neuroscience community.

Microglial functions are complex because many components and pathways upon the activation of microglia cooperatively contribute to the measurable macroscopic features of their signalling responses such as intracellular Ca^{2+}. This complexity calls for a comprehensive biophysical model whose objective is to include many factors that affect the electrophysiology of microglia. This complexity is also reflected in the experimental data sets cited in Section 2.4.11. For instance, Ca^{2+} responses mediated by P2X receptors in [58] and phosphorylated Akt profile mediated by $P2Y_{12}$ receptor reported in [62] have dual humps. Neither of these works tried to explain from where this intricacy originates. It is worth noting that experimental study of such behaviours is very time-consuming and difficult because it is unclear which cellular components raise them. It is thus ideal first to pinpoint the original cause by mathematical modelling and hypothesis making, and then to arrange experiments in the lab to prove the theory. Consequently, an important aspect of this thesis aims to give biophysical origins for such features by leveraging mathematical

tools and computer simulations. In the meantime, the work presented in this thesis mainly focuses on human models of microglial cells which will be very useful to advance the field of glial cells as there are major obstacles to examining this line of human cells as justified in this chapter.

The development of a virtual model of human microglia is fundamental to our understanding of how glial events interact with each other for a holistic physiological response. This thesis lay the groundwork towards this grander goal in neuroscience as microglia perform principally functional roles involved in a broad family of brain diseases surveyed by Chapter 2. To achieve these goals, we reviewed the existing models in this chapter. Markov-based modelling constitutes the basis by which we will develop three novel Markov models for $P2X_7$, $P2X_4$ and IP_3 receptors in human microglia within Chapter 4 by extending the HH formalism also discussed in this chapter. We also elaborated on several existing models, including NCX, PMCA, GPCR and CaMKII, that are directly used in Chapter 4 because microglial literature is still lacking experimental data for these building blocks of our models. Basic mass-action biochemical network modelling is also exploited in Chapter 4 to build a biophysical model of the PI3K/Akt pathway for which a review of the existing body of work is essential for understanding the components given within our model. New model development requires a scalable, efficient optimisation strategy to find the parameters of the system in question. This makes the modelling process more challenging. The requirement of using non-classical optimisation algorithms stems from the complexity and inability of providing data for numerous observables of a Markov model or biochemical reaction network of biological systems. To facilitate the model development, an overview of parameter estimation frameworks was provided in this chapter in order to rationalise why we are using evolutionary algorithms in constructing all the models in Chapter 4.

3.5 Summary

Mathematical modelling of glial cells coupled with computer simulation can establish a link between their dynamics and brain dysfunction. Mathematical models in systems biology are usually founded upon biochemical reactions, where a system of ODEs is inferred to express

a sound translation of the seen patterns in experiments into a computational model. Parameter estimation of such large networks that are often made up of hundred chemicals is indeed challenging, although the lack of measuring all of them makes this process more complex. A series of computational models whose goals are relevant to this project was exemplified and their limitations were also discussed. These show a theoretical basis of mathematical modelling is necessary to increase our understanding of microglial dynamics when a large number of receptors and ion channels are simultaneously activated. Such a complicated model must be built incrementally and its effect on the electrophysiology of microglia should be investigated component by component.

Also, it was identified that there is still no modelling effort towards human microglia that can help us understand how they work upon activation. Additionally, due to several obstacles to studying microglial cells, it is an essential need to build mathematical models to pave the way for experimental research. An in-depth review of all mathematical modelling approaches relevant to this work was given, including, the law of mass action, biochemical networks and receptor modelling utilising Markov models. Related works aligning with this thesis were also explained which is helpful to highlight the contributions made throughout Chapters 4 to 6.

This thesis builds a comprehensive computational framework to study P2-mediated signalling and its effects on PI3K/Akt behaviour with a major emphasis on human microglia as much as human datasets are available. This is achieved by developing novel biophysical sub-models for $hP2X_7$, $hP2X_4$ and hIP_3 receptors coupled with existing NCX, PMCA, GPCR and CaMKII sub-models in order to construct an integrated PI3K/Akt model by a new hypothesis by which we will explain how P2X and P2Y receptors crosstalk to regulate actin polymerisation intricately.

Chapter 4. Mathematical Models

4.1 Introduction

Biophysical models allow researchers to get more information and even knowledge from raw experimental data. Given that a biophysical model is usually developed from principal assumptions using fundamental laws as illustrated in Chapter 3, available experimental data are fitted to the model at the first stage. In Section 2.4.11, experimentally published data in microglial research was discussed. This chapter thereafter develops all biophysical models utilising this set of experimental data for the thesis by which different aspects of the activation of microglial cells are mathematically formalised. Firstly, two novel Markov models are proposed that take the biophysical features of $P2X_7R$ and $P2X_4R$ currents into account where it is shown that there should be exponential dependencies between model parameters and agonist concentration (this assumption is made in agreement with the HH model). Then, a new model of P2X-mediated Ca^{2+} signalling is constructed that in fact integrates the P2X models with a fluid compartmental approach in accordance with the HH formalism. Here, three sub-models given as explicit equations in Section 3.2.4, including PMCA and NCX, are reused to predict three pivotal electrophysiological quantities, namely, Na^+ and Ca^{2+} concentrations, and membrane potential. The modelling of leak channels with the separation of the Na^+ and Ca^{2+} currents is also described. Secondly, we build a complete model from when the microglial $hP2Y_{12}$ receptor is activated and intracellular Ca^{2+} is released from the ER region. For this purpose, the GPCR model from Section 3.2.4 is coupled to a newly developed IP_3R model in this chapter with a simple model of the SERCA channel. Thirdly, we construct a comprehensive biophysical model of the PI3K/Akt pathway which is activated by the CaMKII model given in Section 3.2.4. The CaMKII model is regulated by a total cytosolic Ca^{2+} that is assumed to be a combination of individual Ca^{2+} components stemming from P2X and P2Y receptors. Finally, the general algorithm for curve fitting of the models is presented. Note that further discussion on this process is provided in two subsequent chapters.

4.2 P2X-mediated Signalling in Microglia

The high-level view of the model is shown in Figure 4.1, which includes P2XRs, the Na^+/Ca^{2+} exchanger (NCX) and the plasma membrane Ca^{2+} ATPase (PMCA) along with Ca^{2+} and Na^+ leakage channels. Microglia ionic homeostasis is both dynamic and complex, involving a myriad of receptors, effectors, proteins, channels, and processes. The proposed model for intracellular Ca^{2+} and Na^+ dynamics mediated by P2XRs is based on the mass action kinetics formulated by four state variables to capture the complex mechanics of both $P2X_4$ and $P2X_7$ receptors when activated by ATP.

Increases in extracellular ATP levels (e.g., from damaged neurons) are detected by microglia and they extend their processes towards the elevated ATP levels through chemotaxis principles [14]. Figure 4.1(a) summarises the key intracellular signalling transduction pathways for this purpose. The two P2XRs bind ATP and change their conformation, allowing a rapid rise in intracellular $[Ca^{2+}]$ through Ca^{2+} influx. Published experimental data for hP2XRs obtained from both native preparations and expression systems were employed throughout the model development [59, 94]. While no data for $hP2X_4R$ currently exists for microglia, this thesis uses functional $hP2X_4$ data recorded in expression systems [94]. Given the overexpression of receptor protein and the magnitude of expression system currents, the data has been scaled to better align with native microglial P2X currents [56] (in the order of pA).

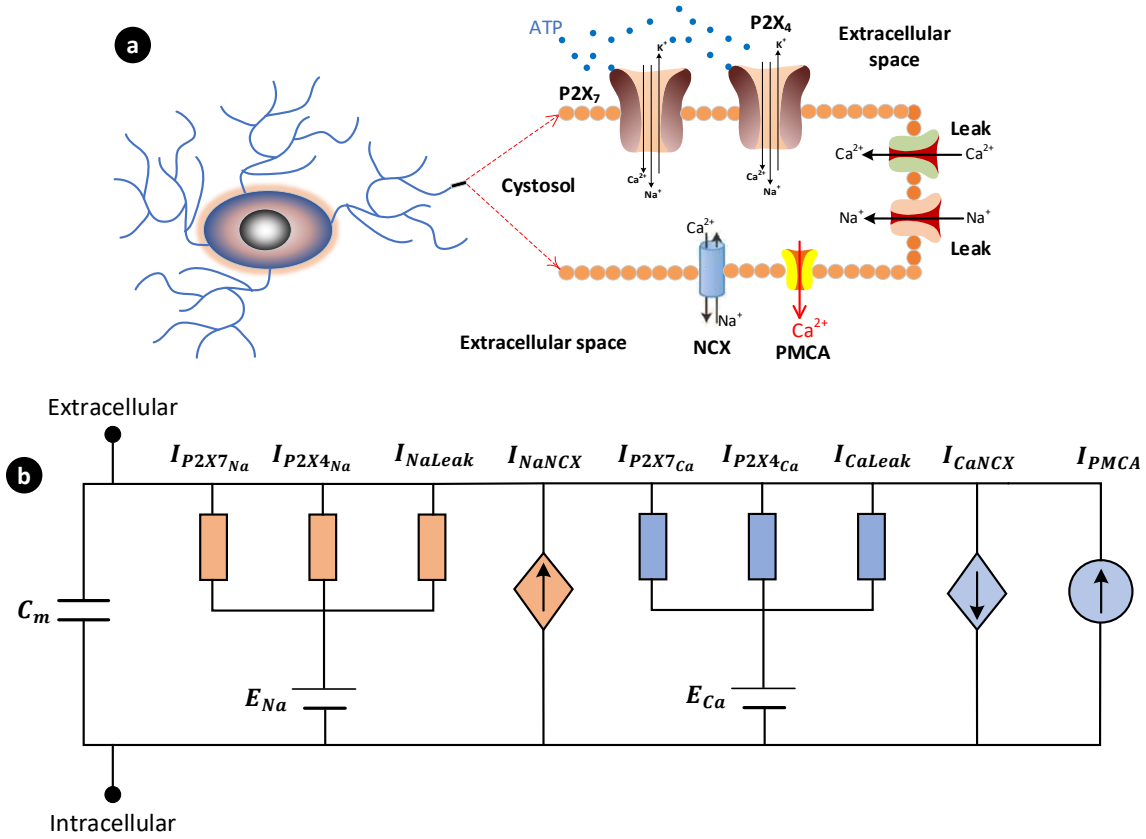

Figure 4.1. P2X-mediated Ca^{2+} signalling network developed for this study involved in microglial directed motility. The computational model is classified into two parts: (a) fluid compartmental model and (b) microglial membrane electrophysiology. The PMCA (I_{PMCA}) and NCX (in the forward mode) remove cytosolic Ca^{2+}. Cellular electrophysiology is included in our model by involving the transmembrane currents that underpin P2X-mediated Ca^{2+} signalling and microglia homeostasis. The P2X currents for each receptor are modelled as two individual Na^+ and Ca^{2+} conductance-based channels ($I_{P2X_{Na}}$ and $I_{P2X_{Ca}}$), and both Na^+ and Ca^{2+} leak channels (I_{NaLeak} and I_{CaLeak}) are also included in the proposed model; the dynamic behaviour of the reversal potentials (E_{Na} and E_{Ca}) are also taken into account. The current through the NCX channel is divided into a sodium current (I_{NaNCX}) and a calcium current (I_{CaNCX}).

4.2.1 P2X Kinetic Models

P2XRs work as cation channels and open after ATP binding. They allow a rapid entrance of Na^+ and Ca^{2+} ions into the cell with an efflux of potassium (K^+): note that it has recently been proposed that K^+ efflux is primarily driven by the TWIK2 K^+ channel [112] but this mechanism needs further investigation, and therefore K^+ dynamics are not considered in this thesis. Both $P2X_4$ and $P2X_7$ receptors in microglia share similar trimeric configurations but display different biophysical properties. $P2X_7$ receptors in the CNS can activate the proliferation of microglia, modulate cell phagocytosis and induce TNF-α production [14]. The $P2X_4$ receptor, which is stimulated at micromolar ranges of ATP, induces an instantaneous peak current and desensitises within seconds [56, 94]. In contrast, millimolar ATP triggers $P2X_7$ receptors and maintains ionic currents during the ATP application [59].

Figure 4.2 shows a biochemical kinetic reaction network that underpins both the $hP2X_7$ and $hP2X_4$ receptors comprised of only four state variables (where C, S, D and O states represent *closed*, *sensitised*, *desensitised* and *open* respectively). By introducing variable exponential kinetic rates into this four-variable model (inspired by other similar biophysical models [113]) in a similar way to the approach of Hodgkin and Huxley (HH) [20], the model becomes a less complex realisation as compared to the existing P2X Markov models, which is capable of capturing the major gating properties of microglial P2XRs. Note that the HH model benefits from voltage-gated exponential rates while the model herein makes use of agonist-gated exponential rates. The gating properties of the P2X channels are broken into four individual stages, including activation (S → O) and sensitisation (C → S and D → S), desensitisation (S → D and then D → C) and deactivation (from O to S and then C, or S to D and then to C). Activation is a quick process, which happens after the receptor is sensitized by the agonist, during which the channel opens resulting in increasing inwardly cationic currents following ATP exposure which slowly tends towards a plateau. This levelling-off of the current is referred to as desensitisation and following this, the current amplitude rapidly goes to zero when the ATP becomes unbound. $P2X_4$ and $P2X_7$ receptors differ in terms of the kinetic machinery actively involved in their sensitivity and function.

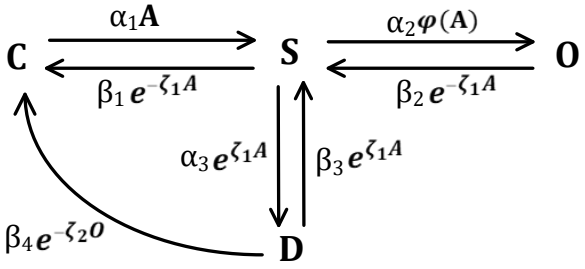

Figure 4.2. The biophysical P2X model: a compact kinetic reaction network which captures the total current induced by microglial hP2X$_7$ or hP2X$_4$ receptors dependant on the model parameters used. The agonist is denoted by the letter *A*. The states C, S, D and O respectively stand for *closed*, *sensitised*, *desensitised* and *open*. The α and β parameters are the forward and reverse kinetic rates. The rate function φ between S and O is expressed as $\varphi(\mathrm{A}) = A$ for the hP2X$_7$ receptor and $\varphi(\mathrm{A}) = e^{\zeta_1 A}$ for the hP2X$_4$ receptor.

In the model, ATP application is potentiated though two forward rate constants of α_1 and α_2. All backward rates were chosen as variable functions in agreement with the HH approach as discussed in [90]. Experimental data show that the desensitisation of P2XRs depends on the level of ATP exposure [66, 94, 114, 115]. Therefore, the gating transition between $\mathrm{S} \rightleftarrows \mathrm{D}$ has an exponential dependency on the agonist. This prevents the desensitisation pathway from disappearing in the model during agonist removal since the exponential terms became unity upon ATP removal. Note that both exponential rates are present on both sides of the transitions guaranteeing the amount of reduction in the S state in the forward reaction returns to the D state in a proportionally balanced fashion. The model conserves all the species because it is a closed system; therefore, the sum of all state variables at any time is equal to unity and the system state variables return to their initial resting state after stimulation has ceased. An important function of a biophysical model is that the state of the system should go back to its resting state because the model can be activated again without affecting the model predictions, for example, when this model is simulated using a repeated application of ATP. In order to ensure this property, the transition between D and C states through a negative exponential rate function makes an extra path that enables D to be depleted to C when O becomes very small (note that the path

is activated because the exponential function goes to its high value when O significantly decreases).

The microglial hP2X$_7$ receptor currents [59] have two significant phases: A to B (activation/sensitisation/desensitisation) and B to C (deactivation) as shown in Figure 5.1(a). The exponential backward rates in Figure 4.2 between O/S and S/C allow this complex behaviour to be captured. The function φ for the hP2X$_7$ model is defined as $\varphi(\mathrm{A}) = A$. The exponential backward rates in Figure 4.2 between O/S and S/C makes this complex behaviour possible to be captured in such a simple manner. In fact, when the agonist is high the exponential terms are low and let the model pass the flow in the forward direction (C/S/O). By contrast, these two terms switch to their maximal values (viz. one) upon agonist removal, so letting the state O deplete (go to zero) to capture the deactivation phase (B to C) in Figure 4.3(a). Strictly speaking, such intricate dynamics can be captured by simpler models when reaction rates are designed such that they dynamically change to avail of existing paths of the model. They are responsible for reproducing the main properties of the experimental data for whole-cell currents, such as persistent sensitised state and monophasic/biphasic dynamics.

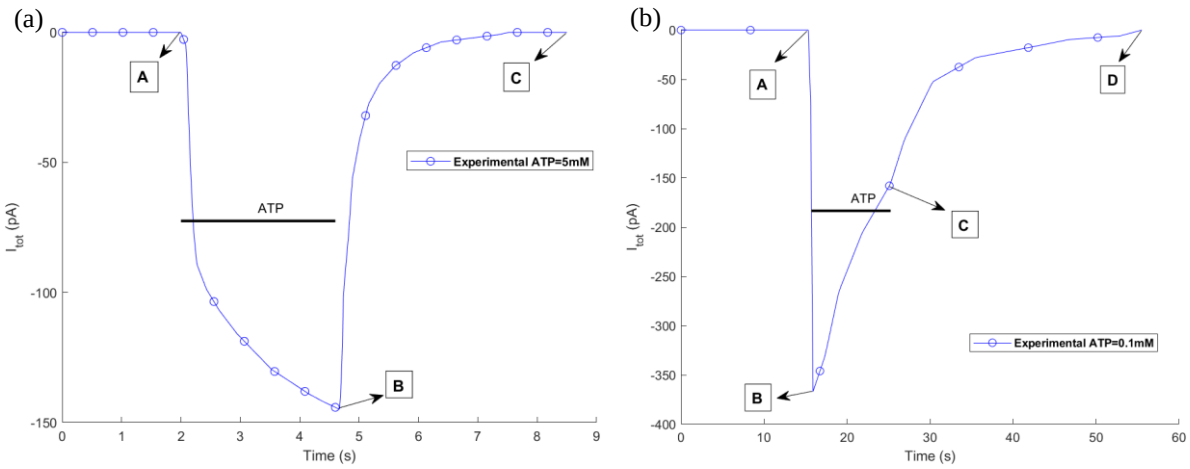

Figure 4.3. Experimental current transients [59, 94] upon ATP treatment of (a) via activation hP2X$_7$ receptor, and (b) via activation hP2X$_4$ in microglia. Horizontal bars show the duration of agonist exposures.

In contrast, hP2X$_4$ receptors mediate a rapid current that is sustainably greater than the peak amplitude of P2X$_7$ receptor as shown in Figure 4.3(b), and their desensitisation is much faster than P2X$_7$R, which is also validated by the model predictions. As seen in Figure 4.3(b), hP2X$_4$ receptor has three significant phases at the macroscopic level: A to B (activation/sensitisation), B to C (desensitisation), and C to D (deactivation). In contrast to microglial rP2X$_4$ [56], the hP2X$_4$ current takes some time to vanish after ATP removal (C to D). This additional phase requires minor changes to the P2X model of Figure 4.2, where $\varphi(\mathrm{A}) = e^{\zeta_1 A}$ is chosen. The transition between S and D states are gated by an exponential form of the agonist in Figure 4.2, which requires no additional state variables and therefore avoids the necessity for a more complex model. When ATP is zero, the transition between C and S is eliminated while $\varphi(\mathrm{A})$ becomes unity. In fact, the bidirectional path between S/D and S/O makes active routes for the current to vanish, namely, the phase of C to D in Figure 4.3(b) is simply realised. For more details on the relevance and necessity of model elements in Figure 4.2, the reader is referred to [90]. Human P2X$_4$R data shows that there are three different phases in the whole-cell patch-clamp current configuration. By assuming $\varphi(\mathrm{A}) = A$ instead of an exponential rate function for P2X$_4$R model, the model response become biphasic and misses capturing the third phase (i.e., deactivation). For a complete treatment of this kind of inference on model elements, see [90].

It is worth noting that in [116, 117] the authors employed time-dependent rates of mode switches (which are expressed as extra differential equations which make their model complex in terms of state variables) to develop an IP$_3$R model using a modified Markov model as our exponential rates (which are explicit functions of the agonist) is similar to HH model which takes fixed values at different levels of membrane potential. Our exponential rates were not originally meant for model simplification but to capture agonist-dependent responses.

To derive the mathematical equations representing the kinetic P2X model, the topology in Figure 4.2 is now translated into a system of time-dependent coupled ordinary differential equations as expressed in Eqs. (4.1) to (4.4) by using the law of mass action:

$$\frac{dC_Z}{dt} = \beta_{1Z} e^{-\zeta_{1Z} A} S_Z + \beta_{4Z} e^{-\zeta_{2Z} O_Z} D_Z - \alpha_{1Z} A C_Z \tag{4.1}$$

$$\frac{dS_Z}{dt} = \alpha_{1Z}AC_Z + \beta_{2Z}e^{-\zeta_{1Z}A}O_Z + \beta_{3Z}e^{\zeta_{1Z}A}D_z - \left(\beta_{1Z}e^{-\zeta_{1Z}A} + \alpha_{2Z}\varphi_Z(\mathrm{A}) + \alpha_{3Z}e^{\zeta_{1Z}A}\right)S_Z \qquad (4.2)$$

$$\frac{d\mathrm{D}_Z}{dt} = \alpha_{3Z}e^{\zeta_{1Z}A}S_Z - (\beta_{3Z}e^{\zeta_{1Z}A} + \beta_{4Z}e^{-\zeta_{2Z}O_Z})D_z \qquad (4.3)$$

$$\frac{dO_Z}{dt} = \alpha_{2Z}\varphi_z(\mathrm{A})S_Z - \beta_{2Z}e^{-\zeta_{1Z}A}O_Z \qquad (4.4)$$

Each state C, S, D and O corresponds to the fraction of a specific P2X receptor that is in the *Closed*, *Sensitised*, *Desensitised* and *Open* state at any given time. The above equations are used for both P2X models ($hP2X_4$ and $hP2X_7$), where Z is used to denote the subtype receptor number (4 or 7). The fitting of the model parameters is discussed in Section 5.2.1. Values and units of rate constants and coefficients in Eqs. (4.1) to (4.4) are also provided in Section 5.2.1.

4.2.2 $hP2X_Z$ Current Model

Having the system of Eqs. (4.1) to (4.4), we can now derive the current equations for the P2XRs (4 and 7). Currents through the receptors are proportional to the state O_Z, where Z is the subchannel number of the receptor, and can be expressed in terms of the familiar conductance channel model. These currents are obtained by a product of the open state, the maximum conductance, g, through the channels, and the difference between the membrane potential (V_m) and the reversal potential of the cell (E). The Ca^{2+} and Na^+ currents for the receptors can be modelled as two separate conductance channels using Eqs. (4.5) and (4.6), as illustrated in Figure 4.1(b), where reversal potentials are expressed in Eqs. (4.8) and (4.9). With regards to K^+ efflux, the mechanisms underpinning this ionic current are poorly understood and are therefore not considered in this thesis. However, the influx of Na^+ affect the NCX and will consequently have a downstream effect on Ca^{2+}. Therefore, the contribution to the Na^+ concentration in the cytoplasm by the P2XRs needs to be considered for a more complete understanding of the observed Na^+ and Ca^{2+} dynamics. This approach, where a conductance type model is used to characterise the P2XRs as individually ATP-gated Ca^{2+} and Na^+ channels, allows the segregation of the Ca^{2+} or Na^+ channel currents while maintaining a similar overall time-dependent response. While we

recognise that this is an assumption, the segregation of these two ions facilitates the calculation of both Ca^{2+} or Na^{+} ionic concentrations in the cytoplasm. Ca^{2+} or Na^{+} channel conductance in the proposed model is set to define channel stoichiometry. The total current is calculated by the summation of the separate channel contributions, as shown in Eq. (4.7).

$$I_{hP2XZ_{Na}} = g_{hP2XZ_{Na}} O_Z (V_m - E_{Na}) \tag{4.5}$$

$$I_{hP2XZ_{Ca}} = g_{hP2XZ_{Ca}} O_Z (V_m - E_{Ca}) \tag{4.6}$$

$$I_{tot_{hP2XZ}} = I_{hP2XZ_{Na}} + I_{hP2XZ_{Ca}} \tag{4.7}$$

The above equations are used for both P2X models ($hP2X_4$ and $hP2X_7$), where Z is used to denote the subtype receptor number (4 or 7). The ionic concentrations in the extracellular space are assumed constant but are dynamic in the cytoplasm due to the influx/efflux of ions giving rise to a dynamic transmembrane concentration gradient. Accordingly, the reversal potentials for Na^{+} and Ca^{2+} in Eqs. (4.5) and (4.6) can be expressed in terms of the Nernst equation as

$$E_{Na} = \frac{RT}{Z_{Na^+} \times F} ln \left(\frac{[\mathrm{Na}^+]_x}{[\mathrm{Na}^+]_i} \right) \tag{4.8}$$

$$E_{Ca} = \frac{RT}{Z_{Ca^{2+}} \times F} ln \left(\frac{[\mathrm{Ca}^{2+}]_x}{[\mathrm{Ca}^{2+}_{\mathrm{P2X}}]_i} \right) \tag{4.9}$$

where x and i are the extracellular and intracellular space respectively, Z_{Na^+} and $Z_{Ca^{2+}}$ are the valencies of Na^{+} and Ca^{2+} respectively, F is Faraday's constant, R is Boltzmann constant and T is the temperature in kelvins.

4.2.3 Sodium Calcium Exchanger (NCX)

The Na^{+} and Ca^{2+} current densities of the exchanger were elaborated in Section 3.2.4.1. Note that in the NCX model, the term $[\mathrm{Ca}^{2+}]_i$ stands for $[\mathrm{Ca}^{2+}_{\mathrm{P2X}}]_i$ within this section.

4.2.4 Plasma Membrane Ca^{2+} ATPase (PMCA)

The Ca^{2+} current density through the PMCA pump in our model was given in Section 3.2.4.2, where *n* is set to one [90]. Note that in the NCX model, the term $[Ca^{2+}]_i$ stands for $[Ca^{2+}_{P2X}]_i$ within this section.

4.2.5 Na^+ and Ca^{2+} Leakage Channels

In our model, two separate membrane-bound leakage channels exist for Na^+ and Ca^{2+} and are modelled as two passive electrochemical gradients by assuming a Nernst-like equation given by

$$J_{NaLeak} = g_{NaLeak}(V_m - E_{Na}) \tag{4.10}$$

$$J_{CaLeak} = g_{CaLeak}(V_m - E_{Ca}) \tag{4.11}$$

where g_y and E_y are conductance and reversal potential for ion *y*, and V_m is the membrane potential. The physiological conditions of these channels change dynamically with both membrane and reversal potentials.

4.2.6 Na^+ and Ca^{2+} Concentration Dynamics

Na^+ and Ca^{2+} signalling is formulated as a fluid compartment model, which is assumed to be well mixed. The changes in $[Na^+]_i$ and $[Ca^{2+}]_i$ are modelled as

$$\frac{d[Na^+]_i}{dt} = -\frac{\frac{I_{hP2X7_{Na}}}{S_m}+\frac{I_{hP2X4_{Na}}}{S_m}+J_{NaNCX}+J_{NaLeak}}{Z_{Na^+}\times F\times V_p}\times S_p \tag{4.12}$$

$$\frac{d[Ca^{2+}_{P2X}]_i}{dt} = -\frac{\frac{I_{hP2X7_{Ca}}}{S_m}+\frac{I_{hP2X4_{Ca}}}{S_m}+J_{CaNCX}+J_{PMCA}+J_{CaLeak}}{Z_{Ca^{2+}}\times F\times V_p}\times S_p \tag{4.13}$$

where S_m, S_p, Z, F and V_p are the microglial membrane surface area, microglial process surface area, the valency of ions, Faraday's constant, and the intracellular process volume respectively: the model assumes that $[Na^+]_i$ and $[Ca^{2+}]_i$ reside in the total cytosolic volume of microglial processes. The conversion of the P2XR's whole-cell patch-clamp currents into current densities is performed by dividing over S_m due to other current components already being expressed as current densities.

4.2.7 Membrane Potential

Taking the same approach as is used for neuronal cells [20, 63], V_m can be related to ionic flow across the membrane as

$$\frac{dV_m}{dt} = -\frac{1}{C_m} \times [I_{tot_{hP2X7}} + I_{tot_{hP2X4}} + (J_{NaNCX} + J_{CaNCX} + J_{PMCA} + J_{NaLeak} + J_{CaLeak}) \times S_p] \quad (4.14)$$

where C_m is the membrane capacitance. The total current flow through P2X channels is added to the transmembrane currents across the NCX exchanger, PMCA pump and leak channels. The terms expressed as current densities in Eq. (4.14) are multiplied by S_p.

4.3 P2Y-mediated Signalling in Microglia

The main goal of this section is to develop biophysical models of ADP-meditated $P2Y_{12}$ Ca^{2+} signalling and transduction and PI3K pathway activation in microglia. We aim to develop a model that can predict ionic behaviour and motility of microglia resulting from ADP-based extracellular disturbance: note that the biophysical model predictions will be verified using available experimental data.

Figure 4.4 portrays a high-level view of the components integrated into the model. In this thesis, it is hypothesised that $P2Y_{12}R$ in microglia is associated with $G_{\alpha i}$-GPCR signalling which triggers intracellular calcium transits as it has been experimentally shown that this receptor is involved with a (yet unknown) PLC pathway [62]. Of course, more work in the future is needed to test this hypothesis because, in contrast, the $P2Y_{12}$ receptor

can couple to the $G_{\alpha i}$ subunit in platelets and gives rise to only adenyl cyclase inhibition and cAMP decrease without meditating Ca^{2+} [118].

In Figure 4.4, the $P2Y_{12}$ receptor first activates phospholipase C (PLC) which then converts phosphatidylinositol 4,5-bisphosphate (PIP_2) that in turn leads to the creation of inositol 1,4,5-trisphosphate (IP_3) as an intracellular second messenger. IP_3 penetrates the cellular space and gates cytosolic calcium stores (such as the endoplasmic reticulum). This channel is sensitive to both IP_3 and calcium whereby Ca^{2+} release takes place. IP_3 and other signalling intermediates are recycled perpetually by a set of signalling events such as phosphorylation and dephosphorylation reactions. Diacylglycerol (DAG) is generated by PLC_β and affects PKC activity through the intracellular calcium.

The complete pathways underpinning microglial PI3K/Akt signalling are not well understood. However, from the literature regarding microglial cells and other cell lines [40, 119, 120], a complex signalling pathway can be constructed as shown in Figure 4.4. It appears that ADP or ATP can activate the G-coupled receptor, $P2Y_{12}$ [6, 62], which directly leads to the production of PIP_3 from PIP_2 by the $G_{\beta\gamma}$ subunit. The $G_{\beta\gamma}$ subunit simultaneously triggers the PLC_β pathway (which is also a large pathway and accompanied by a rapid rise of cytosolic [Ca^{2+}] [5]) and indirectly controls the conversion of PIP_2 to PIP_3 during phosphorylation (i.e. PLC_β converts PIP_2 to IP_3 and so can slow down the rate at which PIP_2 is turned into PIP_3 by $PI3K_\gamma$). PTEN inhibits the elevation of PIP_3. The total mediated PIP_3 leads to the activation of Akt (followed by the generation of pAkt) which in turn directly takes part in F-actin polymerisation, which is critical machinery of directed motility of microglia. Ras is also activated through the leading edge and contribute to the PI3K activation [121]. Although the complexity in Figure 4.4 may provide a research avenue on microglia, unfortunately, there is a scarce source of experimental data for most of the key elements of Figure 4.4, such as PIP_2, PIP_3, IP_3, PDK1, and so on. The only available experimental data capture intracellular [Ca^{2+}] and pAkt by applying a single level of ADP in rat primary cultured microglia [62]. On this basis, a comprehensive model of the PI3K/Akt pathway is developed.

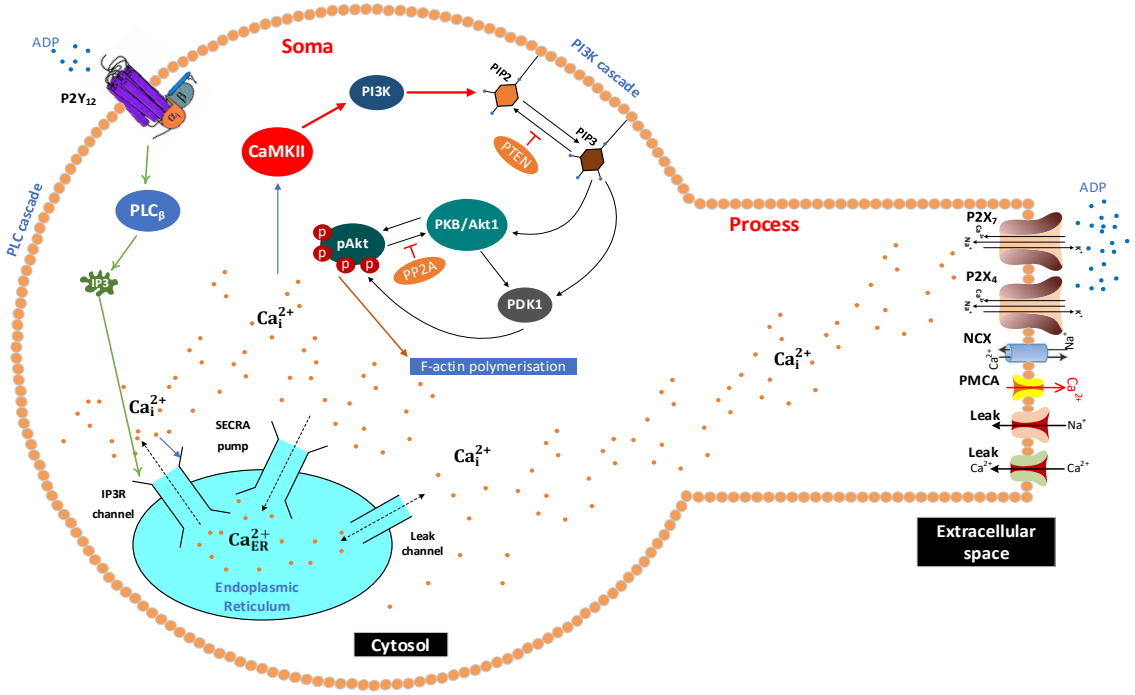

Figure 4.4. A model of $P2Y_{12}$-mediated calcium and PI3K/Akt signalling pathways of a microglial cell involved in chemotaxis (directed motility). $P2Y_{12}$ receptor is activated after ADP binding and phospholipase C (PLC) is evoked. PLC hydrolyses PIP_2 into IP_3 and DAG. IP_3R channels become open when IP_3 and intracellular calcium bind simultaneously and Ca^{2+}_{ER} is released from the endoplasmic reticulum (ER) into the cytoplasmic region. The PI signalling network recycles phosphorylated phosphatidylinositol (PI) substances while the SERCA (Sarco/endoplasmic reticulum Ca^{2+}-ATPase) and leak channel function as major transporters of calcium from the cytosol into the ER. In the microglia process, P2XRs, the Na^+/Ca^{2+} exchanger (NCX) and the plasma membrane Ca^{2+} ATPase (PMCA) along with Ca^{2+} and Na^+ leakage channels bring Ca^{2+} from the extracellular space, which diffuses into the somatic space. Ca^{2+} can trigger CaMKII whose role is to directly control the PI3K/Akt pathway. pAkt production is regulated by a complex network of potentiators (like PDK1), inhibitors (like PTEN) and species convertors.

There is growing evidence in the literature that both P2X and P2Y receptors are involved in the directed motility of microglia and other glial cells followed by activation of

the PI3K/Akt pathway [6, 122, 123]. As shown later (see Section 6.2.1), two peaks exist in the pAkt experimental data in microglia. This thesis makes the hypothesis that the P2Y receptor forms the first peak, whereas the second hump is regulated by P2X receptors. Consequently, the P2X model is included in Figure 4.4, which was detailed in Section 4.2 and [90]. Herein, it is assumed that two sources contribute to the total cytosolic Ca^{2+}: (1) intercellular stores specifically the endoplasmic reticulum (ER), and (2) a diffusion Ca^{2+} current mediated by P2X receptors. The latter Ca^{2+} travels along the process towards the soma that is modelled by a delayed time course of Ca^{2+} originating from P2XRs. There is extensive evidence that P2X receptors are located on the processes of glial cells [124] that is consistent with the compartmental model in Figure 4.4 for supporting the idea of a diffusion time delay arising from P2X receptors. To quantify this hypothesis, Appendix A discusses when P2XRs are switched off the model can only cover only a single peak thereby biophysically implying the presence of both P2YR and P2XRs through mathematical modelling. As stated, the presence of Ca^{2+} is necessary for microglial-directed motility through the PI3K/Akt machinery. Therefore, in this model, it is assumed that when the level of Ca^{2+} elevates, CaMKII is phosphorylated and in turn directly activates the PI3K pathway as strongly evidenced by the literature [53, 125, 126].

4.3.1 The Biophysical Model of IP_3 Receptor

In this section, a biophysical model is developed for $P2Y_{12}$-mediated Ca^{2+} dynamics in human microglia. Our proposed model of the inositol trisphosphate (IP_3) receptor describes this receptor in different states using fitting parameters to facilitate the capturing of calcium transients observed in published experiments. When ADP binds to the $P2Y_{12}$ receptor, the GPCR model given in Section 3.2.4.3 is activated. Note that in the GPCR model, the term Ca^{2+}_{P2Y} stands for $[Ca^{2+}_{P2Y}]_i$ within this section.

To overcome the limitations of existing IP_3R models [74, 95-97] (existing models were unable to get fitted to human microglial data as also encountered and explained in [90]), it is proposed that a new IP_3 receptor model is used. The model uses four state variables inspired by our previously published P2X model [90], as shown in Figure 4.5, and is tested using human microglial data published in [61]. A major challenge in modelling the human

microglial IP_3R is the lack of raw data from electrophysiological measurements in the literature.

The model assumes that the unliganded receptor can bind IP_3 resulting in low permeability (low open probability), namely, the C/S/O path (note that in this state the forward S/O path has a low kinetic rate about 100 times lower than when the channel fully opens). Then, Ca^{2+} releases and can bind to intracellular calcium biding sites. This forms a new open state of the channel with high open probability (the path from S to O). As cytosolic Ca^{2+} reaches very high levels, the receptor can turn into in inactivated state through a complex path between O/S and S/D. Therefore, the gating properties of the IP_3 channel are divided into four individual stages, including, activation (*S* to *O*) and sensitization (*C* to *S*), desensitisation (full-duplex Ca^{2+}-gated transition between S and D) and deactivation (mainly from D to C and partly from *O* to *S* and then *C*). Activation is a quick process (it happens after the receptor is sensitised by IP_3) over which the channel opens and pumps out Ca^{2+} from the ER lumen to the cytosol. The amplification effect of Ca^{2+} to bind the receptor site is likewise modelled in the transition from *S* to *O*. The receptor is fully activated when IP_3 binds through the transition between states *C* and *S*, and calcium gates the receptor through sate *S* to *O*.

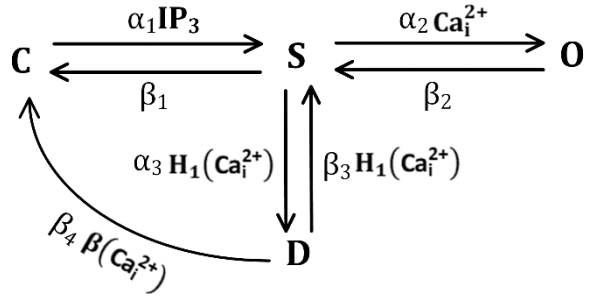

Figure 4.5. A reaction network was developed to capture the calcium current passing through the calcium-gated IP_3 receptor on the ER lumen in human microglia. The states *C*, *S*, *D*, and *O* respectively stand for *closed*, *sensitised*, *desensitised* and *open*. It is assumed that IP_3 has to bind to its binding site before Ca^{2+} is able to bind and the channel can open. H_1 and β functions are defined in Eqs. (4.19-4.20).

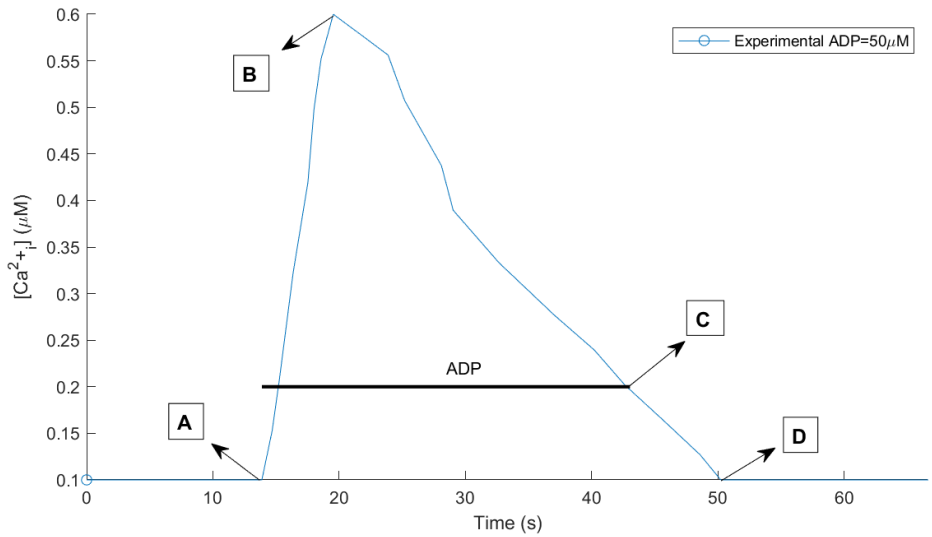

Figure 4.6. Experimental data for intracellular Ca^{2+} upon the activation of the $hP2Y_{12}$ receptor [61]. Note that [61] only provides calcium traces in relative fluorescence units and as there is no direct measurement for baseline and peak Ca^{2+} concentrations, they are approximated from the literature in [60, 127]. Particularly, relative Ca^{2+} fluorescence from [61] was normalised and then rescaled to the values of concentrations (baseline=0.1μM and peak-above-baseline=0.5μM) reported in [128].

As shown in Figure 4.6 microglial human P2Y-mediated Ca^{2+} response has three significant phases at the macroscopic level: A to B (activation with a moderate rising steepness), B to C (desensitisation with a uniform falling steepness), and C to D (deactivation with a falling slope close to its desensitisation stage). In other words, there are virtually two uniformly distributed rising and following slopes in the experimental data and the response returns to the resting state with the same slope observed in phases B to C. It means the Ca^{2+} does not have a new significant baseline after the removal of ADP. The function H_1 is mainly responsible to form this kind of complex steepness in a simplified manner. The first-order Hill function allows the model to control the slope of the response in order to have a moderate value. Note that the function is present on both sides of the S/D transition guaranteeing the amount of reduction in the S state in the forward reaction returns to the D state in a proportionally balanced fashion and vice versa.

The system of time-dependent differential equations formed by the topology in Figure 4.5 is derived in Eqs. (4.15) to (4-18) by directly applying the law of mass action. These

equations describe the rate at which the model states change in the time domain. Each state *C*, *S*, *D* or *O* corresponds to the fraction of IP_3R that remains at it over time, which is a combination of probability such as sensitisation and desensitisation, as discussed earlier. The model equations indicate in agreement with Figure 4.5 that the Hill function introduces a coupled set of non-linearities into the model. They are used to reproduce the main triphasic properties of the experimental data.

$$\frac{dC}{dt} = \beta_1 S + \beta_4 H_1([\mathrm{Ca}^{2+}_{\mathrm{P2Y}}]_i)D - \alpha_1[IP3]C \tag{4.15}$$

$$\frac{dS}{dt} = \alpha_1[IP3]C + \beta_2 O + \beta_3 H_1([\mathrm{Ca}^{2+}_{\mathrm{P2Y}}]_i)D - (\alpha_2[\mathrm{Ca}^{2+}_{\mathrm{P2Y}}]_i + \alpha_3 H_1([\mathrm{Ca}^{2+}_{\mathrm{P2Y}}]_i) + \beta_1)S \tag{4.16}$$

$$\frac{dD}{dt} = \alpha_3 H_1([\mathrm{Ca}^{2+}_{\mathrm{P2Y}}]_i)S - \beta_3 H_1([\mathrm{Ca}^{2+}_{\mathrm{P2Y}}]_i)D - \beta_4\beta([\mathrm{Ca}^{2+}_{\mathrm{P2Y}}]_i)D \tag{4.17}$$

$$\frac{dO}{dt} = \alpha_2[\mathrm{Ca}^{2+}_{\mathrm{P2Y}}]_i S - \beta_2 O \tag{4.18}$$

where the set of α and β parameters are forward and reverse reaction rates for the IP_3R model. The function H_1 is a first-order (*n=1*) version of the standard *Hill* function defined in Eq. (3.18) for human microglia as follows

$$\mathrm{H}_1([\mathrm{Ca}^{2+}_{\mathrm{P2Y}}]_i) = Hill([\mathrm{Ca}^{2+}_{\mathrm{P2Y}}]_i, n, K_S) \tag{4.19}$$

and the function β is defined using an exponential kinetic rate in Eq. (4.29) similar to the approach of Hodgkin–Huxley (HH) model [20]. Note that the HH model benefits from voltage-gated exponential rates while the model herein uses a Ca^{2+}-gated exponential rate.

$$\beta([\mathrm{Ca}^{2+}_{\mathrm{P2Y}}]) \equiv e^{-\frac{[\mathrm{Ca}^{2+}_{\mathrm{P2Y}}]_i - a}{b}} \tag{4.20}$$

In accordance with the HH model [20], flow through the IP_3R channel from the ER region to the cytosol is modelled as two identical rapidly Ca^{2+} activation gates (which

opens with the probability of *O*) and a single inactivation gate (which is activated by a probability of *h*). So, the channel dynamics are assumed to be affected by these two gates. At resting microglia, the *h* gate is open whereas the *O* gates are closed, thus the entire IP_3R is closed. When IP_3 gates the receptor in Figure 4.5, the *O* gates are quickly activated and in turn the *h* gate closes. Since it is expected that these two channels work in tandem, the resultant probability that describes the channel dynamics is simply obtained by multiplying the probability of the gates together. The *D* state is indicative of inactivation in the model, so the equation for the *h* state is given as

$$h = 1 - D \tag{4.21}$$

A typical *h* transient can be seen in Figure 6.1(b). By the notations developed above, the flux passing through the IP_3R channel can be mathematically written as

$$J_{IP3R} = \alpha_4 h O^2 (C_0 - (1 + C_1)[\mathrm{Ca}^{2+}_{\mathrm{P2Y}}]_i) \tag{4.22}$$

where α_4 is the maximal rate of calcium release from the IP_3 channel, C_0 is the free intracellular Ca^{2+} concentration [80] and C_1 stands for ER lumen to the cytoplasm volume ratio [80]. It is worth noting that activation and inactivation of the model is dependent on IP_3 and Ca^{2+} and *h* depends on the activation gates in contrast to the HH model (where they are truly independent). The flow of Ca^{2+} ions through the leak channel is modelled using a simple linear equation as

$$J_{Leak} = \alpha_5 (C_0 - (1 + C_1)[\mathrm{Ca}^{2+}_{\mathrm{P2Y}}]_i) \tag{4.23}$$

where α_5 is the Ca^{2+} leakage rate. The SERCA pump preserves low ER Ca^{2+} profiles by consuming energetic ATP macromolecules and extruding one Ca^{2+} from microglial cytosol against its ionic gradient into the ER region. As the second-order version of the Michaelis-Menten kinetics [79], the Ca^{2+} current density through it is formulated by

$$J_{SECRA} = \bar{J}_{SECRA} \frac{\left[\mathrm{Ca}^{2+}_{\mathrm{P2Y}}\right]_i^{\,2}}{{K_{SECRA}}^2 + \left[\mathrm{Ca}^{2+}_{\mathrm{P2Y}}\right]_i^{\,2}} \tag{4.24}$$

Ca^{2+} signalling is formulated as a fluid compartment model, which we assume is well mixed. We describe the change in Ca^{2+} concentration in the cytosolic region as

$$\frac{d\left[\mathrm{Ca}^{2+}_{\mathrm{P2Y}}\right]_i}{dt} = J_{IP3R} + J_{Leak} - J_{SECRA} \tag{4.25}$$

Note that the signs of the right-hand side of Eq. (4.25) have been chosen such that the amount of J_{IP3R} plus J_{Leak} are added to the cytosol while J_{SECRA} is removed from the cytosol.

4.3.2 Total Ca^{2+} Model

Figure 4.4 introduced two sources of intercellular Ca^{2+}. A major source is mediated from the internal stores activated by the $P2Y_{12}$ receptor in the soma followed by a hypothetical diffusion flow of Ca^{2+} coming from the microglia's process induced through P2X receptors which must travel to the soma, thereby resulting in a time delay. Therefore, it is expected the total calcium profile can be approximated by a linear combination of these two sources because the effect of the second source arrives in the cell's body with a significant delay as compared with the first one. This behaviour is then modelled as follows

$$\mathrm{Ca}^{2+}_{\mathrm{tot}}(t) = \mathrm{Ca}^{2+}_{\mathrm{P2Y}}(t) + \alpha \times \mathrm{Ca}^{2+}_{\mathrm{P2X}}(t - t_d) \tag{4.26}$$

where α is a Ca^{2+} scaling factor, and t_d models the time delay that P2X-mediated Ca^{2+} takes to travel the length of the process. The first term of Eq. (4.26), that is, $\mathrm{Ca}^{2+}_{\mathrm{P2Y}}(t)$, can be calculated by numerically solving Eq. (4.25). To obtain the numerical values for $\mathrm{Ca}^{2+}_{\mathrm{P2X}}(t)$, it is required to solve Eq. (4.13). After calculating $\mathrm{Ca}^{2+}_{\mathrm{P2X}}(t)$ in any desired integration

interval in the time domain, the results can be shifted by the value of t_d and a polynomial function can be fitted to these new data points, where the polynomial acts as a function of time and is used during the Akt model simulation explained in the next two sections.

In this model, α is a very important parameter, the value of α must be greater than one to capture the second hump in the pAkt experimental data. Several possibilities could be investigated behind this interesting behaviour. One may be arising from an increase in the density of P2X receptors or receptor upregulation [123] in the process when microglia are activated. On the other hand, α may be indicative of the P2X source of Ca^{2+} indirectly interacting with intercellular Ca^{2+} stores such as ER and store-operated Ca^{2+} channels (SOCs) in the soma. This unexplored part of the whole model hypothesised by this thesis then can be further explored experimentally.

Finally, it is assumed that the activation of CaMKII is sensitive to any perturbation of Ca^{2+} from its equilibrium level. Whereas the initial value of Ca^{2+} in the cytosol is present in both P2Y and P2X model equations, it must be subtracted from both terms of Eq. (4.26) appropriately, which gives the following equation:

$$\mathrm{Ca}^{2+}_{\mathrm{tot}}(t) = (\mathrm{Ca}^{2+}_{\mathrm{P2Y}}(t) - [Ca_i^{2+}]_0) + \alpha \times (\mathrm{Ca}^{2+}_{\mathrm{P2X}}(t - t_d) - [Ca_i^{2+}]_0) \tag{4.27}$$

where $[Ca_i^{2+}]_0$ is the initial value of Ca^{2+} at equilibrium. Note that the numerical value of Eq. (4.27) becomes zero when the model agonist (i.e., ADP) ceases.

4.3.3 CaMKII Model

The mathematical model used for the CaMKII component of the model was given in Section 3.2.4.4. Note that, by contrast to [82], the order of the hill function in Section 3.2.4.4 is raised to the power of two which allows the model to better capture the experimental data.

4.3.4 Biophysical PI3K/Akt Model

As stated earlier, there are many complex mathematical models for PI3K/Akt signalling pathway. For this study, an attempt is made to incorporate a minimum set of species which are key to Akt signalling involved in the directed motility of microglia. The general overview of these species was shown in Figure 4.4. The developed reaction network is depicted in Table 4-1. They represent the PI3K pathway of Figure 4.4 by applying Michaelis-Menten kinetics (which approximately models the dynamics of an enzyme system). Such an approach is likewise taken for constructing a mass-action Akt model of vascular endothelial growth factor in [108] and heregulin-induced ErbB signalling in [104]). In this model, a_i and b_i stand for association and dissociation rates, while k_i describes the activation rate of a protein; all of which are assumed to be constant. The biochemical reaction network is broken down into three parallel stages, in which phosphorylation, dephosphorylation and potentiation take place.

In the first stage (reactions 1 and 2), the PI3K enzyme phosphorylates PIP_2, thereby producing PIP_3, followed by dephosphorylation of PIP_3 to PIP_2 through PTEN. In these reactions, the PI3K enzyme is assumed to be directly activated by CaMKII. Thus, the first reaction indeed has a variable forward rate controlled by *CaM* activity which is defined using Eq. (4.26) as

$$CaM = CaMK_{active} \tag{4.26}$$

In the next stage, the phosphorylation of Akt to pAkt is carried out by the PIP_3 as shown in reaction 3. pAkt is dephosphorylated back to Akt by the PP2A enzyme in reaction 4. Finally, in the third stage, PDK1 acts as a major potentiator of Akt given by reactions 5 to 7. Since the activity of PDK1 in Figure 4.4 relies on both PIP_3 and Akt, we exploit a slightly generalised variant of Michaelis-Menten kinetics in order for the model to capture this complex behaviour. The first step of the enzymatic kinetics due to PDK1 is divided into two phases. The first is an activated form of PDK1 by PIP_3 described by reaction 5. It is possible that PDK1 also interacts with the PIP_3-Akt compound produced by reaction 3, which is expressed by reaction 5 and forms PIP_3-PDK1-Akt (which is also affected by

reaction 7). Then, the new complex PIP_3-PDK1 instead phosphorylates Akt, and down this way, one original reactant is reproduced leaving pAkt as a final product which contributes to a higher level of pAkt in tandem with reaction 3. In the end, PIP_3-PDK1 is disassociated to PIP_3 and PDK given by reaction 5. The indispensable presence of PDK1 to make a good match of the model with experimental data is worthy of note.

Table 4-1. CaMKII-mediated PI3K/Akt reaction network developed for microglia.

Num.	Reaction
PIP_2 phosphorylation and PIP_3 inhibition by PTEN	
1	$\underbrace{\text{PIP}_2}_{x_1} + \underbrace{\text{PI3K}}_{x_2} \underset{b_1}{\overset{a_1 \times CaM}{\rightleftarrows}} \underbrace{\text{PIP}_2\text{-PI3k}}_{y_1} \xrightarrow{c_1} \underbrace{\text{PIP}_3}_{x_3} + \underbrace{\text{PI3K}}_{x_3}$
2	$\underbrace{\text{PIP}_3}_{x_3} + \underbrace{\text{PTEN}}_{x_4} \underset{b_2}{\overset{a_2}{\rightleftarrows}} \underbrace{\text{PIP}_3\text{-PTEN}}_{y_2} \xrightarrow{c_2} \underbrace{\text{PIP}_2}_{x_1} + \underbrace{\text{PTEN}}_{x_4}$
Akt phosphorylation and pAkt inhibition by PP2A	
3	$\underbrace{\text{PIP}_3}_{x_3} + \underbrace{\text{Akt}}_{x_5} \underset{b_3}{\overset{a_3}{\rightleftarrows}} \underbrace{\text{PIP}_3\text{-Akt}}_{y_3} \xrightarrow{c_3} \underbrace{\text{PIP}_3}_{x_3} + \underbrace{\text{pAkt}}_{x_6}$
4	$\underbrace{\text{pAkt}}_{x_6} + \underbrace{\text{PP2A}}_{x_7} \underset{b_4}{\overset{a_4}{\rightleftarrows}} \underbrace{\text{pAkt-PP2A}}_{y_4} \xrightarrow{c_4} \underbrace{\text{PP2A}}_{x_7} + \underbrace{\text{Akt}}_{x_5}$
pAkt potentiation by PDK1	
5	$\underbrace{\text{PIP}_3}_{x_3} + \underbrace{\text{PDK1}}_{x_8} \underset{b_5}{\overset{a_5}{\rightleftarrows}} \underbrace{\text{PIP}_3\text{-PDK1}}_{y_5}$
6	$\underbrace{\text{PIP}_3\text{-Akt}}_{y_3} + \underbrace{\text{PDK1}}_{x_8} \underset{b_6}{\overset{a_6}{\rightleftarrows}} \underbrace{\text{PIP}_3\text{-PDK1-Akt}}_{y_6}$
7	$\underbrace{\text{PIP}_3\text{-PDK1}}_{y_5} + \underbrace{\text{Akt}}_{x_5} \underset{b_7}{\overset{a_7}{\rightleftarrows}} \underbrace{\text{PIP}_3\text{-PDK1-Akt}}_{y_6} \xrightarrow{c_5} \underbrace{\text{pAkt}}_{x_6} + \underbrace{\text{PIP}_3\text{-PDK1}}_{y_5}$

To drive the mathematical model of the aforementioned reactions in terms of a system of ODEs, the law of mass action is employed. In Table 4-1, all species are denoted by either x_i or y_i to simplify writing the model equations down. Consequently, the non-linear ODE Akt model is described by Eqs. (A.1) through (A.14), which come in Appendix B.

4.4 Curve Fitting using Evolution Strategy

In this thesis, parameter estimation of the models is carried out by CMA-ES which is also available as a MATLAB library [129]. Algorithm 1 portrays three essential phases in the curve fitting of our mathematical models given in Sections 4.2 and 4.3. Data points are prepared for fitting to the model in the first phase. Experimental data is fed into a spline interpolation algorithm, so a uniform distribution of data points can be obtained. In the second stage, the environmental setup of the underlying GA (genetic algorithm) optimiser is carried out, for example, choosing an appropriate estimate of the population size, and lower and upper bounds at which the parameters are estimated (note that all parameters correspond to positive values because they are mostly indicating the kinetic rates of the models), the radius of search (the value of 0.5 was used here) and a function callback.

The estimation process interacts with the CMAES library through a callback function in which the curve fitting handler is invoked on every GA iteration. Finally, the third phase performs the actual fitting. In each iteration, the ODE equations must be numerically solved. To improve the stability of numerical integration, we utilise the Jacobian matrix due to the nonlinearity of model equations. The distance between experimental data and the fitted model response must be calculated in each iteration. A variety of cost functions for this purpose can be defined whose performance may depend on specific problems. Mean Squared Error (MSE) was chosen as a basic loss function that can result in stable and good fits to experimental data. The fitting process terminates when a specific tolerance denoted as *tol* in Algorithm 1 is met (we used $tol = 10^{-6}$).

Algorithm 1. Non-linear, non-convex GA-based curve fitting for the model

Definitions:
S: stoichiometric matrix
$\bar{S}$: sparse matrix
K_0, s_0, K: vector
w: vector of experimental data
pop_size: population size
LB, UB: lower and upper bound for K required by GA optimiser
$fit\_callback$: function pointer handling the fitting process
J: Jacobian matrix of the system of ODEs for the P2X model
$w^{(k)}$: Approximated response curves to ATP in k'th iteration of the GA optimiser
w: Real response curves to ATP in experiments
$r^{(k)}$: Error in k'th iteration of the GA optimiser from experimental data
The Algorithm:
$[S, K_0, s_0] \leftarrow$ Load the model architecture. ← Phase I
$\bar{S} \leftarrow$ Build a sparse matrix from S.
$w \leftarrow$ Import experimental data and apply spline curve smoothing
$pop\_size \leftarrow$ Number of model parameters. ← Phase II
$[LB, UB] \leftarrow [0, Infinite]$
$fit\_callback \leftarrow$ Register model callback with CMAES GA library.
$fit\_callback$ is being invoked by the CMAES runtime. ← Phase III
$[s_0, K] \leftarrow$ Extract information for the current iteration minimized by CMAES.
$w^{(k)} \leftarrow$ Solve the system of ODEs by an appropriate numerical integration algorithm with J utilised.
$|r^{(k)}| \leftarrow$ Calculate deviation from the real data w by a loss function such as Mean Squared Error (MSE)
$MSE: |r^{(k)}| \leftarrow \frac{1}{n}\sum_{i=1}^{n}\left(w^{(k)}{}_i - w_i\right)^2$
if $|r^{(k)}| < tol$ **do**
  Finalize the curve fitting and save K and s_0.
else do
  Return $|r^{(k)}|$ to CMAES library.

4.5 Summary

In this chapter, a theoretical foundation for studying P2X/P2Y-mediated signalling in human microglial cells was developed. The main goal of this chapter was to provide a simple framework by which one can study major players in directed motility and calcium dynamics in human microglia. The proposed computational framework can be extended towards a more complete understanding of microglial function, particularly, *in situ* and *in vivo*, as discussed in Chapters 5 through 7. The model can also be refined as new experimental data becomes available. The proposed model provides a starting point for adding other physiological components discussed in Section 2.4 when their corresponding experimental data or characterisation become available. For example, mathematical modelling of P2Y-mediated electrophysiology is of main interest for studying how ionic responses (such as Na^+, K^+ and Ca^{2+}) and membrane potential may affect microglial

functions or potentially lead to intricate behaviour. As another example, we omitted to include SOCE which could contribute to changing the Ca^{2+} dynamics. Section 7.3 will give a detailed list of possible extensions of the model for further investigations.

Chapter 5. P2X-mediated Electrophysiology and Calcium Dynamics in Human Microglia

5.1 Introduction

The P2X models developed in Chapter 4 are now used to provide a deeper insight into intracellular P2X-triggered Na^+ and Ca^{2+} dynamics in microglial cells. The model was implemented in MATLAB Release 2021a. The *ode23s* routine was used to numerically integrate the non-linear, stiff model equations. The integration was carried out using the default MATLAB ODE solver timestep because it takes advantage of dynamic step sizes for implicit numerical integration. For integration stability during the curve fitting and numerical simulation, the calculation of the right-hand-side terms of the ODEs and the Jacobian matrix of the system equations were implemented for the model. This section investigates four case studies, including, whole-cell currents due to P2XRs, Ca^{2+}, Na^+ and V_m dynamics resulting from the P2X-provoked currents.

5.2 Numerical Results

5.2.1 Model Fitting and Validation

In this section, validation of the P2X models uses available experimental data [59, 94]. An evolutionary strategy as described in Section 4.4 and [90] was used to estimate the optimal values of the P2X model parameters that capture time-dependent kinetics experimentally observed. As illustrated in Figure 5.1, the kinetic P2X model shown in Figure 4.2 is able to reproduce all the major gating properties of $hP2X_7$ and $hP2X_4$ receptors for the whole-cell current experiments, i.e. activation, deactivation, sensitisation and desensitisation. The fitted $hP2X_7$ model is subject to 5mM ATP stimulation [59], while 0.1mM ATP had been used for the $hP2X_4$ receptor [94].

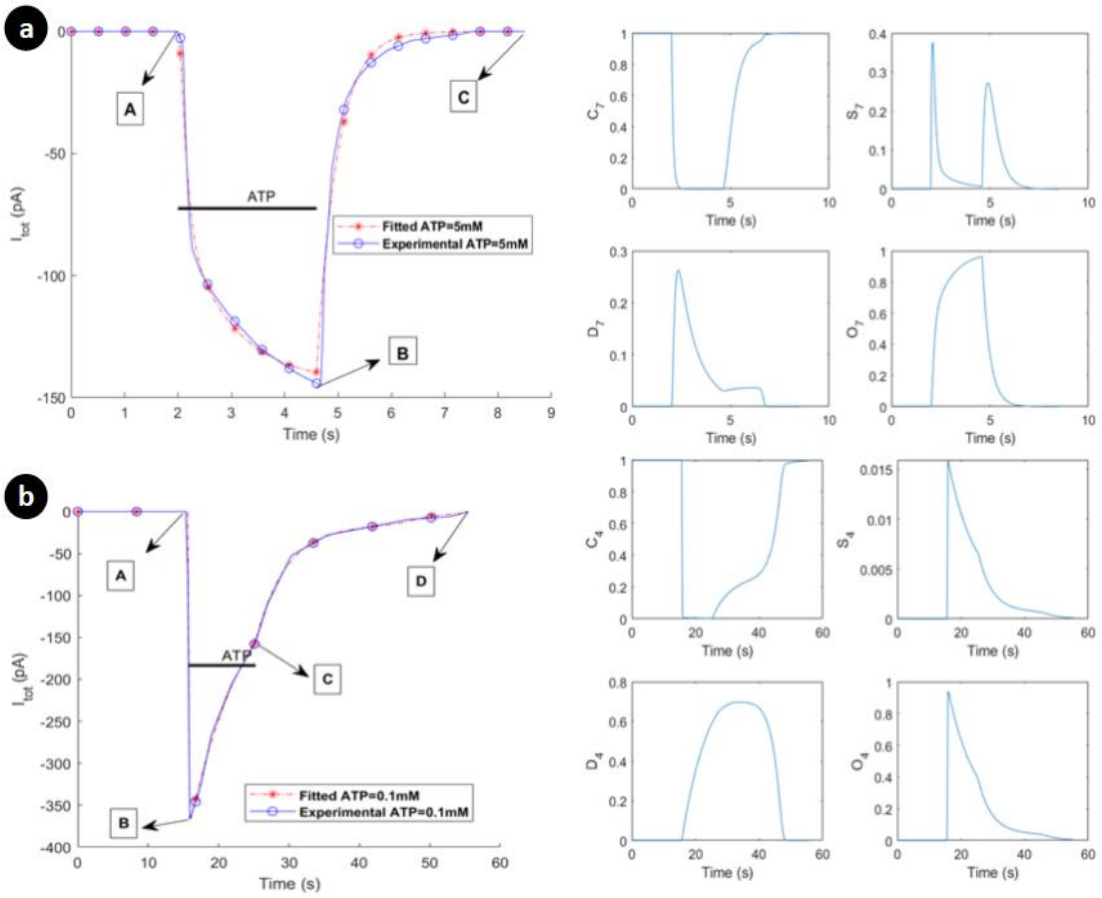

Figure 5.1. Current transient (left panel) and receptor gate C/S/D/O state responses (right panel) upon ATP treatment of (a) 5mM ATP within 2.6 seconds via activation $hP2X_7$ receptor, and (b) 0.1mM ATP within 9.6 seconds via activation $hP2X_4$ in microglia. Horizontal bars show the duration of agonist exposures. Experimental data come from [59, 94]. Corresponding states for both receptors on the right panels have different transient behaviours that are mainly due to the distinction between model parameters and model structure.

In contrast to $hP2X_4$ current profile which peaks at -372pA, $hP2X_7$ responds much slower reaching a peak of -145pA. Clearly, both models closely approximate the experimental data. The right panel of Figure 5.1 illustrates the transient behaviour of the state variables for the whole-cell current. As seen, sensitisation and desensitisation significantly differ in both models. Interestingly, there are two similar transients in state S of Figure 5.1(a) that align with the existing two phases of activation and deactivation. The

first transient relates to the activation phase from point A to B (Figure 5.1(a)) where ATP is present, and the second transient is created upon ATP removal since the state O must be depleted from the only available path (O to S, followed by S to C or S to D and then finally to C in Figure 4.2(a)). The summation of transient responses of all the state variables is equal to unity at all times and all state variables return to their resting state post-stimulation. There are four classes of parameters in the entire model formulated by Eqs. (4.1) to (4.14), including, (a) whole-cell patch-clamp current parameters of α and β, (b) estimated constant parameters such as ζ, (c) morphological parameters such as C_m and S_p, and (d) physically measured parameters such as K_{PMCA} and γ used from the literature. Conductances of both P2X models were fitted to clamped electrophysiological voltage data [59, 94] and then reduced by a factor of 25 (similar to [89]) such that the difference between the resting [Ca^{2+}] and the peak [Ca^{2+}] lies between 50nM and 55nM, in agreement with the general P2X-mediated $[Ca^{2+}]_i$ dynamics found in the literature [58]. PMCA, NCX and leak channel parameters were determined through numerical simulation to fit experimental data [130] such that $[Na^{+}]_i$ and $[Ca^{2+}]_i$ are maintained at their resting concentrations in a steady state. This is a paramount property of the microglial cells where the model takes up the role of maintaining $[Ca^{2+}]_i$ in resting microglia because microglia must be sufficiently sensitive to their microenvironment to generate a quick response to injury. By letting the optimiser calibrate the value of ζ parameters in Figure 4.2, it was unable to give a satisfactory fit quality as detailed in [90]. Hence, ζ was estimated manually by setting different values for ζ and letting the optimiser find all remaining parameters. Therefore, trial and error were used where values of ζ_1 and ζ_2 greater than 1 was chosen, and these values were then used in the optimiser. This process was repeated until the best fit for all remaining parameters was found (see Table 5-1 for the final values of ζ_1 and ζ_2). The reference in [90] gives an example for choosing a typical value of ζ_1 in that the model cannot capture the experimental well.

Morphological changes occur in microglia and while the proposed model does not take this into account, morphological data [131] was used to estimate the surface area and volume of activated microglia by assuming three cylindrical processes and the cell body is represented by a cube: while microglia can dynamically lose their spherical somatic phenotype upon activation, a cube is closer to an image of particular microglia morphology

as reported in [131]. Using these assumptions, the process surface area and volume can be calculated and used as parameters in Eqs. (4.12) to (4.14). Values, units, and descriptions of the parameters used in our model are presented in Table 5-1.

Table 5-1. Parameters for the mathematical model of P2X-mediated calcium and sodium dynamics in human microglia.

Parameter	Value	Unit	Description	Source
α_{17}	2427.508	$M^{-1}s^{-1}$	Rate constant for $C_7 \rightarrow S_7$	Fitted
α_{27}	1473.074	$M^{-1}s^{-1}$	Rate constant for $S_7 \rightarrow O_7$	Fitted
α_{37}	0.0299	s^{-1}	Rate constant for $S_7 \rightarrow D_7$	Fitted
β_{17}	4.277	s^{-1}	Rate constant for $S_7 \rightarrow C_7$	Fitted
β_{27}	2.616	s^{-1}	Rate constant for $O_7 \rightarrow S_7$	Fitted
β_{37}	0.0125	s^{-1}	Rate constant for $O_7 \rightarrow S_7$	Fitted
β_{47}	930.251	s^{-1}	Rate constant for $D_7 \rightarrow C_7$	Fitted
α_{14}	187057.5	$M^{-1}s^{-1}$	Rate constant for $C_4 \rightarrow S_4$	Fitted
α_{24}	1111.369	s^{-1}	Rate constant for $S_4 \rightarrow O_4$	Fitted
α_{34}	6.223	s^{-1}	Rate constant for $S_4 \rightarrow D_4$	Fitted
β_{14}	7.298	s^{-1}	Rate constant for $S_4 \rightarrow C_4$	Fitted
β_{24}	19.369	s^{-1}	Rate constant for $O_4 \rightarrow S_4$	Fitted
β_{34}	0.01341	s^{-1}	Rate constant for $D_4 \rightarrow S_4$	Fitted
β_{44}	528.077	s^{-1}	Rate constant for $D_4 \rightarrow C_4$	Fitted
ζ_{17}	1×10^{3}	M^{-1}	$P2X_7$ exponential rate functions coefficient	Estimated
ζ_{27}	1×10^{3}		$P2X_7$ exponential rate functions coefficient	Estimated
ζ_{14}	0.2×10^{3}	M^{-1}	$P2X_4$ exponential rate functions coefficient	Estimated
ζ_{24}	0.2×10^{3}		$P2X_4$ exponential rate functions coefficient	Estimated
$g_{hP2X7_{Na}}$	10.33×10^{-12}	S	Maximal $hP2X_7$ sodium conductance	Fitted
$g_{hP2X7_{Ca}}$	6.91×10^{-12}	S	Maximal $hP2X_7$ calcium conductance	Fitted
$g_{hP2X4_{Na}}$	31.28×10^{-12}	S	Maximal $hP2X_4$ sodium conductance	Fitted
$g_{hP2X4_{Ca}}$	20.85×10^{-12}	S	Maximal $hP2X_4$ calcium conductance	Fitted
$C_7\|_0 = C_4\|_0$	1		Initial values of C_7 and C_4	
$S_7\|_0 = S_4\|_0$	0		Initial values of S_7 and S_4	
$D_7\|_0 = D_4\|_0$	0		Initial values of D_7 and D_4	
$O_7\|_0 = O_4\|_0$	0		Initial values of O_7 and O_4	
$\bar{J}_{NCX}$	55	Am^{-2}	Maximum NCX current density	Estimated
γ	0.5		NCX partition number	[74]
F	96485	$CMol^{-1}$	Faraday constant	[74]
R	8.314	$JMol^{-1}K^{-1}$	Ideal gas constant	[74]
T	310	K	Temperature	[74]
$\bar{J}_{PMCA}$	0.06	Am^{-2}	Maximum PMCA current density	Estimated
K_{PMCA}	0.1×10^{-6}	M	PMCA Ca^{2+} affinity	[79]
Z_{Na^+}	1		Na^+ valency	[74]
g_{NaLeak}	305×10^{-4}	Sm^{-2}	Na^+ leak conductance	Calculated
$Z_{Ca^{2+}}$	2		Ca^{2+} valency	[74]
g_{CaLeak}	783×10^{-4}	Sm^{-2}	Ca^{2+} leak conductance	Calculated
$[Na_i^+]_0$	8×10^{-3}	M	Initial Na_i^+ concentration	[74]
$[Ca_i^{2+}]_0$	45×10^{-9}	M	Initial Ca_i^{2+} concentration	[74]
$[Na_x^+]$	130×10^{-3}	M	Extracellular Na^+ concentration	[74]

$[Ca_x^{2+}]$	2×10^{-3}	M	Extracellular Ca^{+} concentration	[74]
$V_m\|_0$	-0.06	V	Initial membrane potential	[59]
C_m	12×10^{-12}	F	Microglia membrane capacitance	[89]
S_m	3.178×10^{-10}	m^2	Microglia membrane surface area	[131]
S_p	2.435×10^{-10}	m^2	Microglia process surface area	[131]
V_p	1.67×10^{-13}	L	Microglia process volume	[131]

5.2.2 P2X-mediated Whole-Cell Currents

Microglial $hP2X_4$ and $hP2X_7$ receptors are activated in micromolar and millimolar concentrations of the applied ATP, respectively [56, 58]. We now consider model predictions for both receptors. The simulated whole-cell current responses of $hP2X_7$ and $hP2X_4$ receptors are shown in Figure 5.2 to Figure 5.4 for different applications of ATP stimulus level and duration.

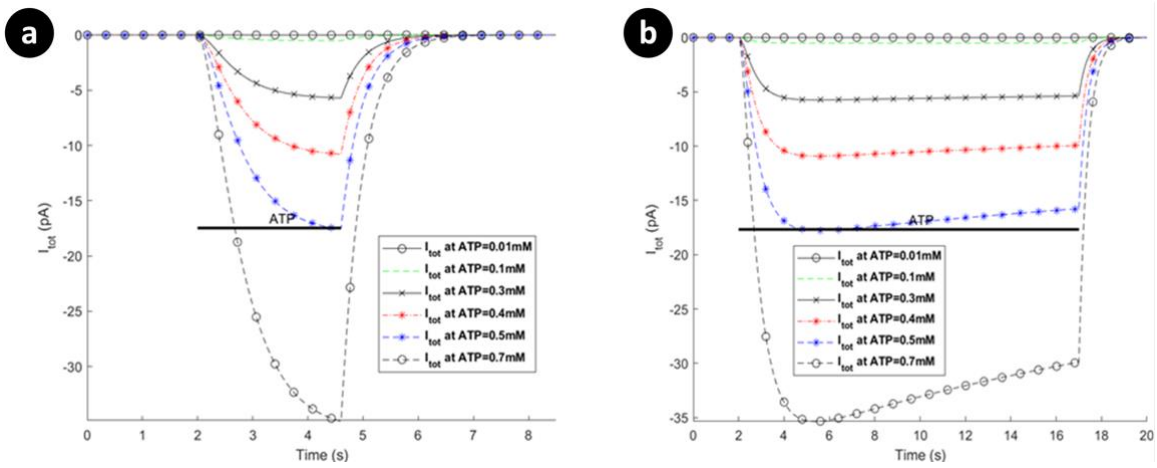

Figure 5.2. Dependence of total $P2X_7$ currents on different ATP treatments under 1 millimolar: (a) 3-second application, and (b) 15-second application via activation of $P2X_7$ for human microglia. Horizontal bars show the duration of agonist exposures.

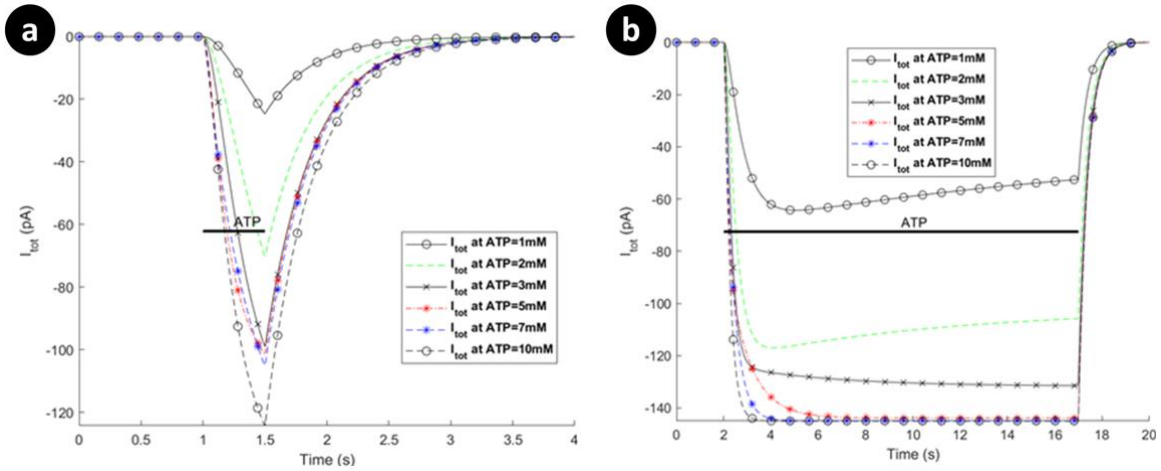

Figure 5.3. Total $P2X_7$ currents on different ATP treatments above 1 millimolar for human microglia: (a) short duration of ATP application (0.5 seconds), versus (b) long duration of ATP exposure (15 seconds).

All the results for the $hP2X_7$ receptor invoked by micromolar or millimolar ATP (see Figure 5.2 and Figure 5.3 respectively) display two biphasically distinguishable phases as observed in [59], namely, current initialisation (rapid effect of ATP) and time-dependent current facilitation. Figure 5.3(a) illustrates a short ATP stimulus in contrast to Figure 5.3(b) where, at 1mM and 2mM, the behaviour conforms to the Ca^{2+} dynamics reported experimentally [59]. Note that: it is inferred that ATP levels of 1-2mM correspond to 300μM of Benzoylbenzoyl-ATP (Bz-ATP) [132]. This is also discussed further in the next section.

The predictions in Figure 5.3(a) and Figure 5.3(b) show that for short ATP application, the current remains in the ascendancy while for long ATP stimulus the current plateaus and thereafter slowly declines. In contrast to rat microglial data [133], the current amplitude appears to saturate with larger ATP levels, which suggests that desensitisation becomes more pronounced for higher levels of ATP. However, this behaviour agrees with what has been reported for mouse $P2X_7$ microglia receptors [57].

The predictions in Figure 5.4(a) show that the amplitude and rate of increase of current is largely unaffected by the magnitude of the ATP stimulus for $hP2X_4R$. Note that this receptor appears to rapidly desensitise until the ATP stimulus is removed, thereafter the current falls off rapidly to baseline. In contrast, Figure 5.4(b) shows that for long ATP

durations the current reaches a steady state after a period of desensitisation and these levels are ATP-dependent. Only when the ATP stimulus is removed does the current return to its baseline level. This dual component indicates a biophysical fingerprint that has been reported through *in vitro* electrophysiology [134]. For example, human monocyte-derived macrophage research shows that $P2X_4Rs$ exhibit fast activation current followed by biphasic desensitisation in [115], particularly for high levels of ATP. Pertinent to dynamic microglia, this biphasic functionality of $P2X_4Rs$ may provide a regulatory pathway to control motility as has been suggested in expression systems [92].

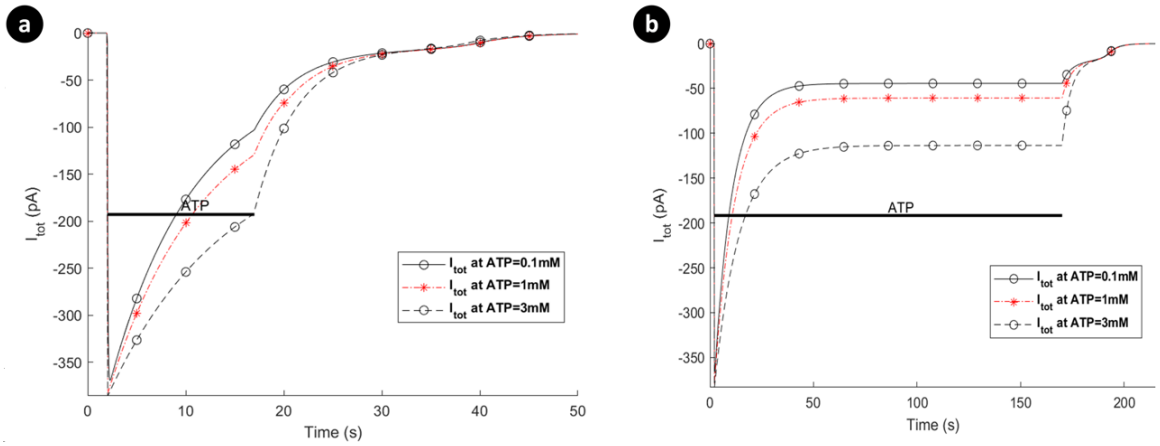

Figure 5.4. Prediction of patterns in total currents via activation of $P2X_4$ for human microglia. The curves represent biphasic responses: (a) short duration of ATP exposure, versus (b) long duration of ATP treatment.

The $hP2X_7$ and $hP2X_4$ receptor models can now be integrated yielding valuable data regarding P2X-mediated Ca^{2+} and Na^{+} signalling in human microglia. These data could be used to guide future experimental design.

5.2.3 P2X-mediated Calcium Dynamics

The interaction between the P2XRs, NCX, PMCA and leak channels dictates the dynamics of Ca^{2+} and Na^{+} concentrations and also V_m, as described by Eqs. (4.12) to (4.14). The model predicts the total Ca^{2+} influx/efflux via the receptors, leak channels, extruders, and pumps. Figure 5.5 shows individual Ca^{2+} transients for each receptor separately assuming the same ATP exposure level and duration. For Figure 5.5(a), the $[Ca^{2+}]_i$ reaches a plateau

for higher levels of ATP and this correlates with the total current carried by this receptor (e.g., at 3mM), as shown in Figure 5.3(b). Figure 5.5(a) agrees with experimental intracellular Ca^{2+} measurements [59] for ATP=1mM, as discussed earlier, in which there exists a local maximum before the Ca^{2+} curve goes to its plateau prior to ATP removal. Figure 5.5(b) shows a very transient-like $[Ca^{2+}]_i$ profile where hP2X$_4$R preserves $[Ca^{2+}]_i$ for higher levels of ATP which is consistent with its equivalent current profile in Figure 5.4.

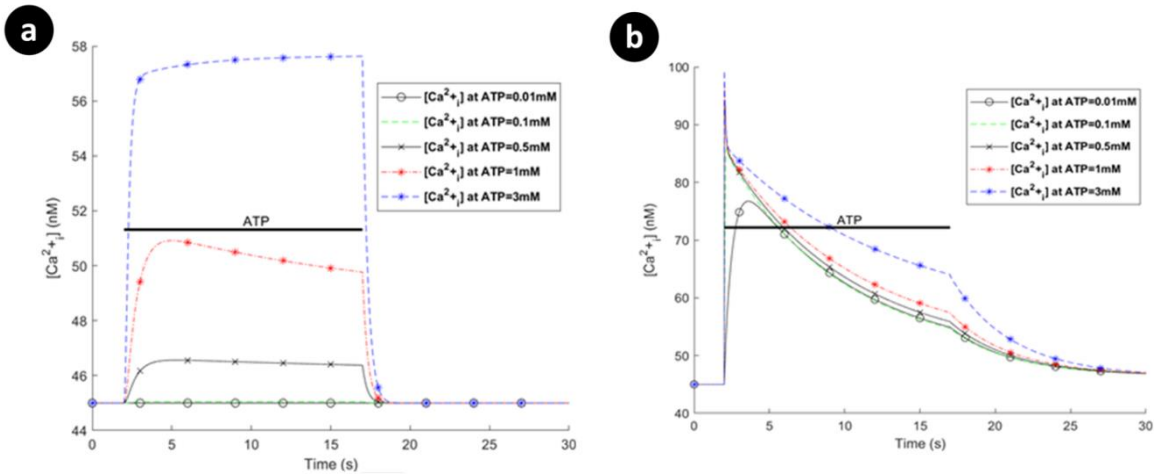

Figure 5.5. Intracellular $[Ca^{2+}]_i$ transients when (a) the hP2X$_4$ receptor is switched off with hP2X$_7$ active, and (b) hP2X$_7$ is switched off with hP2X$_4$ active.

Figure 5.6 shows the absolute currents carried by the P2X$_7$ (P2X$_4$ switched off), NCX, PMCA and leak channels for ATP levels of 0.1mM, 1mM and 3mM. Note that prior to the onset of the ATP stimulus Ca^{2+} efflux by the PMCA is negated by the NCX operating in reverse mode and calcium leak across the membrane via the Ca^{2+} leak channel. As the ATP stimulus is applied, the P2X$_7$ receptor is activated and both Ca^{2+} and Na^{+} current flows into the cytoplasm. However, V_m and $[Ca^{2+}]_i$ are the primary drivers for the NCX ensuring that it operates in reverse mode, as can be seen in Figure 5.6 for higher levels of ATP (1mM and 3mM). Also, after the initial disturbance, both the Ca^{2+} and Na^{+} currents stabilise such that the net Ca^{2+} or Na^{+} current flowing across the membrane becomes zero, and the concentration of both ions in the cytoplasm stabilises, in agreement with Figure 5.5(a).

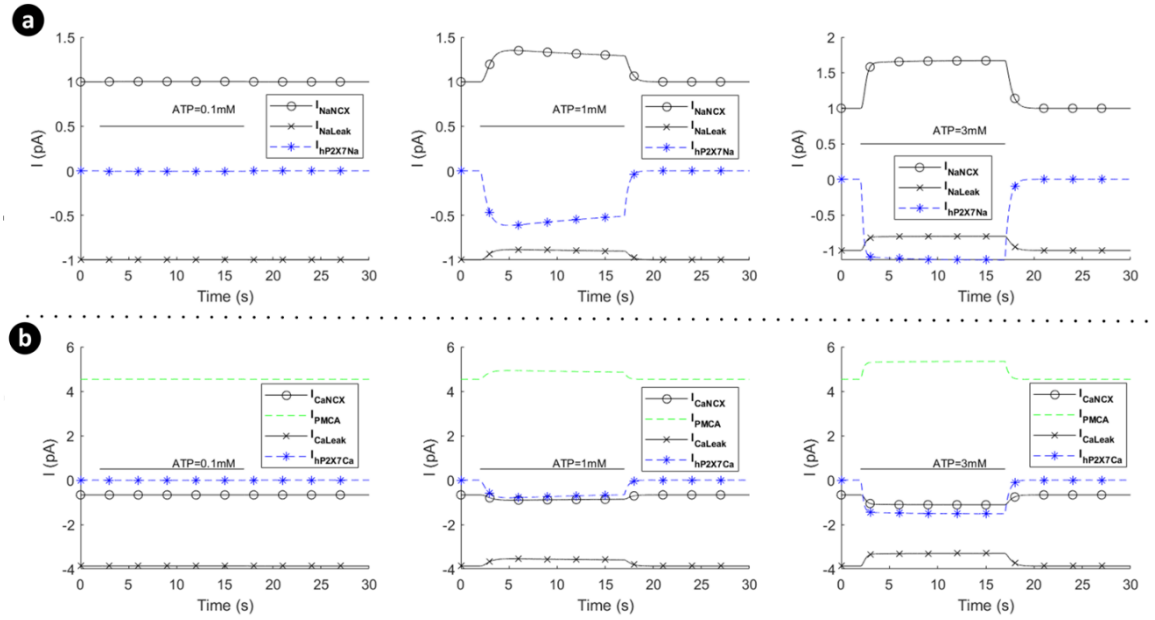

Figure 5.6. Dynamics of absolute currents via activation of $hP2X_7$ when the $hP2X_4$ receptor is switched off. Top (a) and bottom (b) panels respectively quantify the sodium (a) and calcium components of the model receptor for 0.1mM, 1mM and 3mM ATP.

Reversal potentials and V_m for $P2X_7R$ are shown in Figure 5.7 when $P2X_4R$ is switched off. Note that the reversal potential for Na^+ (Figure 5.7) changes much less significant in comparison with $[Ca^{2+}]_i$, because the baseline level of $[Na^+]_i$ is much higher than that of $[Ca^{2+}]_i$. Additionally, experimental data [133] indicates that rectification of V_m occurs following low levels of ATP stimulus while sustained depolarisation occurs with higher ATP concentrations. Our model of V_m (illustrated in Figure 5.7(c)) shows a similar trend to this data.

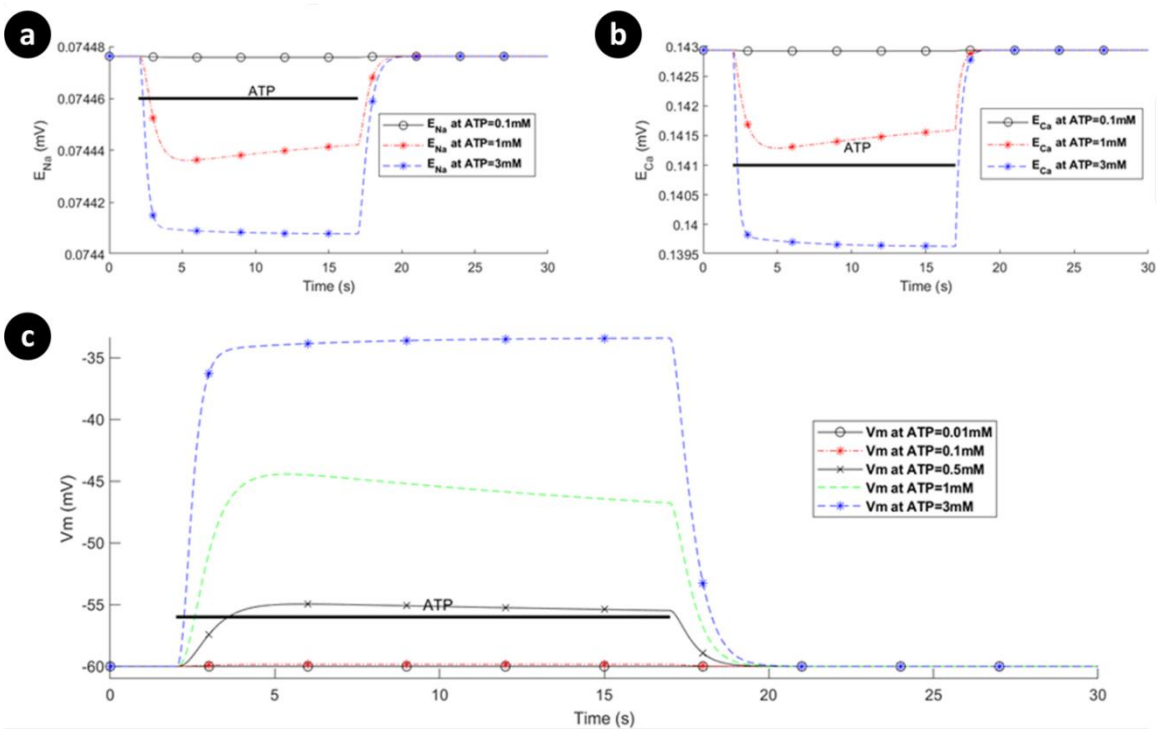

Figure 5.7. Dynamics of the reversal potentials associated with (a) Ca^{2+}, (b) Na^{+}, and (c) the membrane potential as a function of ATP levels when the $hP2X_4$ receptor is turned off.

Note that the mode of operation for the NCX is, to a good approximation, unaffected by influx/efflux of Na^{+} currents since the baseline $[Na^{+}]_i$ in the cytoplasm is high (8mM). In contrast, the mode of operation of the NCX is much more sensitive to the $[Ca^{2+}]_i$ in the cytoplasm as this quantity changes much more significantly by the ATP stimulus because the baseline $[Ca^{2+}]_i$ in the cytoplasm is low (45nM); V_m also drives the NCX. Figure 5.8 shows the absolute currents carried by the $P2X_4$, NCX, PMCA and leak channels for ATP levels of 0.1mM, 1mM and 3mM. Prior to the onset of the ATP stimulus, the Na^{+} leak current is negated by NCX extruded Na^{+} efflux and the Ca^{2+} efflux by the PMCA is negated by the NCX operating in reverse mode and Ca^{2+} leakage across the membrane via the Ca^{2+} leak channel. As the ATP stimulus is applied, the $P2X_4$ receptor is activated and both Ca^{2+} and Na^{+} current flows into the cytoplasm. In contrast to the $P2X_7$ current (see Figure 5.3), the current through the $P2X_4$ (see Figure 5.5) is more transient in nature, reflecting the behaviour of the biological $P2X_4$ receptor. The sharp rise in Na^{+} influx by the $P2X_4$ results in an associated rise in the Na^{+} leakage current and V_m, with the NCX extruder

driven deeper into reverse mode. Also, the sharp rise in Ca^{2+} influx resulting from $P2X_4$ activation causes additional efflux of Ca^{2+} via the PMCA but this is somewhat negated by the influx of Ca^{2+} by the NCX, where the latter is driven by hyperpolarisation of V_m and fluctuations in the $[Ca^{2+}]_i$ in the cytoplasm. As in the case of the $P2X_7$, the reversal potential for Na^+ (Figure 5.9) is virtually unaffected due to the high $[Na^+]_i$ baseline in the cytoplasm but the reversal potential for Ca^{2+} (Figure 5.9) changes much more significantly because of the low $[Ca^{2+}]_i$ baseline in the cytoplasm.

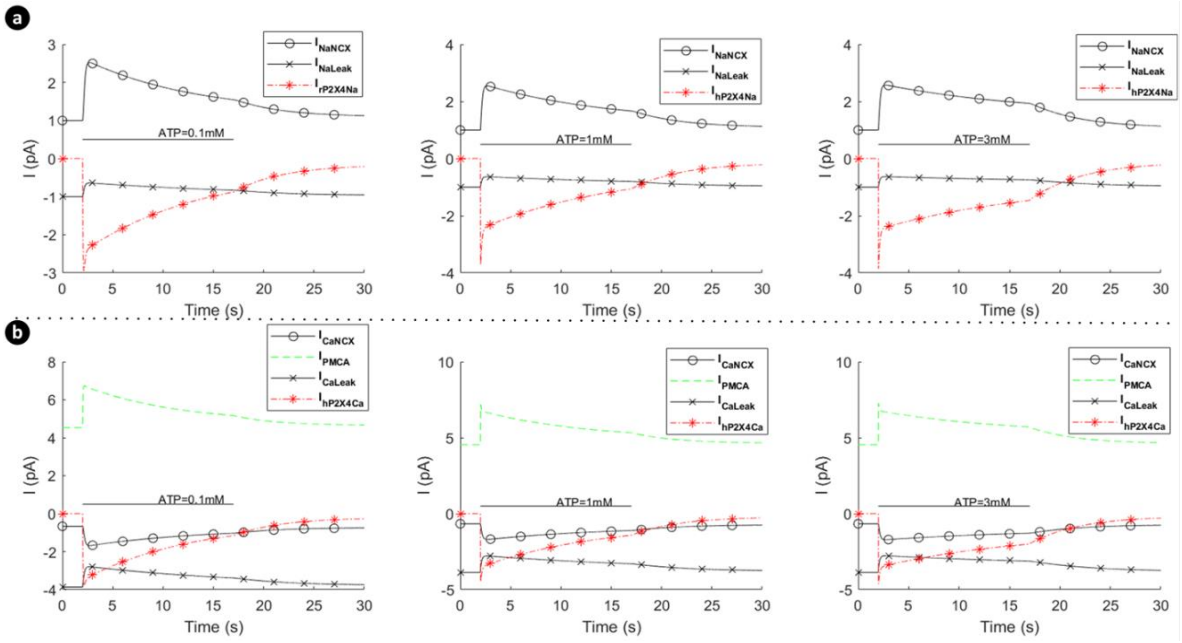

Figure 5.8. Dynamics of absolute currents via activation of the $hP2X_4$ receptor when the $hP2X_7$ receptor is turned off. Top (a) and bottom (b) panels respectively quantify the sodium and calcium components of the model for 0.1mM, 1mM and 3mM ATP.

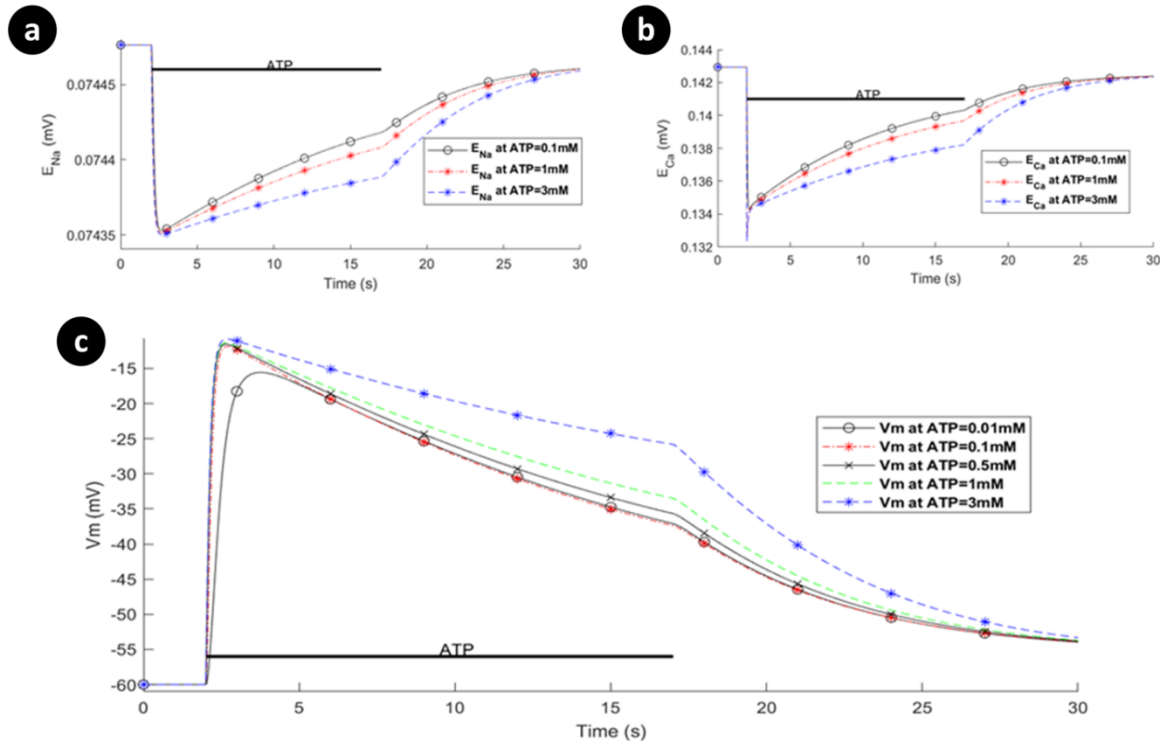

Figure 5.9. Dynamics of the reversal potentials associated with (a) Ca^{2+}, (b) Na^{+}, and (c) the membrane potential as a function of ATP levels when the $P2X_7$ receptor is turned off.

A holistic view of $[Ca^{2+}]_i$ transients by concurrent stimulation of both $hP2X_4$ and $hP2X_7$ receptors is given in Figure 5.10. A significantly distinguished pattern is observed in Figure 5.10 for ATP=1mM and ATP=3mM. As seen in the results of Figure 5.6, both the Ca^{2+} and Na^{+} currents continue towards saturation while the ATP stimulus is sustained. In contrast, for the $P2X_4$ (Figure 5.8) both the Ca^{2+} and Na^{+} current behave more like a transient (affecting V_m) and decay over time irrespective of the level or duration of the ATP stimulus. It is therefore concluded that the kinks in the curves at ATP levels of 1mM and 3mM in Figure 5.10 are because of the fast fall-off in $[Ca^{2+}]_i$ due to the decrease in the Ca^{2+} current through the $P2X_4$ and the relatively slow rise in $[Ca^{2+}]_i$ due to the increasing Ca^{2+} current through the $P2X_7$. When these two $[Ca^{2+}]_i$ cross over (at a comparable concentration) a kink is formed (momentary rise in $[Ca^{2+}]_i$ followed by a slow fall-off in $[Ca^{2+}]_i$). Essentially, both receptors have a direct influence on the total P2X-mediated $[Ca^{2+}]_i$ dynamics where the $P2X_4$ receptor dominates the $[Ca^{2+}]_i$ at the onset of the ATP stimulus but thereafter the $P2X_7$ receptor maintains a high level of $[Ca^{2+}]_i$ in the cytoplasm

until the removal of the ATP stimulus. A wide spectrum of experimental data confirms this theoretical finding where several P2 (i.e., P2X and P2Y variants) receptors are simultaneously triggered by extracellular nucleotides like ATP. Activation of $P2X_4R$ and $P2X_7R$ results in intricate $[Ca^{2+}]_i$ kinks for 1mM and 3mM of ATP in rat microglia [58]. Other works on microglia and astrocytes reveal the kink-style behaviour of $[Ca^{2+}]_i$ [86, 135-137] and such dynamics are also observed in other animal and human cell lines including those experimentally reported in [138-143]. Note that no kink appears for ATP < 1mM because the initial rise in current is dominated by current flow through the $P2X_7$.

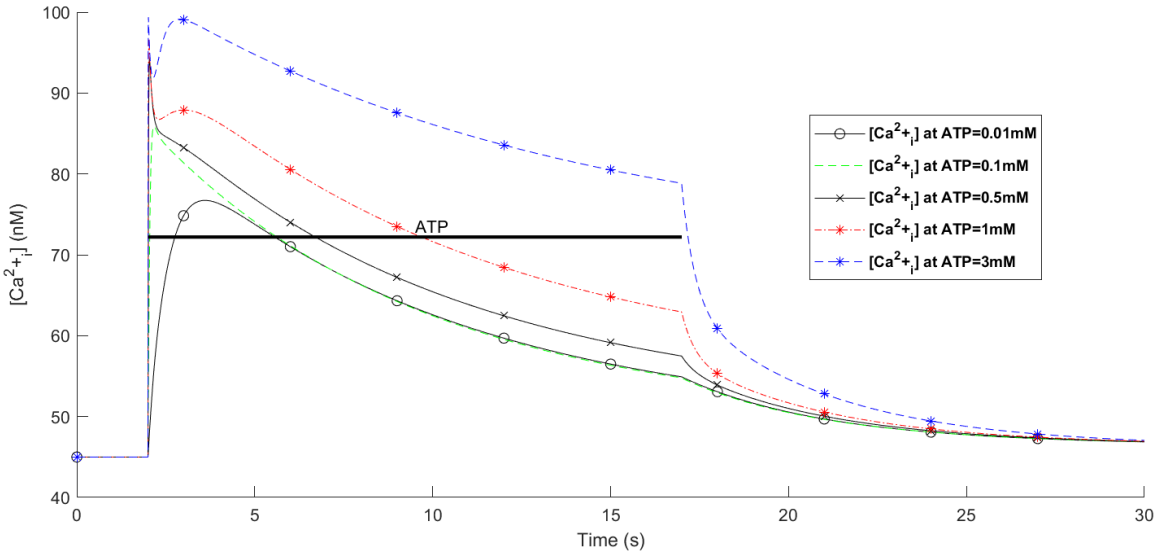

Figure 5.10. Intracellular Ca^{2+} transients from simultaneous activation of both $hP2X_4$ and $hP2X_7$ receptors.

Figure 5.11 shows the $[Na^+]_i$ and V_m dynamics. As is evident, both $[Na^+]_i$ and V_m graphs have similar shapes in contrast to $[Ca^{2+}]_i$ counterparts, as their dynamics are dictated by the action of the P2XRs. It is because NCX channels mainly control the flow of Na^+ cations across the membrane as microglia are reported not to express Na^+/K^+-ATPases [14]. The behaviour of V_m indicates that microglia depolarise rapidly, which is also consistent with experimentally reported data for rate microglia [133]. Emerging evidence shows that the dynamic membrane potential, V_m, plays key role in the regulation/upregulation of biological processes such as cell migration and proliferation [144]. Therefore, the model may be made more biologically plausible by considering

voltage-gated Na^+ channels and $[K^+]_i$ dynamics. It is worth noting that varying the morphological parameters of the model such as S_p and V_p only alters the predicted $[Ca^{2+}]_i$ amplitudes slightly and so does not significantly influence the overall response of the Ca^{2+} dynamics.

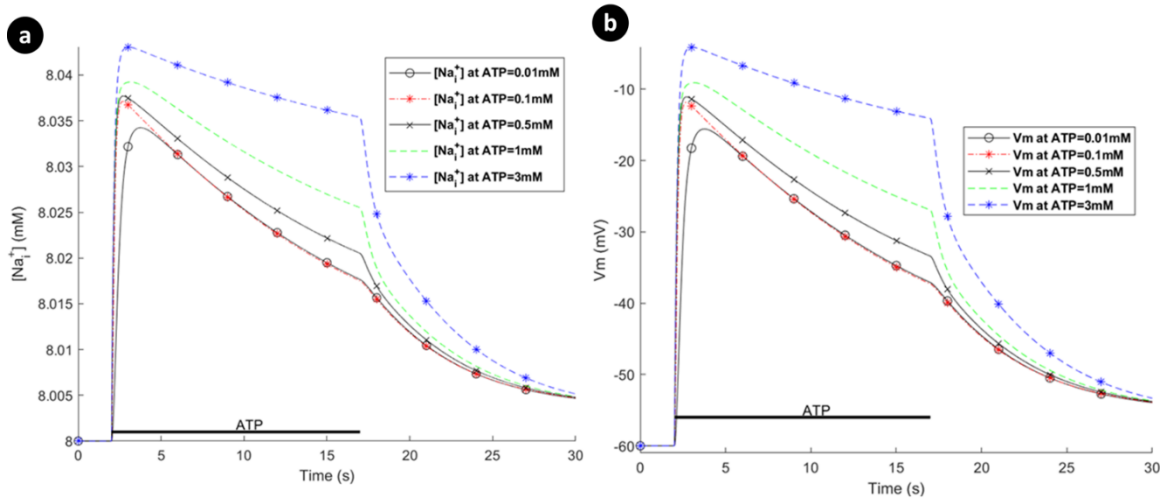

Figure 5.11. (a) Intracellular $[Na^+]_i$, and (b) the membrane voltage dynamics resulting from simultaneous stimulation of $hP2X_7$ and $hP2X_4$ receptors stimulation.

In contrast to the current profile outlined in Figure 5.6 for the $hP2X_7$ only and in Figure 5.8 for the $hP2X_4$ only, the marked difference when both receptors are activated simultaneously (as seen in Figure 5.12), is the domination of the $hP2X_4$ receptor current at high levels of ATP, while the $hP2X_7$ stays constant at higher ATP levels and over a longer duration. In addition, the kink in the concentration profile for Ca^{2+} directly correlates with the initial fall off in the Ca^{2+} current, carried by the PMCA, due to the decaying Ca^{2+} influx by $hP2X_4$ and the increasing Ca^{2+} influx by $hP2X_7$ (see curves for 1mM and 3mM ATP levels).

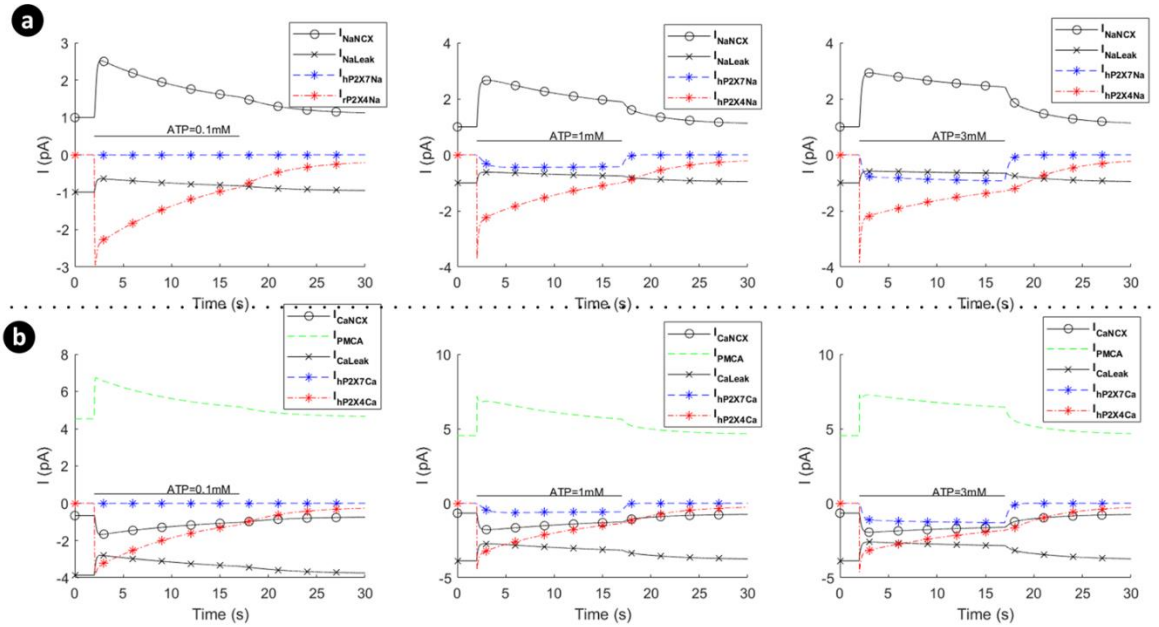

Figure 5.12. Dynamics of absolute currents via simultaneous activation of $hP2X_4$ and $hP2X_7$ receptors. Top (a) and bottom (b) panels quantify the Na^+ and Ca^{2+} components respectively of the model for 0.1mM, 1mM and 3mM ATP.

To summarise, it is inferred that the very transient behaviour of the kinks in Figure 5.10 is indicative of cooperative dynamics between the activation of several P2XRs, PMCA and NCX, where NCX mainly derives the $[Na^+]_i$ extrusion. As such, V_m is similar to the Na^+ dynamic in Figure 5.11 because of a high baseline of $[Na^+]_i$, and leak channels keep microglia sensitive enough to changes in their microenvironment.

5.2.4 Sensitivity Analysis of the Mathematical Model

As demonstrated throughout Chapter 4, P2X-mediated Ca^{2+} dynamics are primarily controlled by ATP-gated P2XRs, NCX, PMCA and leak channels. This section carries out a sensitivity analysis (SA) of the model parameters to elucidate the robustness of the model responses [145]. It is also a powerful means whereby the parameters or components that substantially contribute to the model predictions can be determined. The sensitivity analysis results can provide a detailed insight into the model parameters for future model refinements when new experimental data becomes available in order to calibrate the model

at different levels of agonist. Sensitivity can also be viewed as the inverse of robustness where the sensitivity of parameters gives rise to a quantitative estimate in deviations of model outcomes arising from perturbation of model parameters. Since the behaviour of high-dimensional biochemical reaction networks is often dominated by a small number of parameters, SA helps identify these parameters that can be investigated in further studies.

In this section, two different methods of SA are employed to obtain additional information regarding the P2X model parameters: these methods are local and global sensitivity analysis (LSA and GSA). In LSA, a single parameter (where others are kept constant) is varied and the effect of this perturbation is considered. This process is repeated for all parameters. In contrast to LSA, GSA techniques employ simultaneous perturbations to model parameters, and changes in the model output are monitored. GSA is capable of detecting relationships between a set of parameters. Logarithmic sensitivity analysis (LSA) [146], was initially used to investigate the influence of the model parameters on the model output. LSA is dimensionless and therefore allows comparison of the results conveniently. If *y* is a single response of a system of ODEs, LSA of this variable is defined as

$$S_y = \frac{\partial ln\, y(t,p_i)}{\partial ln\, p_i} = \frac{p_i}{y(t,p_i)} \times \frac{\partial y(t,p_i)}{\partial p_i} \tag{5.1}$$

where p_i denotes the *i*'th parameter. The partial derivative of *y* in Eq. (5.1) with respect to p_i can be approximated by using forward finite difference (FD) [145] as follows

$$\frac{\partial y(t,p_i)}{\partial p_i} \approx \frac{y(t,p_i+\Delta p_i)-y(t,p_i)}{\Delta p_i} \tag{5.2}$$

where Δp_i is a notation for a small change of the parameter p_i.

As a general rule of understanding sensitivity analysis robustness, if the results do not change significantly after the fitted model parameters are perturbed then the sensitivity analysis is said to be robust [145]. For this study, the sensitivity analysis was carried out on the cytosolic Ca^{2+} concentration with respect to the maximum NCX current density ($\bar{J}_{NCX}$), the maximum PMCA current density ($\bar{J}_{PMCA}$), and the parameter sets of the P2X models by

stimulating the model under 1mM ATP. Figure 5.13 illustrates a plot of Eq. (4.2) for parameter perturbations of 0.1% and 1% (note that *x7* and *x4* subscripts represent $P2X_7$ and $P2X_4$ in Figure 5.13). Both graphs are similar, and this verifies the sensitivity analysis robustness of the fitted model. More importantly, the uptake of Ca^{2+} is mainly affected by $\bar{J}_{NCX}$, $\bar{J}_{PMCA}$, g_{x7}, α_{2x4} and β_{2x4}. The intracellular Ca^{2+} concentration exhibits negative and positive sensitivity to PMCA and NCX parameters respectively.

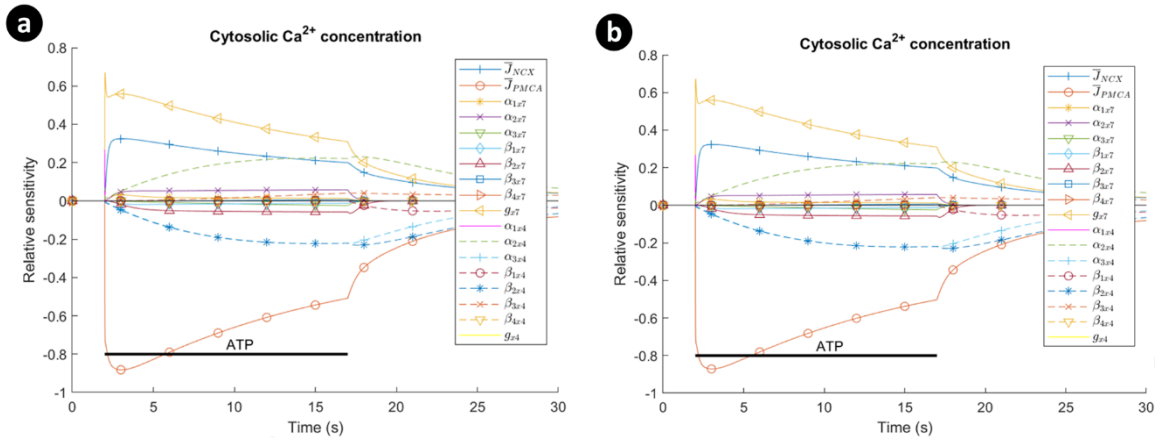

Figure 5.13. The sensitivity analysis of the intracellular Ca^{2+} for ATP=1mM with respect to maximum NCX current density ($\bar{J}_{NCX}$), maximum PMCA current density ($\bar{J}_{PMCA}$), and the parameter sets of $hP2X_7$ and $hP2X_4$ receptors: (a) 0.1% perturbation of the model parameters was employed, namely, $\Delta p_i = 0.001 \times p_i$, and (b) 1% perturbation of the model parameters was used in this case, viz., $\Delta p_i = 0.01 \times p_i$. Horizontal bars show the duration of agonist exposure.

Several techniques exist to carry out GSA. Sobol's method is used in this section, which is a variance-based method [147]. The method does not make any assumption for the input and output relationships of a model. The variance of the model output is decomposed into a combination of variances. A Joint Probability Function (PDF) is employed to make Sobol's terms. A MATLAB implementation of this method developed by [148] was used to perform GSA and study the effect of simultaneous changes of model parameters on cytosolic Ca^{2+} for ATP=1mM. Figure 5.14 shows the computed Sobol's total indices for the peak duration. A peak duration is defined as the time interval at which the transient values of the model output are greater than or equal to the mean of the output throughout the

simulation time. According to Figure 5.14 for total Sobol indices. The five most dominant parameters are α_{3x4}, $\alpha_{2x4,}$ β_{2x4}, β_{2x7} and β_{3x4} in decreasing order. β_{2x7} and g_{x7} have more influence on the output among all other parameters of the $P2X_7$ model. The effect of both P2X conductances is nearly close, while there is a significant variation for most of the corresponding parameters of both P2X models. β_{2x7} and β_{2x4} have the biggest impact on the output among all other backward rate coefficients for each individual model. Interestingly, the global sensitivity of g_{x7} in Figure 5.14 is significantly less influential than its local sensitivity illustrated in Figure 5.13. These LSA and GSA results show that the parameters of the $P2X_4R$ model are mostly dominant in the model sensitivity as a whole.

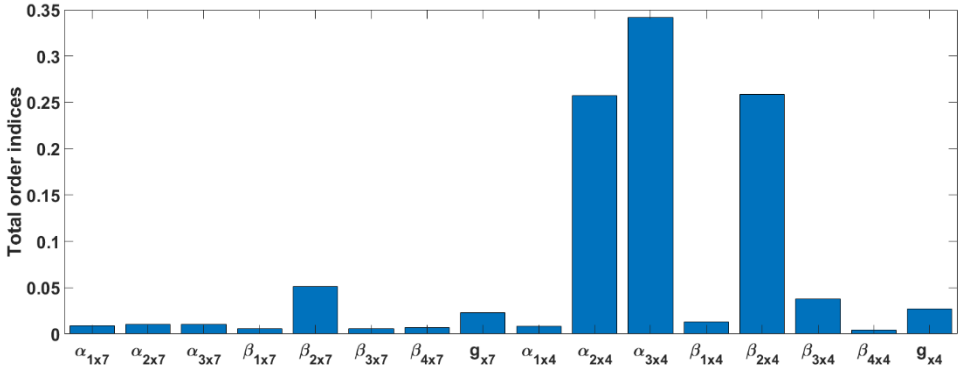

Figure 5.14. Total order Sobol's indices of the intracellular Ca^{2+} model at ATP=1mM for the peak duration.

5.3 Discussion and Summary

Neurotransmitters can modulate intracellular Ca^{2+} and Na^{+} via the activation of microglial receptors, which regulate their homeostatic mechanisms [14]. Microglia express $P2X_4$ and $P2X_7$ purinergic receptors which impact local Ca^{2+} homeostasis. Mathematical models that result in a formal description of agonist binding to purinergic receptors with receptor activation, provide unique tools to unravel the underlying regulatory dynamics of intracellular ionic concentrations. In this research, a minimal computational model for Ca^{2+}, Na^{+} and V_m dynamics of microglia was developed. The binding of ATP to P2XR on microglial processes leads to receptor activation, with the associated influx of Ca^{2+} and Na^{+}. This results in a rise mainly in $[Ca^{2+}]_i$ and V_m hyperpolarising, leading to activation of

the PMCA, NCX and leak channels: it is worthwhile noting that this model allows a detailed investigation into the interplay between the P2XRs, pumps, extruders, membrane voltage and leak channels. The model predictions show that activation and deactivation of $P2X_4$ and $P2X_7$ receptors in microglia generate monophasic and biphasic shapes in conformance to microglia-specific P2X data or other cell-specific data at lower and higher ATP concentrations. Particularly, for the $P2X_7$ receptor, there are two different phases of current initialisation and current facilitation. Simulation observations show that monophasic and biphasic transients are also present in single-cell Ca^{2+} and Na^{+} profiles. The model indicates that the $P2X_7$ receptor maintains significant currents and therefore effect ionic concentrations much more than $P2X_4$ at higher levels of ATP. These data have implications for brain pathology, where elevated levels of ATP are evident [149, 150]. The relative contributions of the P2XRs studied here may provide insight into therapeutic strategies targeting either receptor. For example, $P2X_7$ antagonism has been suggested as a therapeutic intervention for a range of CNS disorders [151-153]; here the modelling data present a read-out of this pharmacological intervention in relation to ionic homeostasis and microglia function. In addition, there are implications from the model with respect to microglial function where their levels of the P2XRs are known to be altered (e.g. Parkinson's disease; [154]).

The model demonstrates that Ca^{2+} dynamics not only rely on different gating properties of P2XRs as a function of ATP pulse protocol but also on the opposing Ca^{2+} currents carried by PMCA and NCX: the latter being continually in the forward mode due to the hyperpolarisation of V_m and $[Ca^{2+}]_i$ fluctuations in the cytoplasm. At ATP levels of 1mM and 3mM, unexpected kinks are observed in the concentration of Ca^{2+} regulated by $[Na^{+}]_i$ and V_m. This kink is a direct consequence of the fast fall-off in $[Ca^{2+}]_i$ due to the continual decrease in the Ca^{2+} influx, via the $P2X_4$ competing with the slow rise in $[Ca^{2+}]_i$ due to the increasing Ca^{2+} influx via the $P2X_7$. Hence there exists a cross-over in the $[Ca^{2+}]_i$ and a kink appears followed by a gradual decrease in $[Ca^{2+}]_i$: the $P2X_4$ receptor dominates the $[Ca^{2+}]_i$ at the onset of the ATP stimulus and thereafter the $P2X_7$ receptor maintains a high level of $[Ca^{2+}]_i$ in the cytoplasm until the removal of the stimulus. The abstraction level of the proposed model facilitates the reproduction of meaningful responses arising from the interplay between the P2XRs, PMCA, NCX and leak channels.

The current experimental data shows a total cellular current where the contribution to the total current comes from Ca^{2+} and Na^{+} influx, and K^{+} efflux. With regards to the latter, the mechanisms underpinning K^{+} efflux are poorly understood and are therefore not considered in this thesis. However, the influx of Na^{+} will affect the NCX and therefore have a downstream effect on Ca^{2+}. Because of this, the contribution to the Na^{+} concentration in the cytoplasm by the P2XRs was considered for a better understanding of the observed Na^{+} and Ca^{2+} dynamics. To the best of our knowledge, there is no theoretical or experimental study of the activation of multiple ionotropic receptors in human microglia. Cultured human microglia experiments failed to isolate $P2X_4$ currents [59] nor did they provide data on the interaction between different P2XRs. However, the model presented in this paper does provide insight into both receptors and how they collectively contribute in terms of Ca^{2+} and Na^{+} dynamics. Moreover, the simulation results in this paper used human data in so far as possible and can inform experimentalists as to the role of Na^{+} influx and how this can affect downstream Ca^{2+} dynamics.

The proposed computational framework provides a strong foundation that can be extended towards a more complete understanding of microglial function, particularly, *in situ* and *in vivo*. The model can also be refined as new experimental data becomes available and to this end, the expansion in human microglia research through the use of induced pluripotent stem cells is of interest [155].

Chapter 6. P2Y-mediated Calcium and PI3K/Akt Signalling in Microglia

6.1 Introduction

This chapter discusses two case studies, including, P2Y-provoked intracellular $[Ca^{2+}]_i$ dynamics, and PI3K/Akt dynamics resulting from simultaneous activation of P2 receptors in microglia. Note that the configuration for numerical model simulations in this chapter was explained in Section 5.1. Firstly, the parameter estimation for the two models is explained with the use of Algorithm 1 given in Section 4.4. The fitted models generate a set of responses for model state variables that are also quantified. Interestingly, it is shown how the optimising framework manages to find the time delay between the two P2X and P2Y mediated Ca^{2+} responses and the upregulation factor of P2X receptors. Secondly, the Ca^{2+} transient responses of the P2Y model are studied along with an estimation of current flows through SERCA and leak channels. Finally, insight is given into the whole model on how P2 receptors regulate Akt dynamics through a cooperative activation of CaMKII. Simulated results provide interesting quantitative insights into different ADP-mediated P2Y calcium and Akt dynamics. Throughout this chapter, it is observed that both Ca^{2+} and Akt dynamics heavily depend on the duration and amplitude of the ADP treatments.

6.2 Numerical Results

6.2.1 Model Fitting and Validation

An evolutionary strategy as described in Section 4.4 and [90] was used to find the optimal values of the P2Y and PI3K/Akt model parameters that capture time-dependent kinetics experimentally observed. Parameters were fitted using an evolutionary optimiser where the aim is to reproduce and experimentally observed the relationship between calcium or pAkt dynamics and ADP stimulus magnitude and duration, as illustrated in Figure 6.1 and Figure 6.2(a). As can be seen in these figures good fits were obtained using the parameters given

in Table 6-1 for the biophysical Ca^{2+} model and Table 6-2 for the mathematical PI3K/Akt model. The P2Y model is crucial as it provides a method of addressing fundamental questions such as how calcium dynamics is governed by the concentration of cytosolic IP_3, IP_3R density and state and also calcium uptake by intracellular Ca^{2+} stores. The complete set of state changes of both models are shown in Figure 6.1(b) and Figure 6.2(b). Interestingly, Figure 6.2(b) unravels how two delayed Ca^{2+} spikes in the model make CaMKII induce two peaks in the pAkt regime (more importantly, this is reflected in all state variables of the model where all have two humps as well).

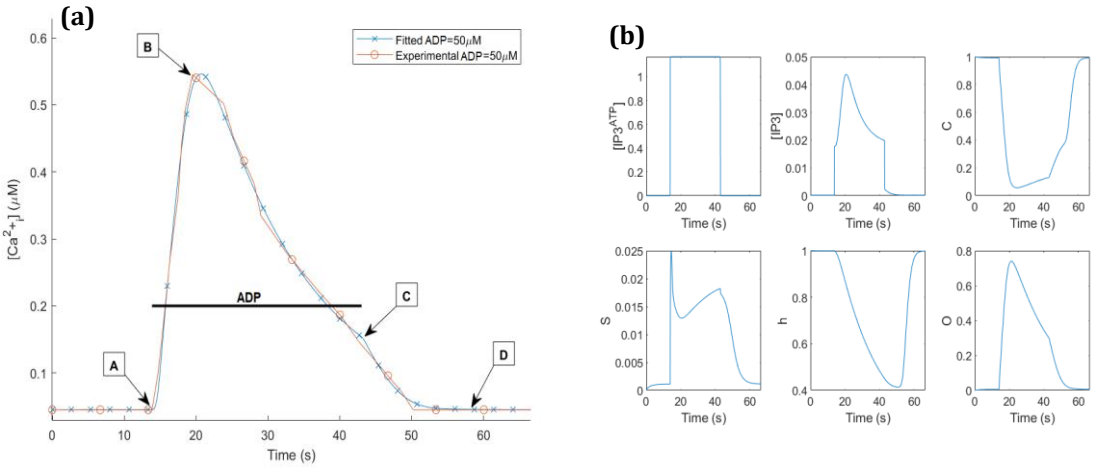

Figure 6.1. (a) Fitted intracellular Ca^{2+} upon an ADP treatment of 50μM within 29 seconds via activation of the $P2Y_{12}$ receptor in human microglia in comparison with experiments [61], and (b) transient responses of the state space to 50μM ADP for the $P2Y_{12}$ model in human microglia. These diagrams are derived from the response of the model to (a) by numerical simulation. It shows the IP_3R model is mainly responsible to form the shape of the cytosolic Ca^{2+} in contrast to the PLC pathway and IP_3 degradation just by its four state variables and using three variable kinetic rates as depicted in Figure 4.5.

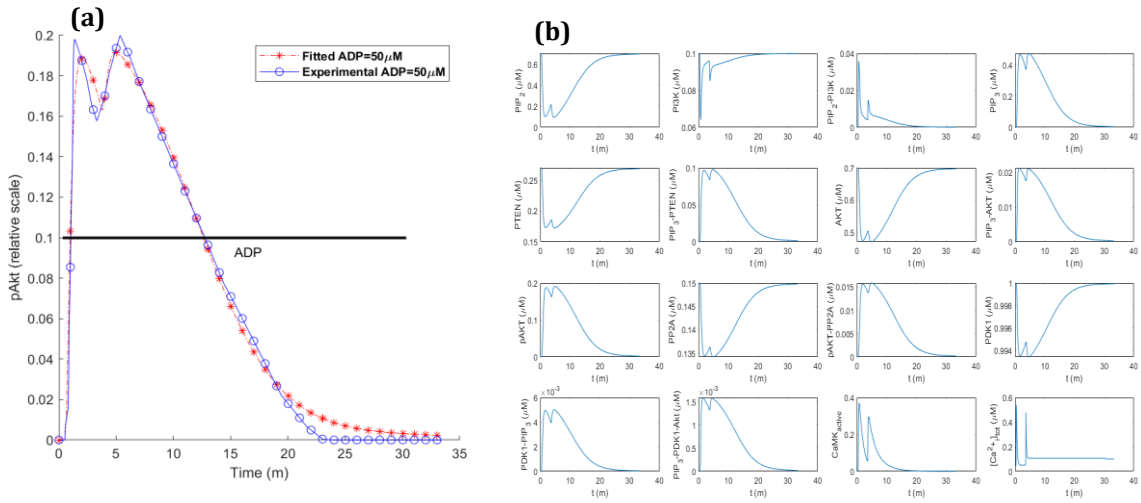

Figure 6.2. (a) Fitted pAkt upon an ADP exposure of 50μM within 30 minutes via activation of the $P2Y_{12}$ receptor in rat microglia, and (b) transient responses of the state space to 50μM ADP for the PI3K/Akt model. Experimental data comes from [62]. Note that the pAkt trace in (a) was obtained by interpolating five data points reported in [62] to a spline curve, where all data points were first normalised and then rescaled to a nominal of 0.2 to show pAkt relative activity.

Table 6-1. Parameters for the mathematical model and non-zero initial conditions of the P2Y-mediated calcium signalling in human microglia.

Parameter	Value	Unit	Description	Source
τ_{ip3}	0.0113	s^{-1}	IP_3 degradation time constant	Fitted
r_{ip3}	2.0644	μMs^{-1}	Rate of IP_3 production	Fitted
K_{PLC_δ}	2.083	μM	Ca^{2+} affinity of PLC_δ	Fitted
$\overline{PLC'_\delta}$	27.136	μMs^{-1}	Maximal rate of IP_3 production by PLC_δ	Fitted
K_δ	4.404	μM	Inhibition constant of PLCδ activity	Fitted
$\bar{r}_{5p}$	66.168	s^{-1}	IP_3 degradation rate by IP_3^{5p}	Fitted
$\bar{v}_{3K}$	14.844	μMs^{-1}	Maximum degradation rate by IP_3^{3k}	Fitted
K_D	66.974	μM	Ca^{2+} affinity of IP_3^{3k}	Fitted
K_3	27.798	μM	IP_3 affinity of IP_3^{3k}	Fitted
α_1	14.771	$(\mu M)^{-1}s^{-1}$	Rate constant for C → S	Fitted
α_2	321.253	$(\mu M)^{-1}s^{-1}$	Rate constant for S → O	Fitted
α_3	6.782	s^{-1}	Outward rate constant for S → D	Fitted

α_4	4.105	s^{-1}	Maximal IP_3R rate	Fitted
α_5	0.0158	s^{-1}	Ca^{2+} leakage rate from ER	Fitted
β_1	2.296	s^{-1}	Rate constant for S → C	Fitted
β_2	3.053	s^{-1}	Rate constant for O → S	Fitted
β_3	0.0789	s^{-1}	Rate constant for D → S	Fitted
β_4	1	s^{-1}	Rate constant for D → C	Fitted
K_s	1	μM	Ca^{2+} affinity of H_1 function for IP_3R	Fitted
a	45×10^{-3}	μM	Coefficient of exponential β function for IP_3R	Fitted
b	1×10^{-3}	μM	Coefficient of exponential β function for IP_3R	Fitted
C_0	2	μM	Total free cytosol Ca^{2+} concentration	[80]
C_1	0.185		Ratio of ER volume to cytosol volume	[80]
$\bar{J}_{SECRA}$	6.516	$\mu M s^{-1}$	Maximum SERCA current density	Fitted
K_{SECRA}	0.656	μM	Ca_i^{2+} for half activation of SERCA in IP_3 sensitive store	Fitted
$C\|_0$	1		Initial value of C	
$[Ca_i^{2+}]_0$	45×10^{-3}	μM	Initial Ca_i^{2+}concentration	

Table 6-2. Parameters and non-zero initial conditions of the total Ca^{2+}, CaMKII and PI3K/Akt models in microglia

Parameter	Value	Unit	Description	Source
α	14.108		Ca^{2+} scaling factor	Fitted
t_d	3.293	m	Delay due to Ca^{2+} diffusion	Fitted
$CaMK_0$	1.999		Fraction of active CaMKII at equilibrium	Fitted
$K_{m,CaM}$	7.041	μM	Hill coefficient for CaMKII model	Fitted
α_{CaMK}	2920.712	m^{-1}	A rate of CaMKII	Fitted
β_{CaMK}	0.7317	m^{-1}	A rate of CaMKII	Fitted
a_1	121.149	$(\mu M)^{-1}m^{-1}$	An association rate for the PI3K pathway	Fitted
a_2	7.101	$(\mu M)^{-1}m^{-1}$	An association rate for the PI3K pathway	Fitted
a_3	5.407	$(\mu M)^{-1}m^{-1}$	An association rate for the PI3K pathway	Fitted
a_4	45.950	$(\mu M)^{-1}m^{-1}$	An association rate for the PI3K pathway	Fitted
a_5	9.312	$(\mu M)^{-1}m^{-1}$	An association rate for the PI3K pathway	Fitted
a_6	1.009	$(\mu M)^{-1}m^{-1}$	An association rate for the PI3K pathway	Fitted
a_7	0.514	$(\mu M)^{-1}m^{-1}$	An association rate for the PI3K pathway	Fitted
b_1	0.010	m^{-1}	A rate for activation of protein in the PI3K pathway	Fitted
b_2	3.345	m^{-1}	A rate for activation of protein in the PI3K pathway	Fitted
b_3	23.888	m^{-1}	A rate for activation of protein in the PI3K pathway	Fitted
b_4	30.080	m^{-1}	A rate for activation of protein in the PI3K pathway	Fitted
b_5	832.201	m^{-1}	A rate for activation of protein in the PI3K pathway	Fitted
b_6	10.085	m^{-1}	A rate for activation of protein in the PI3K pathway	Fitted
b_7	0.0945	m^{-1}	A rate for activation of protein in the PI3K pathway	Fitted
c_1	33.859	m^{-1}	A disassociation rate for the PI3K pathway	Fitted

c_2	2.572	m^{-1}	A disassociation rate for the PI3K pathway	Fitted
c_3	33.196	m^{-1}	A disassociation rate for the PI3K pathway	Fitted
c_4	44.274	m^{-1}	A disassociation rate for the PI3K pathway	Fitted
c_5	4.602	m^{-1}	A disassociation rate for the PI3K pathway	Fitted
$[\mathbf{PIP_2}]_0$	0.7	μM	Initial PIP_2 concentration	[108]
$[\mathbf{PI3K}]_0$	0.1	μM	Initial PI3K concentration	[108]
$[\mathbf{PTEN}]_0$	0.27	μM	Initial PTEN concentration	[108]
$[\mathbf{Akt}]_0$	0.7	μM	Initial Akt concentration	[108]
$[\mathbf{PP2A}]_0$	0.15	μM	Initial PP2A concentration	[108]
$[\mathbf{PDK1}]_0$	1	μM	Initial PDK1 concentration	[108]

6.2.2 Human P2Y-mediated Calcium Dynamics Predictions

In this section, we aim to study calcium dynamics in human microglia due to the activation of the $P2Y_{12}$ receptor. Figure 6.3 predicts transient responses of $[Ca^{2+}]_i$ of the model as a function of different ADP applications. The graphs prompt that the calcium curves rapidly decrease in the presence of ADP followed by a steep increase, particularly, for ADP levels greater than 20μM. When ADP is shortly applied at high concentrations for 2.5 seconds in Figure 6.1(a), a fast Ca^{2+} is evoked but its amplitude is smaller than for a wide range of ADP exposures in comparison with all other cases.

Microglia preserves a stable submicromolar level of cytosolic Ca^{2+} at rest. For Ca^{2+} homeostasis, microglia are required to balance three interacting components in the model, including, IP_3R, SERCA and leak channel. Furthermore, when the receptor is activated, IP_3 dynamics induce a large increase in $[Ca^{2+}]_i$ that is usually restored to its resting levels. Figure 6.4 shows how microglia achieve these important tasks where SERCA is mainly responsible by pumping Ca^{2+} back into the intracellular store. This kind of active homeostatic state is an illustration of the microglial function *in vivo*, because if SERCA is inhibited then Ca^{2+} stores are depleted. $[Ca^{2+}]_i$ generally, peaks within 4-7 seconds of ADP application. A typical theoretical time course of human IP_3 has been shown in Figure 6.1(b) where it reaches a maximum at approximately 6.8s after the application of ADP and the initial rise of Ca^{2+} and IP_3 follows the initial increase of IP_3^{ADP} which models activated GPCR levels. Desensitisation of the receptor gives rise to a fall in IP_3^{ADP}, IP_3 and $[Ca^{2+}]_i$ on a time space of seconds.

The different patterns of Ca^{2+} predicted for human microglial $P2Y_{12}$ receptor by different agonist concentrations and durations show that this receptor is capable of notifying the microglia about the event that happened in the host tissue (such as neurons and astrocytes) requiring the attention of microglia. More notably, the model succeeds in capturing the dual requirement of preserving homeostasis while providing a response when there is enough agonist concentration. Microglia must be sufficiently sensitive to their microenvironment to generate a response in case of an injury without being activated prematurely.

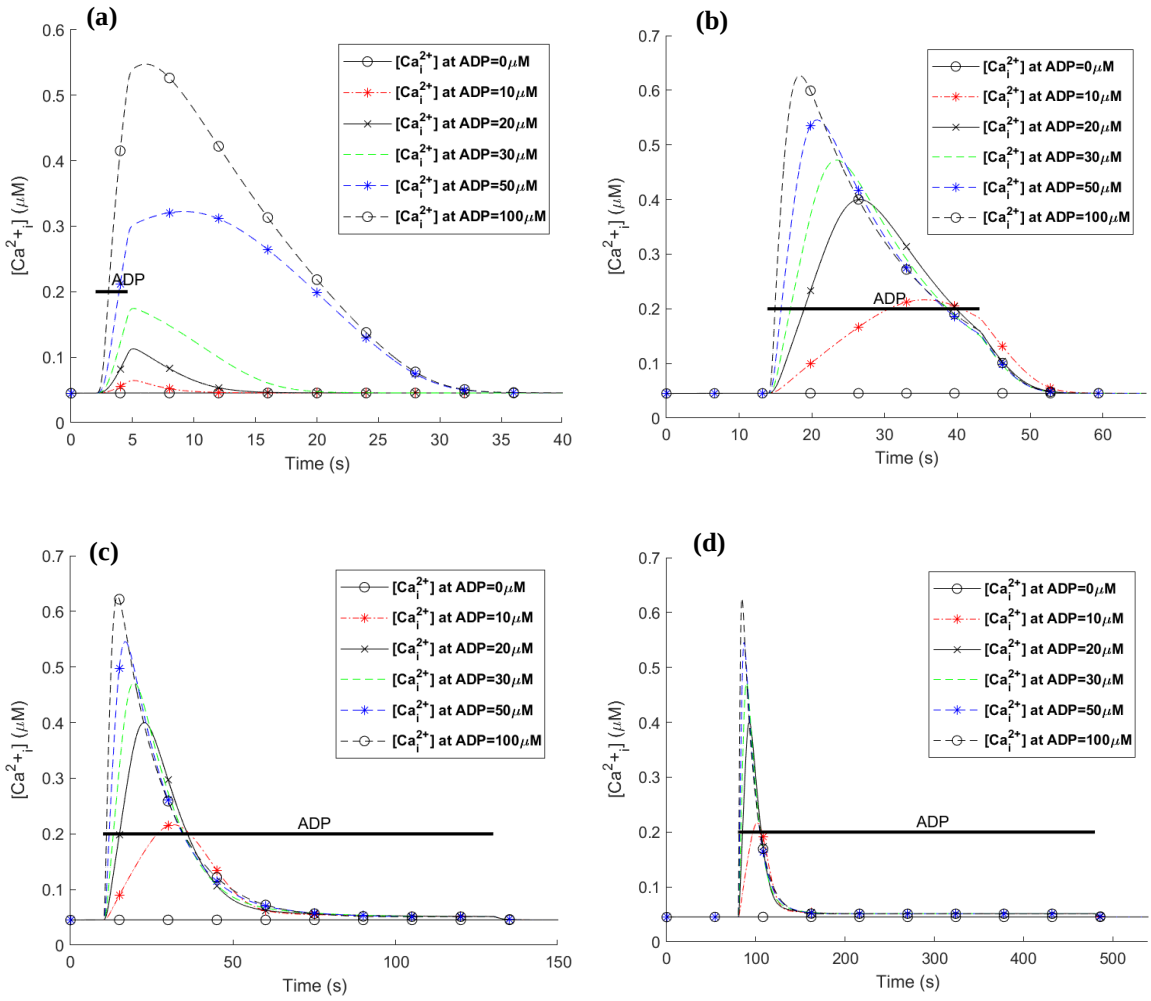

Figure 6.3. Prediction of different patterns in intracellular calcium transients upon different ADP pulse treatments within various time intervals via activation of the $P2Y_{12}$ receptor. Horizontal bars show the duration of ADP application that activates human microglial cells.

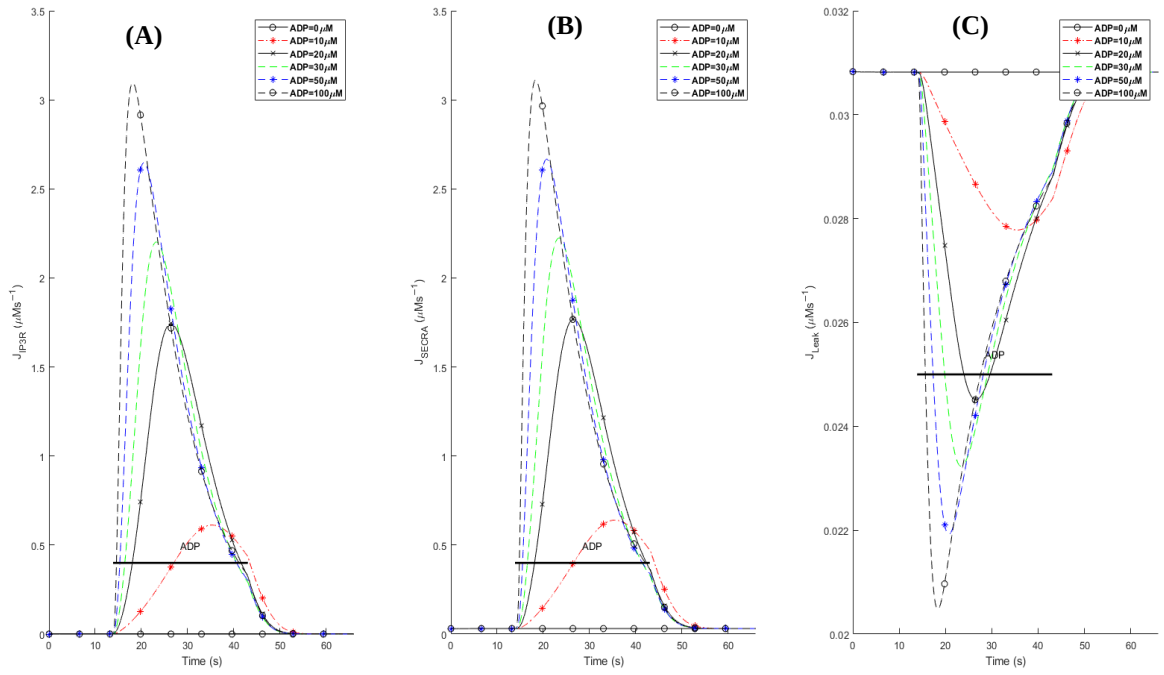

Figure 6.4. Estimation of current components for Figure 6.3(b). (A) Ca^{2+} flux through IP_3R enters the intracellular compartment. (B) Ca^{2+} flux that is pumped out by SERCA. (C) Ca^{2+} flux that is due to the leak channel.

6.2.3 PI3K/Akt Signalling

As the last simulation-based experiment, the PI3K/Akt model was activated by different levels of ADP to investigate the effect of input amplitude on the production of pAkt. Transient responses of total Ca^{2+} followed by pAkt are shown in Figure 6.5. As Figure 6.5(a) promotes both $P2Y_{12}$ and P2X receptors elevate the intracellular Ca^{2+}, in where the first and second spikes correspond respectively to $P2Y_{12}$ receptor and P2X receptors. The Ca^{2+} response of the $P2Y_{12}$ receptor rapidly vanishes within a few minutes (i.e., goes to baseline), while P2X receptors quakily trigger a fast response followed by a consistent Ca^{2+} flow throughout ADP exposition but lower than its peak.

Distinguishably different patterns of pAkt appear in Figure 6.5(b) as a function of ADP amplitude. For lower ADP levels, the amplitude of the first peak in the pAkt profile is significantly less than the second. As the first hump in Figure 6.5(b) is formed by the first Ca^{2+} spike of Figure 6.5(a), it implies that the peak magnitude of Ca^{2+} must be the main

factor for the difference between the amplitude of the two humps in Figure 6.5(b). As seen in the first Ca^{2+} spike of Figure 6.5(a), Ca^{2+} mediated by $P2Y_{12}$ is smaller than Ca^{2+} mediated by P2X receptors for lower ADP levels. In other words, because Ca^{2+} dynamics dictate the activation and regulation of the PI3K/Akt pathway, it is concluded that for high levels of ADP both types of receptors almost evenly contribute to the model response.

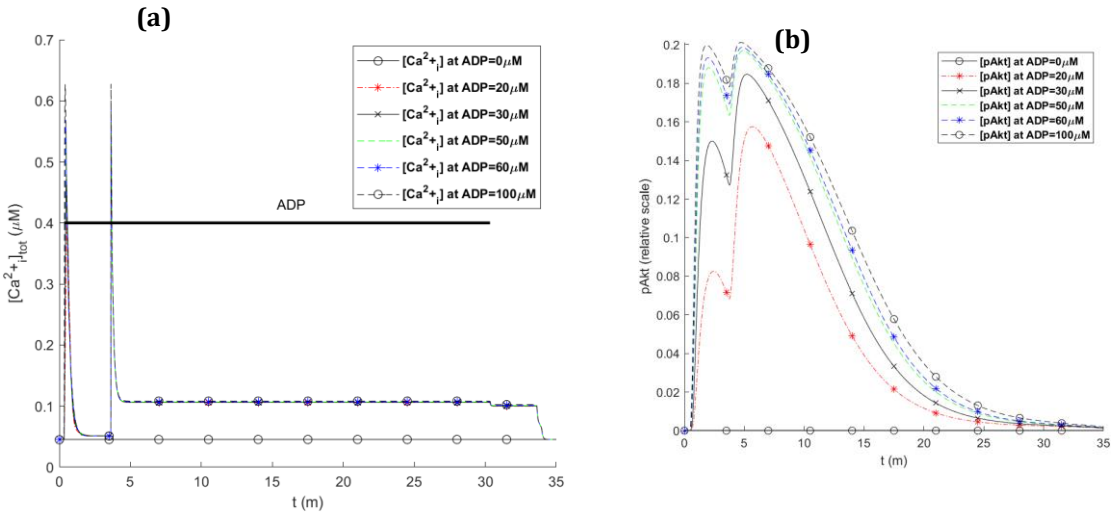

Figure 6.5. Prediction of different patterns in induced pAkt with respect to different ADP pulse treatments when $P2Y_{12}$ and P2X receptors are simultaneously activated in microglia: (a) total cytosolic Ca^{2+} in the somatic region, and (b) simulation of pAkt.

6.3 Discussion and Summary

Mathematical modelling has been performed to study different phases from binding ADP to $P2Y_{12}$ receptor and subsequently IP_3 and Ca^{2+} transient responses in microglial cells and how PI3K/Akt is controlled in pursuit of investigating the machinery behind microglial directed motility. A biophysical model of the PI3K/Akt pathway was proposed and subsequently developed that can capture the intricacy of experimentally published data for microglial pAkt. The model can capture the intricate behaviour of the elements taking part in the signal transduction pathways ending up at cytosolic Ca^{2+} and pAkt production in microglia. Regulation of cytosolic calcium (Ca^{2+}) dynamics is fundamental to microglial functions. Temporal and spatial Ca^{2+} fluxes are induced from a complicated signal

transduction pathway linked to brain ionic homeostasis. Subsequently, a quantitative description was given to provide insights into the secondary messenger system of microglial cells. The precise details of how a metabotropic receptor activation results in intracellular responses depend on receptor and cell type and there is a scarce body of research sources on how $P2Y_{12}$ works in microglia, particularly for humans that are of interest. Very little is known about the internals of this receptor. This peculiarity was specifically found for human IP_3R receptor where none of the existing models was able to conform to experimental Ca^{2+} responses (in compliance with our previous work [90] on microglial human P2X receptors). Consequently, a compact biophysical model was proposed for the capture of Ca^{2+} current associated with the IP_3 receptor on the ER region, which is composed of only four state variables. The intricate pAkt experimental data which is supported by experimental evidence suggests that both P2Y and P2X receptors actively take control over how PI3K/Akt signalling is regulated. It was shown that, through mathematical modelling, a two-compartmental computational Akt model consisting of a soma (which hosts the P2Y receptor) and a process (which hosts both $P2X_7$ and $P2X_4$ receptors) can faithfully capture two peaks observed in experimentally published data. This hypothesis is made possible chiefly due to the assumption that cytosolic Ca^{2+} mediated by P2X receptors takes time to arrive in the soma compartment through diffusion, therefore, total Ca^{2+} was modelled as a linear superposition of P2Y and P2X Ca^{2+} responses.

The computational framework proposed here provides a primary basis that can be extended towards a better understanding of microglial activation, particularly, *in vivo*. The model can also be refined as new experimental data becomes available. The development of a more elaborate model for P2Y-mediated calcium signalling clearly calls for both kinetic and steady-state data of the PLC pathway and IP_3R channel by the neuroscience community. Fitting of the model parameters must be performed using automated optimisation techniques discussed in this thesis and [90].

The entire model shows that intracellular Ca^{2+} dynamics arise from the coupled interaction between the $P2Y_{12}$ receptor, IP_3 channel, Ca^{2+} removal from the cytosol by SERCA pump and Ca^{2+} leak channel. Ca^{2+} responses are dominated by IP_3R and SERCA pump in that the Ca^{2+} leak channel takes up the role of maintaining $[Ca^{2+}]_i$ at resting microglia. Parameter adjustment was used to allow these models to capture human $P2Y_{12}$

microglia data. The model architecture allowed a high degree of simplicity, accuracy, and predictability of P2Y-mediated Ca^{2+} levels. Simulations in Figure 6.3 show that microglial human $P2Y_{12}$ works very fast by generating IP_3 and activating the IP_3 receptor in a time scale of seconds. The model likewise will direct researchers to investigate which types of SERCA isoforms and IP_3R are involved in human microglia with their underlying kinetic data. This means that many of the unknown rate parameters will be determined in the future to refine this model. It was also shown that the $P2Y_{12}$-mediated response is highly a function of ADP for its both duration and amplitude. For long applications of ADP, levels of $[Ca^{2+}]_i$ is independent of the duration but dependent on the amplitude; namely, the rise and fall of the response are very fast in a monotonic manner that completes in seconds and there is no basal-level plateau before ATP is removed as compared to other cell-specific $P2Y_{12}$ receptors and widely seen in other types of metabotropic receptors (e.g., $P2Y_2$ and $P2Y_6$ receptors) [60]. Therefore, it is necessary for experimental investigation to study if increased levels of Ca^{2+} want to stay over a prolonged space of time whether recycling the PI network and $P2Y_{12}R$ and resupplying PIP_2 are required or not. Furthermore, it is highly desirable to experimentally characterise the activity of elements in the PI3K pathway (such as PIP_2, PIP_3, PTEN, etc.) individually and incorporate them within the model in this thesis to provide more accurate insight for conducting further research on human microglia motility.

The biophysical P2Y and PI3K/Akt models developed in this project will improve our quantitative understanding of P2Y-mediated microglial physiology. Understanding the mechanisms underpinning the PI3K/Akt pathway and the interactions between microglial receptors activated by extracellular nucleotides and other cytosolic transporters provides a step forward in resolving the qualitative link between purinergic receptors and microglial physiology and their contribution to brain pathology. Additionally, understanding the interplay between Ca^{2+} and PI3K signalling can provide a basis for the development of new therapeutic interventions.

Chapter 7. Conclusion and Future Works

7.1 Introduction

Although tremendous advances have been made by different research fields in the neuroscience community, today's available drugs can imperfectly control brain disorders and diseases, mainly due to a central focus on neural drug development. Glial cells play essential roles in maintaining a healthy brain microenvironment and extensively dictating how neurons operate. Therefore, a malfunction of the interaction between neurons and glia or glial dysfunction itself is reflected in neurodegenerative and neurological diseases. Microglia, a type of glial cells, perform many tasks while interacting with neurons, astrocytes, and oligodendrocytes. Despite moderate advances in the characterisation of microglia in laboratory rodents, very little information is known about the physiology of microglia in the human brain. This is a challenging task as discussed in Chapter 1, and consequently, this thesis attempts to reduce this gap through mathematical modelling.

The literature review was presented from physiological and mathematical modelling points of view in Chapters 2 and 3 respectively. An exploration of a wide range of ionotropic and metabotropic receptors along with ion channels that form complex, coordinated machinery for regulating microglial cells was given in Chapter 2. From the discussion, it was clear that $P2X_4$, and $P2X_7$ and $P2Y_{12}$ receptors drive significant dynamics of microglial functions such as intracellular Ca^{2+} transients and reorganisation of the actin cytoskeleton involved in the directed motility of microglia.

As there is a scarce amount of research sources for the mathematical modelling of microglial functions and little experimental data is available, Chapter 3 is mainly dedicated to investigating candidate strategies that could be exploited throughout this research. More importantly, two major modelling requirements are discussed, including, Markov modelling of cellular receptors and optimisation of model parameters to data sets. In the former, several examples are given to illustrate how a chain of Markov states in terms of ordinary differential equations can precisely describe the gating properties of a variant of ion channels and receptors. In contrast, the requirement of using non-classical optimisation

algorithms in the latter stems from the complexity and inability of providing data for numerous observables of a Markov model or biochemical reaction network of biological systems. Finally, this chapter studies previous works in the context of this thesis for modelling P2X/P2Y-mediated calcium signalling and PI3K/Akt dynamics. It is concluded that it is essential to build models capable of producing and predicting meaningful, biological transient responses specific to human microglia even though some efforts had been made in other cell lines.

Chapter 4 introduced the development of all the mathematical models for the thesis. The main purpose was to capture different aspects of human microglia as much as experimental data was available. The novel models, as follows, addressed the shortcomings in existing models where they were unable to represent a vast majority of human microglial data.

Firstly, we developed a novel biophysical model of P2X-mediated electrophysiology of human microglia (i.e., intracellular sodium Na^+ and calcium Ca^{2+} dynamics, and membrane potential) in response to agonist/ATP binding. Specifically, a novel compact biophysical model was proposed for the capture of whole-cell patch-clamp currents associated with $P2X_4$ and $P2X_7$ receptors utilising human data, which is composed of only four state variables. Variable exponential kinetic rates as functions of the agonist were introduced into the model in a similar way to the approach of Hodgkin and Huxley formalism; therefore, both P2X models became a minimal realisation of all the existing Markov-based P2X models, while representing all major gating properties of P2XRs. The entire model showed that intricate intracellular ion dynamics arise from the coupled interaction between $P2X_4$ and $P2X_7$ receptors, NCX, Ca^{2+} extrusion by PMCA, and Ca^{2+} and Na^+ leak channels. Both P2XRs are modelled as two separate ATP-gated Ca^{2+} and Na^+ conductance channels, where stoichiometry is the removal of one Ca^{2+} for the hydrolysis of one ATP molecule. Two unique sets of model parameters were determined using an evolutionary algorithm to optimise fitting to experimental data for each of the receptors.

Secondly, microglial-directed motility involves a complex family of intracellular signalling pathways that are mainly controlled by cytosolic Ca^{2+} signalling and activation of PI3K/Akt. The main goal of the next model was to develop a mathematical model for these two complex intracellular events and investigate the interconnecting role of the PI3K

pathway to Ca^{2+}. A biophysical model for Ca^{2+} activation of the PI3K/Akt pathway in microglia is developed where Ca^{2+} influx via P2YR and P2XR contribute to intracellular Ca^{2+} concentration. The proposed model supports the hypothesis that Ca^{2+} influx via P2YR and P2XR can explain the experimentally observed twin peaks in the pAkt profile. In the biophysical model, the PI3K/pAkt pathway was activated by CAMKII that was in turn regulated directly through two cytosolic Ca^{2+} sources mediated by P2 receptors. The model was shown to be capable of capturing the response of Ca^{2+} and phosphorylated Akt to extracellular ADP amplitude and duration. Furthermore, a new IP_3 receptor model extending the P2XR base model was proposed to tackle the limitations of existing IP_3R models for human microglia.

Two subsequent chapters describe the results of the models by performing an extensive set of simulation-based experiments.

In Chapter 5, the activation of P2XRs by ATP on microglial processes leads to an influx of Ca^{2+} and Na^{+}. This subsequently increases $[Ca^{2+}]_i$ rapidly and hyperpolarises the membrane potential, thereby resulting in the activation of the PMCA, NCX and leak channels. It was shown that different dynamics of P2XRs not only affect Ca^{2+} as a function of ATP but rather the opposing Ca^{2+} currents carried by PMCA and NCX intricately change the form of the time course of $[Ca^{2+}]_i$. Particularly, in high levels of ATP, unexpected kinks are formed in the Ca^{2+} concentration which was previously unexplained.

Chapter 6 investigates P2Y-mediated Ca^{2+} dynamics in human microglia and the influx of Ca^{2+} meditates the PI3K/Akt pathway. Simulated results provide interesting quantitative insights into different ADP-mediated P2Y calcium and Akt dynamics. For example, cytosolic calcium only spreads in the cytosol in a short amount of time for long ADP pulse exposures. In all predictions, pAkt behaves intricately by generating kink-like transient responses, which is postulated due to a direct interplay between P2Y and P2X receptors. It was also predicted how the agonist concentration regulates twin peaks in the time course of pAkt.

7.2 Summary of Thesis Contributions

This thesis set out with the objective of investigating P2-mediated signalling in human microglia. Due to the lack of enough experimental information and a theoretical basis for the biology of microglial cells in the human brain, which is attributed to the difficulty in studying them, this research addressed these obstacles through mathematical modelling. Not only do the findings of this study pave the way for neuroscientists for carrying out experimental research and conducting the development of novel therapeutic strategies, but also they bring us a major step closer to a *virtual microglia model* (namely, the computational framework can be further extended to include other components, thereby realising a complete model of microglial plasma membrane electrophysiology). The outcomes of this study were published in two journals as given in Appendix C. The contributions of this thesis as demonstrated in Chapters 4 to 6 are fourfold.

7.2.1 Mathematical Model of Human P2X-mediated Electrophysiology in Microglia

From Chapter 2, it was evident that both $P2X_4$ and $P2X_7$ receptors are found in human microglia. However, unfortunately, previous studies were unable to characterise $P2X_4$ current in human microglia. On the other hand, Ca^{2+} dynamics are utterly unknown upon simultaneous activation of P2X receptors in human microglia. These shortcomings coupled with the limitation in studying human microglia encouraged us to resort to mathematical modelling in our quest for providing the first-time insight into P2X-mediated Ca^{2+} signalling. Two novel, new Markov models were developed from scratch using human data. As discussed, they were less computationally complex in terms of the number of state variables as compared to existing models. Consequently, this minimality allowed us to assume that kinetic rates are exponential in favour of more reliable predictions for the models as a function of agonist. Finally, a compartmental model exploited these P2X models along with a model of known microglial transports and pumps by which three significant quantities were quantified, including, intracellular Ca^{2+} and Na^{+}, and membrane

potential, in microglia processes. To the best of our knowledge, this was the first attempt to feasibly investigate the P2X-mediated electrophysiology of human microglia.

7.2.2 Mathematical Model of Human P2Y-mediated Calcium Signalling in Microglia

$P2Y_{12}R$ substantially contributes to the intercellular Ca^{2+} by regulating the IP_3 receptor which resides on the ER region. This thesis constructed the first biophysical model of calcium dynamics in human microglia when the second messenger system is activated by the $P2Y_{12}$ receptor. Specifically, a Markov model comprised of four state variables was proposed by modifying the base P2X model and changing its variable kinetic rates. In the IP_3R model, a first-order hill function was used in the transition between the sensitisation and desensitisation stages of the receptor, where all other rates were assumed to be constant or directly controlled by its ligand. We estimated the parameters of the entire model by taking benefit from the same optimisation algorithm used for the P2X model. Overall, even though experimental data for all species of the model except Ca^{2+} was unavailable, the developed model managed to capture the interplay between extracellular ADP, IP_3 and cytosolic Ca^{2+} dynamics.

7.2.3 Mathematical Model of PI3K/Akt Pathway in Microglia

Directed motility of microglia is driven by the elevation of intracellular Ca^{2+}, where the PI3K/Akt pathway is potentially involved in the polymerisation of the actin cytoskeleton. Another major contribution of this study focused on modelling this highly complex pathway in microglia for the first time as we were aware of. On one side of the coin, as supported by experimental evidence, the existence of intracellular Ca^{2+} is mandatory for observing the production of pAkt in microglia which is followed by its activation. On the other hand, experimentally published pAkt data for microglial cells contains two peaks. This research work postulated that they were a confluence of two sources of Ca^{2+} mediated by P2Y and P2Y receptors, in which the first and second peaks are formed by P2Y and P2X receptors respectively. Subsequently, a comprehensive mathematical model of the

PI3K/Akt pathway consisting of three major components, including, a superposition of P2Y-mediated Ca^{2+} and delayed P2X-mediated diffusion Ca^{2+}, CaMKII, and the main regulators of Akt phosphorylation, was built for microglia. It was shown that a minimum set of elements involved in the model was necessary to aid the parameter estimator in proving our hypothesis mathematically. Intriguingly, it was found that the Ca^{2+} response of the P2X-initiated compartment must be potentiated, which could be highly likely as an influence of $P2X_4R$ and/or $P2X_7R$ upregulation.

7.2.4 New Insights into P2-mediated Signalling in Microglia

The simulation-based prediction in this thesis significantly contributes to our understanding of the physiology of human microglia. The models were numerically simulated with a wide range of agonist concentrations and durations indicating how they affect intercellular events upon the activation of microglia. It was shown that when P2X receptors are simultaneously activated, the presence of voltage-dependent transporters (i.e., the NCX) can unexpectedly change the behaviour of Ca^{2+} for certain agonist levels. It is also indicative of the importance of the membrane potential in creating intricate behaviours in non-excitable cells such as microglia. The P2X model disclosed the dynamics of Na^{+}, Ca^{2+} and the membrane potential for the first time in human microglia. In addition, this thesis showed which kinetic parameters are dominant and responsible for regulating P2X-mediated Ca^{2+} dynamics. The model predictions showed that the effect of the $P2Y_{12}$ receptor is very short in contrast to P2X receptors in the long presence of the agonist. The hypothesis, that both P2X and P2Y receptors significantly modulate the Akt phosphorylation, backed by the PI3K/Akt model was also observable in all simulations. This work unveiled how the ADP amplitude can create twin peaks with distinct heights.

The results of this study urge carrying out extensive experiments with help of mathematical tools for a better understanding of microglial electrophysiology with as many channels and receptors involved as possible. Finally, the results of this thesis can form a basis for the investigation of therapeutic approaches for brain dysfunction [11, 29-31, 34].

7.3 Future Works

This thesis has added a considerable wealth of work to the physiology of microglia for which our developed mathematical tools have successfully provided profound biological information. The computational framework proposed here provides a primary basis that can be extended towards a better understanding of microglial activation, particularly, *in vivo*. The model can also be refined as new experimental data becomes available. Although there remains a substantial body of theoretical and experimental works to be done in the scope of this thesis, there are further extensions to the base framework presented in this thesis to assist neuroscientists.

The development of a more elaborate model for P2Y-mediated calcium signalling clearly calls for both kinetic and steady-state data of the PLC pathway and IP_3R channel by the neuroscience community. A major extension is to model potassium dynamics through $P2Y_{12}$ activation, which depends on protein kinase C (PKC), intracellular Ca^{2+} and membrane potential. This modelling requires building a new model of a leak channel that depends on these drivers. We hypothesize that an intermediate Markov model similar to our IP_3R model that is gated by its key drivers must be built from scratch. Other future work on extending the model proposed here can be the inclusion of distinct types of potassium (K^+) channels which are involved in functions such as proliferation and ramification, and voltage-gated sodium channels which have rapid kinetics and depend on membrane voltage. Additionally, there is no model developed for microglia-specific aspects of voltage-gated sodium channels, A_3, and A_{2A}, particularly, by using microglial human data. Therefore, extensive research can be devoted to this channel and these receptors to further extend the biophysical models given in this research.

Furthermore, another interesting work can be to couple the kinetics of the receptors to different types of movement and deformation in glial cells through mathematical modelling. The Patlak-Keller-Segel (PKS) is the de-facto mathematical language to study chemotaxis, which is presented as a PDE formulation [156]. In [157], PKS is extended for mathematical modelling of the density of microglial cells around implanted electrodes in the brain. The authors in [158] developed an interesting technique to involve actin dynamics in terms of a PDE system which captures cell expansion, cell contraction, etc.

Therefore, further work can examine the feasibility to construct a comprehensive model for process extension and retraction of microglial cells and to couple it with receptor dynamics.

7.4 Summary

Mathematical modelling and computer simulation are powerful tools by which we can analyse complex biological systems, particularly, neural phenomena involved in brain dysfunction. The research detailed in this thesis developed a theoretical foundation for studying P2-mediated calcium and PI3K/Akt signalling in human microglial cells. A literature review was given in two individual chapters and provided the rationale behind the project. Mathematical models of the thesis were all presented in Chapter 4, which made an essential attempt to establish the relationship between microglial activation and several intercellular events either explicitly or implicitly controlled by a wide, complex range of membrane-resident ion channels and receptors, and cytosolic components and pathways. The subsequent two chapters studied the behaviour of the most important cytosolic signalling substances in human microglia, which are observed and analysed for the first time through numerical simulation.

The main goal of this thesis was to develop mathematical models for complex intracellular events in microglia and investigate the interconnecting role of the PI3K/Akt pathway to Ca^{2+}. Cytosolic calcium dynamics are vital to the functionalities of microglial cells. Calcium transients emerge from a highly coupled, complicated signal transduction pathway in these brain-resident macrophages. In this thesis, we developed biophysical models for PI3K/Akt signalling and calcium dynamics in microglia and quantified how different molecular machinery of purinergic receptors (P2Y/P2X) contribute to intracellular calcium levels in response to the agonist aiming at directed motility. To the best of our knowledge, this is the first biophysical model that aims to predict complicated Akt and Ca^{2+} responses in microglia. The biophysical models provide directions for new fundamental experimental research. We believe that our models are good candidates for expressing microglial activation which can be expanded and utilised in future to suggest new therapeutical strategies.

References

1. Vazza, F., *On the complexity and the information content of cosmic structures.* Monthly Notices of the Royal Astronomical Society, 2017. 465(4): p. 4942-4955.
2. Von Bartheld, C.S., J. Bahney, and S. Herculano-Houzel, *The search for true numbers of neurons and glial cells in the human brain: A review of 150 years of cell counting.* Journal of Comparative Neurology, 2016. 524(18): p. 3865-3895.
3. Verkhratsky, A. and A. Butt, *Glial neurobiology: a textbook*. 2007: John Wiley & Sons.
4. Franco-Bocanegra, D.K., et al., *Molecular mechanisms of microglial motility: changes in ageing and Alzheimer's disease.* Cells, 2019. 8(6): p. 639.
5. Madry, C. and D. Attwell, *Receptors, ion channels, and signaling mechanisms underlying microglial dynamics.* Journal of Biological Chemistry, 2015. 290(20): p. 12443-12450.
6. Ohsawa, K., et al., *Involvement of P2X4 and P2Y12 receptors in ATP-induced microglial chemotaxis.* Glia, 2007. 55(6): p. 604-616.
7. Umpierre, A.D., et al., *Microglial Calcium Signaling is Attuned to Neuronal Activity.* bioRxiv, 2019.
8. Brawek, B. and O. Garaschuk, *Microglial calcium signaling in the adult, aged and diseased brain.* Cell Calcium, 2013. 53(3): p. 159-169.
9. Younger, D., et al., *Microglia receptors in animal models of traumatic brain injury.* Molecular neurobiology, 2019. 56(7): p. 5202-5228.
10. Honda, S., et al., *Extracellular ATP or ADP induce chemotaxis of cultured microglia through Gi/o-coupled P2Y receptors.* Journal of Neuroscience, 2001. 21(6): p. 1975-1982.
11. Wolf, S.A., H. Boddeke, and H. Kettenmann, *Microglia in physiology and disease.* Annual review of physiology, 2017. 79: p. 619-643.
12. North, R.A., *P2X receptors.* Philosophical Transactions of the Royal Society B: Biological Sciences, 2016. 371(1700): p. 20150427.
13. Domercq, M., N. Vazquez, and C. Matute, *Neurotransmitter signaling in the pathophysiology of microglia.* Frontiers in Cellular Neuroscience, 2013. 7: p. 49.
14. Kettenmann, H., et al., *Physiology of microglia.* Physiological reviews, 2011. 91(2): p. 461-553.
15. Timmerman, R., S.M. Burm, and J.J. Bajramovic, *An overview of in vitro methods to study microglia.* Frontiers in cellular neuroscience, 2018. 12: p. 242.
16. Smith, A.M. and M. Dragunow, *The human side of microglia.* Trends in neurosciences, 2014. 37(3): p. 125-135.
17. Bohlen, C.J., et al., *Diverse requirements for microglial survival, specification, and function revealed by defined-medium cultures.* Neuron, 2017. 94(4): p. 759-773. e8.
18. Lund, S., et al., *The dynamics of the LPS triggered inflammatory response of murine microglia under different culture and in vivo conditions.* Journal of neuroimmunology, 2006. 180(1-2): p. 71-87.

19. Reich, M., et al., *Alzheimer's Risk Gene TREM2 Determines Functional Properties of New Type of Human iPSC-Derived Microglia.* Frontiers in immunology, 2021. 11: p. 3918.
20. Hodgkin, A.L. and A.F. Huxley, *A quantitative description of membrane current and its application to conduction and excitation in nerve.* The Journal of physiology, 1952. 117(4): p. 500-544.
21. Butt, A. and A. Verkhratsky, *Neuroglia: Realising their true potential.* Brain and Neuroscience Advances, 2018. 2: p. 2398212818817495.
22. Ding, X., X. Zhang, and L. Ji, *Contribution of calcium fluxes to astrocyte spontaneous calcium oscillations in deterministic and stochastic models.* Applied Mathematical Modelling, 2018. 55: p. 371-382.
23. Tewari, S.G. and K.K. Majumdar, *A mathematical model of the tripartite synapse: astrocyte-induced synaptic plasticity.* Journal of biological physics, 2012. 38(3): p. 465-496.
24. Breslin, K., et al., *Potassium and sodium microdomains in thin astroglial processes: A computational model study.* PLoS computational biology, 2018. 14(5): p. e1006151.
25. Liu, J., et al., *GABA regulation of burst firing in hippocampal astrocyte neural circuit: A biophysical model.* Frontiers in cellular neuroscience, 2019. 13: p. 335.
26. Wade, J.J., et al., *Bidirectional coupling between astrocytes and neurons mediates learning and dynamic coordination in the brain: a multiple modeling approach.* PloS one, 2011. 6(12): p. e29445.
27. Welsh, T.G. and S. Kucenas, *Purinergic signaling in oligodendrocyte development and function.* Journal of neurochemistry, 2018. 145(1): p. 6-18.
28. De Vellis, J., *Neuroglia in the aging brain*. 2001: Springer Science & Business Media.
29. Hickman, S., et al., *Microglia in neurodegeneration.* Nature neuroscience, 2018. 21(10): p. 1359-1369.
30. Erb, L., et al., *Purinergic signaling in Alzheimer's disease.* Brain research bulletin, 2019. 151: p. 25-37.
31. Thei, L., et al., *Microglia in alzheimer's disease: a role for ion channels.* Frontiers in neuroscience, 2018. 12: p. 676.
32. Hanisch, U.K., *Microglia as a source and target of cytokines.* Glia, 2002. 40(2): p. 140-155.
33. Ransohoff, R.M. and J. El Khoury, *Microglia in health and disease.* Cold Spring Harbor perspectives in biology, 2016. 8(1): p. a020560.
34. Bachiller, S., et al., *Microglia in neurological diseases: a road map to brain-disease dependent-inflammatory response.* Frontiers in cellular neuroscience, 2018. 12: p. 488.
35. Trapp, B.D., et al., *Evidence for synaptic stripping by cortical microglia.* Glia, 2007. 55(4): p. 360-368.
36. Kandel, E.R., et al., *Principles of neural science*. Vol. 4. 2000: McGraw-hill New York.
37. Habermacher, C., et al., *Molecular structure and function of P2X receptors.* Neuropharmacology, 2016. 104: p. 18-30.

38. Roth, B.L., *Molecular pharmacology of metabotropic receptors targeted by neuropsychiatric drugs.* Nature structural & molecular biology, 2019. 26(7): p. 535-544.
39. Sanz, J.M., et al., *Activation of microglia by amyloid β requires P2X7 receptor expression.* The Journal of Immunology, 2009. 182(7): p. 4378-4385.
40. Kölsch, V., P.G. Charest, and R.A. Firtel, *The regulation of cell motility and chemotaxis by phospholipid signaling.* Journal of cell science, 2008. 121(5): p. 551-559.
41. Tran, N.L., et al., *Signal transduction from n-cadherin increases bcl-2 regulation of the phosphatidylinositol 3-kinase/akt pathway by homophilic adhesion and actin cytoskeletal organization.* Journal of Biological Chemistry, 2002. 277(36): p. 32905-32914.
42. Keren-Shaul, H., et al., *A unique microglia type associated with restricting development of Alzheimer's disease.* Cell, 2017. 169(7): p. 1276-1290. e17.
43. Madry, C., et al., *Microglial ramification, surveillance, and interleukin-1β release are regulated by the two-pore domain K+ channel THIK-1.* Neuron, 2018. 97(2): p. 299-312. e6.
44. Sheth, S., et al., *Adenosine receptors: expression, function and regulation.* International journal of molecular sciences, 2014. 15(2): p. 2024-2052.
45. Haselkorn, M.L., et al., *Adenosine A1 receptor activation as a brake on the microglial response after experimental traumatic brain injury in mice.* Journal of neurotrauma, 2010. 27(5): p. 901-910.
46. Orr, A.G., et al., *Adenosine A 2A receptor mediates microglial process retraction.* Nature neuroscience, 2009. 12(7): p. 872.
47. Koscsó, B., et al., *Adenosine augments IL-10 production by microglial cells through an A2B adenosine receptor-mediated process.* The Journal of Immunology, 2012. 188(1): p. 445-453.
48. Hammarberg, C., G. Schulte, and B.B. Fredholm, *Evidence for functional adenosine A3 receptors in microglia cells.* Journal of neurochemistry, 2003. 86(4): p. 1051-1054.
49. Luongo, L., et al., *The A1 adenosine receptor as a new player in microglia physiology.* Glia, 2014. 62(1): p. 122-132.
50. Ohsawa, K., et al., *Adenosine A3 receptor is involved in ADP-induced microglial process extension and migration.* Journal of neurochemistry, 2012. 121(2): p. 217-227.
51. Nörenberg, W., P. Illes, and P.J. Gebicke-Haerter, *Sodium channel in isolated human brain macrophages (microglia).* Glia, 1994. 10(3): p. 165-172.
52. Colton, C.A., et al., *K+ modulation of microglial superoxide production: involvement of voltage-gated Ca2+ channels.* American Journal of Physiology-Cell Physiology, 1994. 266(6): p. C1650-C1655.
53. Jing, Z., et al., *SKF-96365 activates cytoprotective autophagy to delay apoptosis in colorectal cancer cells through inhibition of the calcium/CaMKIIγ/AKT-mediated pathway.* Cancer letters, 2016. 372(2): p. 226-238.
54. Zhang, X., et al., *Calcium/Calmodulin–Dependent Protein Kinase II in Cerebrovascular Diseases.* Translational Stroke Research, 2021. 12(4): p. 513-529.

55. Toulme, E., et al., *P2X4 receptors in activated C8-B4 cells of cerebellar microglial origin.* Journal of General Physiology, 2010. 135(4): p. 333-353.
56. Toulme, E. and B.S. Khakh, *Imaging P2X4 receptor lateral mobility in microglia regulation by calcium and p38 MAPK.* Journal of Biological Chemistry, 2012. 287(18): p. 14734-14748.
57. Chessell, I., A. Michel, and P. Humphrey, *Properties of the pore-forming P2X7 purinoceptor in mouse NTW8 microglial cells.* British journal of pharmacology, 1997. 121(7): p. 1429-1437.
58. Hide, I., et al., *Extracellular ATP triggers tumor necrosis factor-α release from rat microglia.* Journal of neurochemistry, 2000. 75(3): p. 965-972.
59. Janks, L., C.V. Sharma, and T.M. Egan, *A central role for P2X7 receptors in human microglia.* Journal of neuroinflammation, 2018. 15(1): p. 325.
60. Visentin, S., C. De Nuccio, and G. Bellenchi, *Different patterns of Ca 2+ signals are induced by low compared to high concentrations of P2Y agonists in microglia.* Purinergic signalling, 2006. 2(4): p. 605.
61. Moore, C.S., et al., *P2Y12 expression and function in alternatively activated human microglia.* Neurology-Neuroimmunology Neuroinflammation, 2015. 2(2).
62. Irino, Y., et al., *Akt activation is involved in P2Y12 receptor-mediated chemotaxis of microglia.* Journal of neuroscience research, 2008. 86(7): p. 1511-1519.
63. Keener, J. and J. Sneyd, *Mathematical physiology I: Cellular physiology*. Second ed. 2009: Springer.
64. Goldstein, B., J.R. Faeder, and W.S. Hlavacek, *Mathematical and computational models of immune-receptor signalling.* Nature Reviews Immunology, 2004. 4(6): p. 445-456.
65. Higham, D.J., *Modeling and simulating chemical reactions.* SIAM review, 2008. 50(2): p. 347-368.
66. Yan, Z., et al., *Experimental characterization and mathematical modeling of P2X7 receptor channel gating.* Journal of Neuroscience, 2010. 30(42): p. 14213-14224.
67. Lemon, G., *Mathematical modelling of some aspects of intracellular second messenger signalling*. 2003: School of Mathematics and Statistics, Faculty of Science, University of Sydney.
68. Tveito, A. and G.T. Lines, *Computing characterizations of drugs for ion channels and receptors using Markov models*. 2016: Springer Nature.
69. Sterratt, D., et al., *Principles of computational modelling in neuroscience*. 2011: Cambridge University Press.
70. Patneau, D.K. and M.L. Mayer, *Kinetic analysis of interactions between kainate and AMPA: evidence for activation of a single receptor in mouse hippocampal neurons.* Neuron, 1991. 6(5): p. 785-798.
71. Gábor, A. and J.R. Banga, *Robust and efficient parameter estimation in dynamic models of biological systems.* BMC systems biology, 2015. 9(1): p. 1-25.
72. Briggs, G.E. and J.B.S. Haldane, *A note on the kinetics of enzyme action.* Biochemical journal, 1925. 19(2): p. 338.
73. Khananshvili, D., *Sodium-calcium exchangers (NCX): molecular hallmarks underlying the tissue-specific and systemic functions.* Pflügers Archiv-European Journal of Physiology, 2014. 466(1): p. 43-60.
74. Gabbiani, F. and S.J. Cox, *Mathematics for neuroscientists*. 2017: Academic Press.

75. Weber, C.R., et al., *Na+-Ca2+ exchange current and submembrane [Ca2+] during the cardiac action potential.* Circulation research, 2002. 90(2): p. 182-189.
76. Wade, J.J., et al., *Calcium microdomain formation at the perisynaptic cradle due to NCX reversal: a computational study.* Frontiers in cellular neuroscience, 2019. 13: p. 185.
77. Toman, M., et al., *The influence of astrocytic leaflet motility on ionic signalling and homeostasis at active synapses.* Scientific Reports, 2023. 13(1): p. 3050.
78. Weber, C.R., et al., *Allosteric regulation of Na/Ca exchange current by cytosolic Ca in intact cardiac myocytes.* The Journal of general physiology, 2001. 117(2): p. 119-132.
79. Silva, H.S., A. Kapela, and N.M. Tsoukias, *A mathematical model of plasma membrane electrophysiology and calcium dynamics in vascular endothelial cells.* American Journal of Physiology-Cell Physiology, 2007. 293(1): p. C277-C293.
80. Wade, J., et al., *Self-repair in a bidirectionally coupled astrocyte-neuron (AN) system based on retrograde signaling.* Frontiers in computational neuroscience, 2012. 6: p. 76.
81. De Pittà, M., et al., *Glutamate regulation of calcium and IP 3 oscillating and pulsating dynamics in astrocytes.* Journal of biological physics, 2009. 35(4): p. 383-411.
82. Hund, T.J., et al., *Role of activated CaMKII in abnormal calcium homeostasis and INa remodeling after myocardial infarction: insights from mathematical modeling.* Journal of molecular and cellular cardiology, 2008. 45(3): p. 420-428.
83. Hansen, N., *The CMA evolution strategy: a comparing review*, in *Towards a new evolutionary computation*. 2006, Springer. p. 75-102.
84. Luengo, D., et al., *A survey of Monte Carlo methods for parameter estimation.* EURASIP Journal on Advances in Signal Processing, 2020. 2020(1): p. 1-62.
85. Chhatbar, C. and M. Prinz, *The roles of microglia in viral encephalitis: from sensome to therapeutic targeting.* Cellular & Molecular Immunology, 2021: p. 1-9.
86. Liu, L., et al., *Microglial Calcium Waves During the Hyperacute Phase of Ischemic Stroke.* Stroke, 2021. 52(1): p. 274-283.
87. Bianco, F., et al., *Pathophysiological roles of extracellular nucleotides in glial cells: differential expression of purinergic receptors in resting and activated microglia.* Brain Research Reviews, 2005. 48(2): p. 144-156.
88. Xiang, Z., et al., *Microglial morphology and its transformation after challenge by extracellular ATP in vitro.* Journal of neuroscience research, 2006. 83(1): p. 91-101.
89. Chun, B.J., et al., *Simulation of P2X-mediated calcium signalling in microglia.* The Journal of physiology, 2019. 597(3): p. 799-818.
90. Poshtkohi, A., et al., *Mathematical modelling of human P2X-mediated plasma membrane electrophysiology and calcium dynamics in microglia.* PLOS Computational Biology, 2021. 17(11): p. e1009520.
91. Mackay, L., et al., *Deciphering the regulation of P2X4 receptor channel gating by ivermectin using Markov models.* PLoS computational biology, 2017. 13(7): p. e1005643.
92. Khadra, A., et al., *Dual gating mechanism and function of P2X7 receptor channels.* Biophysical journal, 2013. 104(12): p. 2612-2621.

93. Khadra, A., et al., *Gating properties of the P2X2a and P2X2b receptor channels: experiments and mathematical modeling.* Journal of General Physiology, 2012. 139(5): p. 333-348.
94. Ilyaskin, A.V., et al., *Bile acids inhibit human purinergic receptor P2X4 in a heterologous expression system.* Journal of General Physiology, 2019. 151(6): p. 820-833.
95. De Young, G.W. and J. Keizer, *A single-pool inositol 1, 4, 5-trisphosphate-receptor-based model for agonist-stimulated oscillations in Ca2+ concentration.* Proceedings of the National Academy of Sciences, 1992. 89(20): p. 9895-9899.
96. Li, Y.-X. and J. Rinzel, *Equations for InsP3 receptor-mediated [Ca2+] i oscillations derived from a detailed kinetic model: a Hodgkin-Huxley like formalism.* Journal of theoretical Biology, 1994. 166(4): p. 461-473.
97. Sneyd, J. and J.-F. Dufour, *A dynamic model of the type-2 inositol trisphosphate receptor.* Proceedings of the National Academy of Sciences, 2002. 99(4): p. 2398-2403.
98. Lemon, G., W. Gibson, and M. Bennett, *Metabotropic receptor activation, desensitization and sequestration—I: modelling calcium and inositol 1, 4, 5-trisphosphate dynamics following receptor activation.* Journal of Theoretical Biology, 2003. 223(1): p. 93-111.
99. Song, S.O. and J. Varner, *Modeling and analysis of the molecular basis of pain in sensory neurons.* PLoS One, 2009. 4(9): p. e6758.
100. Purvis, J.E., et al., *A molecular signaling model of platelet phosphoinositide and calcium regulation during homeostasis and P2Y12 activation.* Blood, The Journal of the American Society of Hematology, 2008. 112(10): p. 4069-4079.
101. Shakhidzhanov, S., et al., *Modulation and pre-amplification of PAR1 signaling by ADP acting via the P2Y12 receptor during platelet subpopulation formation.* Biochimica et Biophysica Acta (BBA)-General Subjects, 2015. 1850(12): p. 2518-2529.
102. Dolan, A.T. and S.L. Diamond, *Systems modeling of Ca2+ homeostasis and mobilization in platelets mediated by IP3 and store-operated Ca2+ entry.* Biophysical journal, 2014. 106(9): p. 2049-2060.
103. Mishra, J. and U.S. Bhalla, *Simulations of inositol phosphate metabolism and its interaction with InsP3-mediated calcium release.* Biophysical Journal, 2002. 83(3): p. 1298-1316.
104. Hatakeyama, M., et al., *A computational model on the modulation of mitogen-activated protein kinase (MAPK) and Akt pathways in heregulin-induced ErbB signalling.* Biochemical Journal, 2003. 373(2): p. 451-463.
105. Koh, G., et al., *A decompositional approach to parameter estimation in pathway modeling: a case study of the Akt and MAPK pathways and their crosstalk.* Bioinformatics, 2006. 22(14): p. e271-e280.
106. Pappalardo, F., et al., *Computational modeling of PI3K/AKT and MAPK signaling pathways in melanoma cancer.* PLoS One, 2016. 11(3): p. e0152104.
107. Ji, B., et al., *Mathematical modelling of Her2 (ErbB2) PI3K/AKT signalling pathways during breast carcinogenesis to include PTPD2.* AIMS Mathematics, 2020. 5(5): p. 4946-4958.

108. Tan, W.H., A.S. Popel, and F. Mac Gabhann, *Computational model of Gab1/2-dependent VEGFR2 pathway to Akt activation.* PloS one, 2013. 8(6): p. e67438.
109. Anderson, W.D., et al., *Computational modeling of cytokine signaling in microglia.* Molecular BioSystems, 2015. 11(12): p. 3332-3346.
110. Silchenko, A. and P.A. Tass, *Computational modeling of chemotactic signaling and aggregation of microglia around implantation site during deep brain stimulation.* The European Physical Journal Special Topics, 2013. 222(10): p. 2647-2653.
111. Amato, S. and A. Arnold, *Modeling Microglia Activation and Inflammation-Based Neuroprotectant Strategies During Ischemic Stroke.* Bulletin of Mathematical Biology, 2021. 83(6): p. 1-27.
112. Li, X.-L., et al., *Regulation of TWIK-related K+ channel 1 in the anterior hippocampus of patients with temporal lobe epilepsy with comorbid depression.* Epilepsy & Behavior, 2021. 121: p. 108045.
113. Destexhe, A., Z.F. Mainen, and T.J. Sejnowski, *Kinetic models of synaptic transmission.* Methods in neuronal modeling, 1998. 2: p. 1-25.
114. Klapperstück, M., et al., *Functional evidence of distinct ATP activation sites at the human P2X7 receptor.* The Journal of physiology, 2001. 534(1): p. 25-35.
115. Vargas-Martínez, E.M., et al., *Functional expression of P2X1, P2X4 and P2X7 purinergic receptors in human monocyte-derived macrophages.* European Journal of Pharmacology, 2020. 888: p. 173460.
116. Cao, P., et al., *A stochastic model of calcium puffs based on single-channel data.* Biophysical journal, 2013. 105(5): p. 1133-1142.
117. Cao, P., et al., *A deterministic model predicts the properties of stochastic calcium oscillations in airway smooth muscle cells.* PLoS Computational Biology, 2014. 10(8): p. e1003783.
118. Koupenova, M. and K. Ravid, *Biology of platelet purinergic receptors and implications for platelet heterogeneity.* Frontiers in pharmacology, 2018. 9: p. 37.
119. Sasaki, A.T. and R.A. Firtel, *Regulation of chemotaxis by the orchestrated activation of Ras, PI3K, and TOR.* European journal of cell biology, 2006. 85(9-10): p. 873-895.
120. Fan, Y., L. Xie, and C.Y. Chung, *Signaling pathways controlling microglia chemotaxis.* Molecules and cells, 2017. 40(3): p. 163.
121. Castellano, E. and J. Downward, *RAS interaction with PI3K: more than just another effector pathway.* Genes & cancer, 2011. 2(3): p. 261-274.
122. Jacques-Silva, M.C., et al., *P2X7 receptors stimulate AKT phosphorylation in astrocytes.* British journal of pharmacology, 2004. 141(7): p. 1106-1117.
123. Tsuda, M., et al., *Mechanisms underlying fibronectin-induced up-regulation of P2X4R expression in microglia: distinct roles of PI3K–Akt and MEK–ERK signalling pathways.* Journal of cellular and molecular medicine, 2009. 13(9b): p. 3251-3259.
124. Ashour, F. and J. Deuchars, *Electron microscopic localisation of P2X4 receptor subunit immunoreactivity to pre-and post-synaptic neuronal elements and glial processes in the dorsal vagal complex of the rat.* Brain research, 2004. 1026(1): p. 44-55.

125. Yano, S., H. Tokumitsu, and T.R. Soderling, *Calcium promotes cell survival through CaM-K kinase activation of the protein-kinase-B pathway.* Nature, 1998. 396(6711): p. 584-587.
126. Agell, N., et al., *Modulation of the Ras/Raf/MEK/ERK pathway by Ca2+, and calmodulin.* Cellular signalling, 2002. 14(8): p. 649-654.
127. Sanada, M., et al., *Increase in intracellular Ca2+ and calcitonin gene-related peptide release through metabotropic P2Y receptors in rat dorsal root ganglion neurons.* Neuroscience, 2002. 111(2): p. 413-422.
128. Wang, X., et al., *Activation of purinergic P2X receptors inhibits P2Y-mediated Ca2+ influx in human microglia.* Cell Calcium, 2000. 27(4): p. 205-212.
129. *The CMA Evolution Strategy*. 2021; Available from: http://cma.gforge.inria.fr/index.html.
130. Boscia, F., et al., *NCX1 expression and functional activity increase in microglia invading the infarct core.* Stroke, 2009. 40(11): p. 3608-3617.
131. Torres-Platas, S.G., et al., *Morphometric characterization of microglial phenotypes in human cerebral cortex.* Journal of neuroinflammation, 2014. 11(1): p. 12.
132. Michel, A., M. Xing, and P. Humphrey, *Serum constituents can affect 2'-& 3'-O-(4-benzoylbenzoyl)-ATP potency at P2X7 receptors.* British journal of pharmacology, 2001. 132(7): p. 1501-1508.
133. Visentin, S., et al., *Two different ionotropic receptors are activated by ATP in rat microglia.* The Journal of Physiology, 1999. 519(3): p. 723-736.
134. Ase, A.R., É. Therrien, and P. Séguéla, *An allosteric inhibitory site conserved in the ectodomain of P2X receptor channels.* Frontiers in cellular neuroscience, 2019. 13: p. 121.
135. Verderio, C. and M. Matteoli, *ATP mediates calcium signaling between astrocytes and microglial cells: modulation by IFN-γ.* The Journal of Immunology, 2001. 166(10): p. 6383-6391.
136. Nobile, M., et al., *ATP-induced, sustained calcium signalling in cultured rat cortical astrocytes: evidence for a non-capacitative, P2X7-like-mediated calcium entry.* FEBS letters, 2003. 538(1-3): p. 71-76.
137. Carrasquero, L.M.G., et al., *P2X7 and P2Y13 purinergic receptors mediate intracellular calcium responses to BzATP in rat cerebellar astrocytes.* Journal of neurochemistry, 2009. 110(3): p. 879-889.
138. Pubill, D., et al., *ATP induces intracellular calcium increases and actin cytoskeleton disaggregation via P2x receptors.* Cell calcium, 2001. 29(5): p. 299-309.
139. White, S.M., et al., *Calcium signaling pathways utilized by P2X receptors in freshly isolated preglomerular MVSMC.* American Journal of Physiology-Renal Physiology, 2001. 280(6): p. F1054-F1061.
140. Emmett, D.S., et al., *Characterization of ionotrophic purinergic receptors in hepatocytes.* Hepatology, 2008. 47(2): p. 698-705.
141. Zhang, X.-J., et al., *Expression of P2X7 in human hematopoietic cell lines and leukemia patients.* Leukemia research, 2004. 28(12): p. 1313-1322.
142. Berchtold, S., et al., *Human monocyte derived dendritic cells express functional P2X and P2Y receptors as well as ecto-nucleotidases.* FEBS letters, 1999. 458(3): p. 424-428.

143. Solini, A., et al., *Multiple P2X receptors are involved in the modulation of apoptosis in human mesangial cells: evidence for a role of P2X4.* American Journal of Physiology-Renal Physiology, 2007. 292(5): p. F1537-F1547.
144. Abdul Kadir, L., M. Stacey, and R. Barrett-Jolley, *Emerging roles of the membrane potential: action beyond the action potential.* Frontiers in physiology, 2018. 9: p. 1661.
145. Zi, Z., *Sensitivity analysis approaches applied to systems biology models.* IET systems biology, 2011. 5(6): p. 336-346.
146. Noykova, N. and M. Gyllenberg, *Sensitivity analysis and parameter estimation in a model of anaerobic waste water treatment processes with substrate inhibition.* Bioprocess Engineering, 2000. 23(4): p. 343-349.
147. Sobol, I.M., *Global sensitivity indices for nonlinear mathematical models and their Monte Carlo estimates.* Mathematics and computers in simulation, 2001. 55(1-3): p. 271-280.
148. Marelli, S. and B. Sudret, *UQLab: A framework for uncertainty quantification in Matlab*, in *Vulnerability, uncertainty, and risk: quantification, mitigation, and management*. 2014. p. 2554-2563.
149. Beamer, E., G. Conte, and T. Engel, *ATP release during seizures–A critical evaluation of the evidence.* Brain Research Bulletin, 2019. 151: p. 65-73.
150. Velasquez, S., et al., *Circulating levels of ATP is a biomarker of HIV cognitive impairment.* EBioMedicine, 2020. 51: p. 102503.
151. Thawkar, B.S. and G. Kaur, *Inhibitors of NF-κB and P2X7/NLRP3/Caspase 1 pathway in microglia: Novel therapeutic opportunities in neuroinflammation induced early-stage Alzheimer's disease.* Journal of Neuroimmunology, 2019. 326: p. 62-74.
152. Bartlett, R., L. Stokes, and R. Sluyter, *The P2X7 receptor channel: recent developments and the use of P2X7 antagonists in models of disease.* Pharmacological reviews, 2014. 66(3): p. 638-675.
153. Savio, L.E., et al., *The P2X7 receptor in inflammatory diseases: angel or demon?* Frontiers in pharmacology, 2018. 9: p. 52.
154. Saez-Orellana, F., et al., *Modulation of the neuronal network activity by P2X receptors and their involvement in neurological disorders.* Pharmacological Research, 2015. 101: p. 109-115.
155. Hedegaard, A., et al., *Honing the double-edged sword: improving human iPSC-microglia models.* Frontiers in Immunology, 2020. 11.
156. Painter, K.J., *Mathematical models for chemotaxis and their applications in self-organisation phenomena.* Journal of theoretical biology, 2019. 481: p. 162-182.
157. Silchenko, A.N. and P.A. Tass, *Mathematical modeling of chemotaxis and glial scarring around implanted electrodes.* New journal of physics, 2015. 17(2): p. 023009.
158. George, U.Z., A. Stéphanou, and A. Madzvamuse, *Mathematical modelling and numerical simulations of actin dynamics in the eukaryotic cell.* Journal of mathematical biology, 2013. 66(3): p. 547-593.

Appendix A – The Effect of P2XR Absence on Model Dynamics

As discussed in the thesis and Section 4.3.2, the model supports the hypothesis that Ca^{2+} influx via P2YR and P2XR can explain the experimentally reported biphasic transient responses in measuring pAkt levels [62]. To show this mathematically, P2XRs were turned off and the model was refitted to the experimental pAkt data reported in [62]. As illustrated in Fig. A.1, the model activated only by the $P2Y_{12}$ receptor is unable to capture double pAkt peaks in the absence of P2XRs. Therefore, both receptors (P2Y and P2X) must simultaneously induce Ca^{2+} influx for the activation of CaMKII.

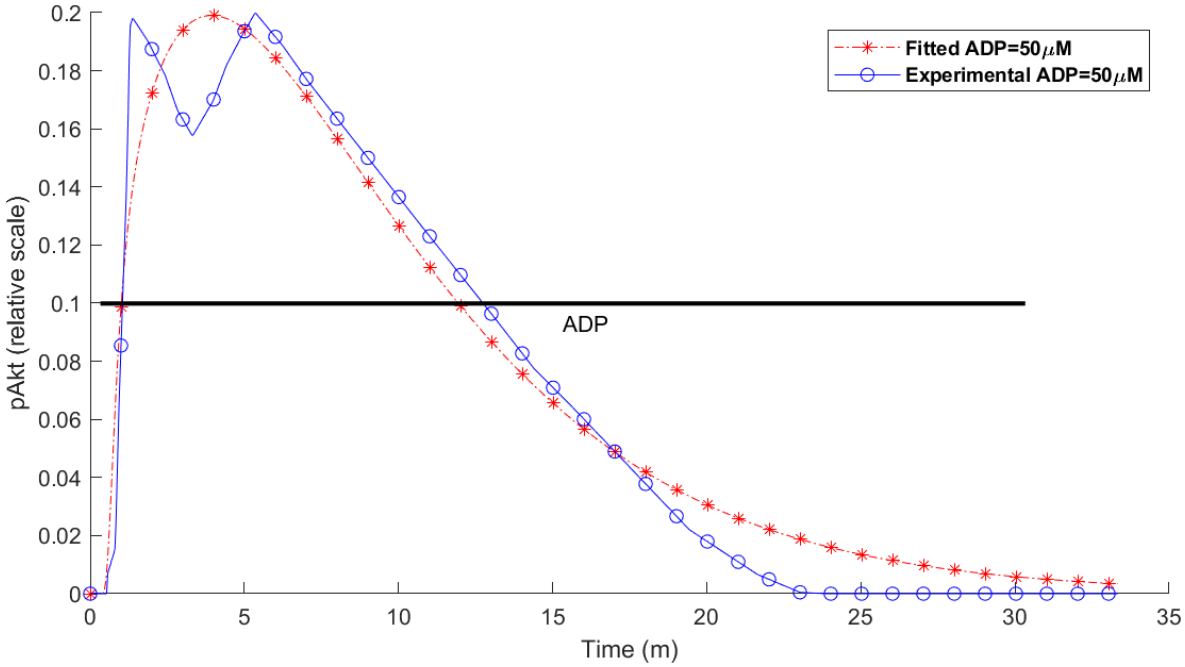

Figure A.1: Fitted intracellular pAkt upon an ADP treatment of 50μM within 30 minutes via activation of the $P2Y_{12}$ receptor in microglia as compared with experiments [62] when P2XRs are turned off.

Appendix B – Equations of PI3K/Akt Reaction Network

The governing equations for the CaMKII-mediated PI3K/Akt reaction network developed in Section 4.3.4 are as follows:

$$\frac{dx_1}{dt} = -a_1 \times CaM \times x_1 x_2 + b_1 y_1 + c_2 y_2 \quad \text{(A.1)}$$

$$\frac{dx_2}{dt} = -a_1 \times CaM \times x_1 x_2 + (b_1 + c_1) y_1 \quad \text{(A.2)}$$

$$\frac{dy_1}{dt} = a_1 \times CaM \times x_1 x_2 - (b_1 + c_1) y_1 \quad \text{(A.3)}$$

$$\frac{dx_3}{dt} = -a_2 x_3 x_4 + b_2 y_2 + c_1 y_1 - a_3 x_3 x_5 + (b_3 + c_3) y_3 - a_5 x_3 x_8 + b_5 y_5 \quad \text{(A.4)}$$

$$\frac{dx_4}{dt} = -a_2 x_3 x_4 + (b_2 + c_2) y_2 \quad \text{(A.5)}$$

$$\frac{dy_2}{dt} = a_2 x_3 x_4 - (b_2 + c_2) y_2 \quad \text{(A.6)}$$

$$\frac{dx_5}{dt} = -a_3 x_3 x_5 + b_3 y_3 + c_4 y_4 - a_7 y_5 x_5 + b_7 y_6 \quad \text{(A.7)}$$

$$\frac{dx_6}{dt} = -a_4 x_6 x_7 + b_4 y_4 + c_3 y_3 + c_5 y_6 \quad \text{(A.8)}$$

$$\frac{dy_3}{dt} = a_3 x_3 x_5 - (b_3 + c_3) y_3 - a_6 y_3 x_8 + b_6 y_6 \quad \text{(A.9)}$$

$$\frac{dx_7}{dt} = -a_4 x_6 x_7 + (b_4 + c_4) y_4 \quad \text{(A.10)}$$

$$\frac{dy_4}{dt} = a_4 x_6 x_7 - (b_4 + c_4) y_4 \quad \text{(A.11)}$$

$$\frac{dx_8}{dt} = -a_5 x_3 x_8 + b_5 y_5 - a_6 y_3 x_8 + b_6 y_6 \quad \text{(A.12)}$$

$$\frac{dy_5}{dt} = a_5 x_3 x_8 - a_7 y_5 x_5 + (b_7 + c_5) y_6 - b_5 y_5 \quad \text{(A.13)}$$

$$\frac{dy_6}{dt} = a_6 y_3 x_8 - (b_6 + b_7 + c_5) y_6 + a_7 y_5 x_5 \quad \text{(A.14)}$$

Appendix C – Publications

1. Poshtkohi, A., et al., *Mathematical modelling of human P2X-mediated plasma membrane electrophysiology and calcium dynamics in microglia.* PLOS Computational Biology, 2021. 17(11): p. e1009520
2. Poshtkohi, A., et al., *Mathematical Modelling of PI3K/Akt Pathway in Microglia.* submitted, 2023.